

# **Structural and Physical Studies of Co(III) Salen Derivatives**

Submitted in fulfilment of the requirements for the degree of

**MASTER OF SCIENCE**

**By**

**Santham Govender**

*B.Sc. (Hons) (Chem Tech) (KwaZulu-Natal)*

March 2007

School of Chemistry  
University of KwaZulu-Natal  
Pietermaritzburg

## Declaration

I hereby certify that this research is as a result of my own investigation which has not already been accepted in substance for any degree and is not submitted in candidature for any other degree.

Signed.....

**Santham Govender**

I hereby certify that this statement is correct.

Signed.....

**Professor O.Q. Munro**

**Supervisor**

School of Chemistry  
University of KwaZulu-Natal  
Pietermaritzburg

March 2007

## Acknowledgments

Firstly, I would like to thank my supervisor, Professor Orde Munro, for his support and guidance throughout the project as well as for the effort and time he has put into the project. His enthusiasm and encouragement really made a difference to this project.

I would also like to thank the following people:

- Mr Craig Grimmer for his assistance in the processing of NMR spectra.
- Messrs Raj Somaru, Faizel Sheik and Shawn Ball and Miss Nozibele Mbangula for their invaluable assistance in everyday laboratory matters.

A big thank you to Sandra Joubert for her continuous encouragement, never-ending support and guidance as well as her advice in chemistry and non-chemistry issues throughout this project. I would also like to thank friends and colleagues in the Chemistry Department for their support and encouragement.

I wish to thank the National Research Fund for funding.

To my dad, thank you for being my inspiration and giving me the opportunity to do what I wanted to do. To my mum and brother, thank you for your never-ending support, encouragement and patience. To Neshalin, thank you for being my pillar of strength and for your continuous encouragement and your understanding. To all my friends and family, thank you for your continuous support and encouragement.

Lastly to Bhagawan Sri Sathya Sai Baba, thank you for being in my life and for your continuous guidance throughout my life and helping me achieve my goals.

## Conference Proceedings

A talk entitled 'Synthesis and Characterisation of Bis(amine) Co(III) Schiff Base Complexes' was presented at SACI at University of KwaZulu-Natal, Howard College in November 2005. A poster of this work was presented at the INORG 2005 conference in Pietermaritzburg entitled 'Synthesis and Characterisation of Bis(amine) Co(III) Schiff Base Complexes'.

## Publications

1. Orde Q. Munro, Santham Govender. A New Polymorph of cobalt(III) Schiff base complex exhibits a one-dimensional C–H...O hydrogen-bonded extended structure with helical  $2_1$  symmetry. *Acta Crystallogr., Sect. C.* **2007**, *63*, 150-152. (See **Appendix A.3.4.**)

## List of Abbreviations and Symbols

2-MeIm	2-methylimidazole
$\alpha$ -MeBzNH <sub>2</sub>	alpha-methylbenzylamine
ACACEN	Bis(acetylacetonate)(ethylene diimine)
CSD	Cambridge Structural Database
BAE	Bis(acetylacetonate)ethylenediimine
BBE	Bis(benzolacetonate)ethylenediimine
BuNH <sub>2</sub>	Butylamine
Bu <sub>2</sub> NH	Dibutylamine
BzNH <sub>2</sub>	Benzylamine
DBM	Dibenzoylmethanate
DCM	Dichloromethane
DMSO	Dimethyl sulfoxide
Hsalmal	(2 <i>Z</i> )-2-amino-3-[[ <i>(1E)</i> -(2-hydroxyphenyl)methylene]amino]but-2-enedinitrile
H <sub>2</sub> salen	<i>N,N'</i> -ethylenebis(salicylideneiminato)
H <sub>2</sub> saldiprop	2-([3-([3-[(2-hydroxybenzylidene)amino]propyl]amino)propyl]imino)methyl]phenol
H <sub>2</sub> saldmprop	2-[( <i>E</i> )-[3-[[ <i>(1E)</i> -(2-hydroxyphenyl)methylene]amino]-2,2-dimethylpropyl]imino]methyl]phenol
H <sub>2</sub> salmal	(2 <i>Z</i> )-2,3-bis[[ <i>(1E)</i> -1-(2-hydroxyphenyl)ethylidene]amino]but-2-enenitrile
H <sub>2</sub> salophen	<i>N,N'</i> -disalicylidene-1,2-phenylenediamine
HIm	Imidazole
HOMO	Highest occupied molecular orbital
ImzH	Imidazole
IR	Infrared
ISE	Ion selective electrode
IUCR	International Union of Crystallography

KBr	Potassium bromide
LUMO	Lowest unoccupied molecular orbital
Me	Methyl
Mrpln	Morpholine
<i>N</i> -MePipz	<i>N</i> -methylpiperazine
N <sub>ax</sub>	axial ligand nitrogen
NADH	Nicotinamide adenine dinucleotide
NMR	Nuclear Magnetic Resonance
OAc	Acetate
ORTEP	Oak Ridge Thermal Ellipsoid Plot Program
Ph	Phenyl
Pip	Piperidine
Prldn	Pyrrolidine
Py	Pyridine
SALOMPHEN	<i>N,N'</i> -3,4-dimethylphenylenebis(salicylideneimine)
THF	Tetrahydrofuran
UV	Ultraviolet

## Abstract

A number of ligands that belong to the salen-type family were synthesized in this thesis. These ligands were synthesized from salicylaldehyde and 1,2-phenylenediamine, 1,3-diamino-2-hydroxypropane, 1,2-diamino-ethane, *N*-(3-aminopropyl)-1,3-propanediamine, diethylenetriamine, diaminomaleonitrile, 2,2-dimethyl-1,3-propanediamine and 1,3-diaminopropane. From this range of ligands, H<sub>2</sub>salophen was chosen as the ligand for further studies.

This work is aimed primarily at elucidating the structures and spectroscopic properties of [Co(salophen)(amine)<sub>2</sub>](OAc) derivatives, where salophen is *N,N'*-disalicylidene-1,2-phenylenediamine and the amines used were butylamine, benzylamine,  $\alpha$ -methylbenzylamine, dibutylamine, *N*-methylpiperazine and piperidine. Three novel crystal structures of [Co<sup>III</sup>(salophen)L<sub>2</sub>](Cl) derivatives, where L = butylamine, benzylamine, and piperidine, with Co-N distances that range from 1.901 Å to 2.024 Å, have been reported in this thesis. The novel crystal structure of [Co(salophen)(*N*-MePipz)(OAc)] is also reported in this thesis. These cobalt complexes have been analysed by <sup>1</sup>H, <sup>13</sup>C and <sup>59</sup>Co NMR as well as electronic and IR spectroscopy. A <sup>59</sup>Co NMR spectrum was obtained for the [Co(salophen)(BuNH<sub>2</sub>)<sub>2</sub>](CH<sub>2</sub>Cl<sub>2</sub>·Cl) complex. The spectrum exhibits a single line at 8504 ppm.

The binding constants of all [Co(salophen)(amine)<sub>2</sub>](OAc) complexes, where amine = butylamine, benzylamine,  $\alpha$ -methylbenzylamine, dibutylamine, *N*-methylpiperazine and piperidine, were determined by spectroscopic titrations. The titrations were carried out at various concentrations of the amine and at temperatures ranging from 25°C to 45°C. It was found that the primary amines had much larger values of K<sub>1</sub> and K<sub>2</sub> compared to the secondary amines. Typical values of K<sub>1</sub> and K<sub>2</sub> were 8000 M<sup>-1</sup> and 63.6 M<sup>-1</sup> respectively at 25°C, for  $\alpha$ -methylbenzylamine. Of the primary amines, it was found that  $\alpha$ -methylbenzylamine had the largest value of K<sub>1</sub> and K<sub>2</sub> compared to the other two amines. For the secondary amines, it was found that *N*-methylpiperazine had the bigger value of K<sub>1</sub> compared to that of dibutylamine.

# Contents

<b>Acknowledgments</b>	<b>III</b>
<b>Conference Proceedings</b>	<b>IV</b>
<b>Publications</b>	<b>IV</b>
<b>List of Abbreviations and Symbols</b>	<b>V</b>
<b>Abstract</b>	<b>VII</b>
<b>Chapter One: Introduction</b>	<b>I</b>
1.1 Schiff Base Ligands	1
1.2 Schiff Base Complexes of Metal Ions	5
1.3 Co(II) Schiff Base Complexes	7
1.4 Co(III) Schiff Base Complexes	9
1.5 Objectives:	11
<b>Chapter Two: Experimental</b>	<b>12</b>
2.1 General Procedure	12
2.2 Instrumentation	12
2.3 Synthesis of Schiff Base Ligands	13
2.4 Synthesis of Cobalt Complexes:	21
<b>Chapter Three: Synthesis of Cobalt(III) complexes</b>	<b>28</b>
3.1 Ligand Synthesis	28
3.2 Synthesis of [Co(L)(OAc)]	37
3.3 Synthesis of [Co(salophen)(L) <sub>2</sub> ](OAc)	42
<b>Chapter Four: Spectroscopy</b>	<b>48</b>
4.1 Infrared Spectroscopy	48
4.2 NMR Spectroscopy	51
4.3 UV-vis Spectroscopy	57
<b>Chapter Five: X-ray Crystal Structures of Co(III) Schiff Base Complexes</b>	<b>62</b>
5.1 Introduction	62
5.2 Experimental: X-ray structure determinations	68
5.3 Results and Discussion	71
<b>Chapter Six: Thermodynamics</b>	<b>89</b>
6.1 Introduction	89

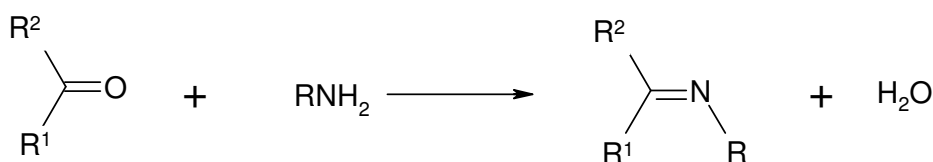
6.2 Experimental	91
6.3 Results and Discussion	94
<b>Chapter Seven: Conclusions and Future Work</b>	<b>125</b>
<b>References</b>	<b>127</b>
<b>Appendix A:</b> Crystallographic Data of Hsalmal, H <sub>2</sub> salmal and Co <sup>III</sup> Complexes	<b>136</b>
<b>Appendix B:</b> <sup>1</sup> H NMR spectrum of [Co(salophen)(OAc)].	<b>159</b>
<b>Appendix C:</b> Co(III) salophen complexes Crystallographic Data.	<b>161</b>
<b>Appendix D:</b> Spectroscopic and Thermodynamic data.	<b>186</b>
<b>Appendix E:</b> Full Crystallographic data tables and CIF files for additional structures.	
<b>Appendix F:</b> Full Crystallographic data tables and CIF files for Co(III) salophen complexes.	

# Chapter One: Introduction

## 1.1 Schiff Base Ligands

Schiff bases are chemical compounds containing a carbon-nitrogen double bond with the nitrogen atom connected to an aryl or an alkyl group but not hydrogen. In 1840 Ettlign synthesised the first example of such a compound during the reaction between salicylaldehyde and ammonia to isolate a copper complex of the product.<sup>1</sup> However in 1869, Hugo Schiff, discovered the 1: 2 metal: ligand stoichiometry of this complex and as a result lent his name to the class of compounds.<sup>2</sup>

Schiff bases are formed by the condensation reaction between an aldehyde or ketone and a primary amine which leads to the formation of an azomethine or imine linkage together with the release of one water molecule:<sup>1,2,3</sup>



**Scheme 1.1.1** Condensation reaction between an aldehyde or ketone and a primary amine to yield a Schiff base where R, R<sup>1</sup> and R<sup>2</sup> are alkyl substituents.<sup>2</sup>

Condensation of two moles of salicylaldehyde with a diamine affords a tetradentate ligand that features two neutral nitrogen atoms and two hydroxyls, which are easily ionisable. The two nitrogen atoms and two hydroxyls are located in a planar arrangement which allows for suitable coordination to transition metals.<sup>4</sup> Many different metals in various oxidation states are stabilized by Schiff bases thereby controlling the performance of the metals.<sup>5</sup>

Schiff base ligands are among the most popular ligands. The main reasons for this are their ease of formation as well as their rich coordination chemistry with a variety of metal ions.<sup>4</sup>

Schiff base compounds are used in coordination chemistry, as ligands, for their metal binding ability. Schiff base-metal complexes are characterized by important properties such as biological activity, complexing ability towards toxic metals, the ability to reversibly bind oxygen in epoxidation reactions, as catalysts in the hydrogenation of olefins and photochromic properties.<sup>6</sup>

Reacting two equivalents of salicylaldehyde with a diamine leads to the formation of an extremely important class of ligands, known as “salens” (salen = *N,N'*-ethylenebis(salicylideneiminato))<sup>3,5</sup> (**L7**). Although salen refers to the tetradentate Schiff bases derived from ethylenediamine and salicylaldehyde, a more general term, salen-type, is used in the literature to describe the class of [N,N,O,O] tetradentate bis-Schiff base ligands.<sup>5</sup> This class of ligands has four coordinating sites and two axial sites open to additional ligands.<sup>3,5</sup> This tetradentate-binding pattern is indicative of the porphyrin framework. However, the salen derivatives are more easily synthesised than the porphyrins and their structures are easier to manipulate to create an asymmetric environment around the active metal site.<sup>7</sup>

In this project, a number of salen derivatives have been synthesised, as illustrated by **Figure 1.1.1**. Of these ligands, H<sub>2</sub>salophen (H<sub>2</sub>salophen = *N,N'*-*o*-phenylenebis(salicylideneiminato)) (**L1**) in particular was chosen for metallation with cobalt (III) and further studies of the coordination chemistry of the [Co(salophen)X] system, where X is an anion such as Cl<sup>-</sup> or CH<sub>3</sub>CO<sub>2</sub><sup>-</sup>.

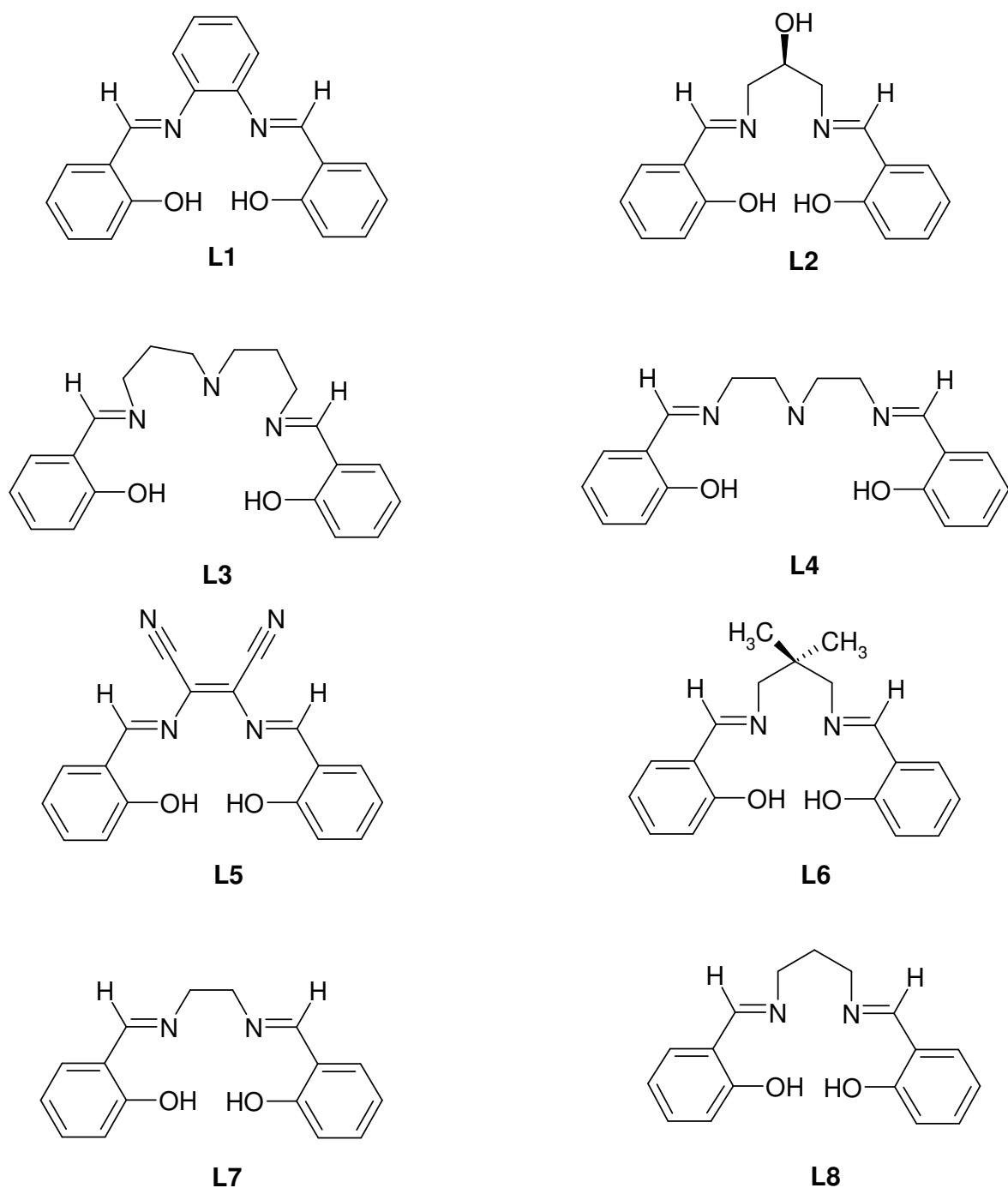


**Figure 1.1.1:** Salen-type ligands that were synthesized during this project.

Schiff base ligands, in particular salen and its derivatives, have been the ligands of choice for many reasons. Firstly the ease with which these ligands can be prepared means that large quantities of the ligand may be prepared cheaply. Secondly, these ligands are multidentate, so for most metals, several binding sites are occupied hence leaving unoccupied sites

available for potential catalytic or biomimetic activity.<sup>8</sup> These ligands show great importance in asymmetric catalysis due to their relevant synthetic ligand systems. They are important as catalysts for a wide range of transition-metal catalysis reactions such as the epoxidation of olefins, hydroxylation, lactide polymerization and asymmetric ring opening of epoxides. The significance of these ligands and their transition-metal complexes, as catalysts, have attracted considerable attention, due to the relevance of their applications, particularly in the development of agrochemical and pharmaceutical industries.<sup>9</sup>

Due to their accessibility, diverse chemical activity, broad spectrum of biological and pharmacological properties, e.g. analgesic, antipyretic, anti-inflammatory, anticancerous, bacteriocidal and fungicidal activity, the study of imines and their metal complexes has become topical in the quest for improved drugs and catalysts ultimately for the betterment of human life.<sup>10</sup>

## 1.2 Schiff Base Complexes of Metal Ions

Metal complexes of Schiff bases have been known since the mid-nineteenth century.<sup>1</sup> Transition metal complexes containing Schiff base ligands have attracted considerable interest for many years<sup>11</sup> and they have occupied a central role in the development of coordination chemistry.<sup>1,12</sup>

Schiff base complexes of transition metals have received the most attention because they can display a variety of structural and magnetic properties. In addition, the metal ion can exist in different spin states, depending on the chemical environment.<sup>13</sup>

The redox chemistry of transition metal complexes containing macrocyclic or polydentate ligands involves the oxidation state of the metal centre. Very seldom does the redox chemistry of the ligand have chemical consequences such as the formation or cleavage of bonds. This could lead to the possibility of storing and releasing electrons to produce a type of molecular battery.<sup>14</sup> Franceschi *et al.* studied the redox chemistry of the transition metals bonded to tetradentate, highly  $\pi$ -delocalized Schiff bases, viz., H<sub>2</sub>salophen. They chose titanium(III) and vanadium(III) bound to H<sub>2</sub>salophen as model compounds. In this particular chemical environment, it is difficult to reduce titanium and vanadium to lower oxidation states. As a result, reduction takes place only of the ligand.<sup>15</sup>

The best known biological role of cobalt is its participation in the coenzyme catalyzed reactions based on vitamin B<sub>12</sub>.<sup>15</sup> Consequently, cobalt complexes with tetradentate Schiff base ligands have been widely used to mimic cobalamin (B<sub>12</sub>) coenzymes, particularly as dioxygen carriers and oxygen activators.<sup>16</sup>

One of the primary applications of cobalt Schiff base complexes is to provide simple models of the vitamin B<sub>12</sub>.<sup>17,18</sup> These systems are 'electron rich' and have a greater resemblance to cobalamins than the 'electron-poor' cobalaximes.<sup>18</sup>

In the last decade, significant attention has been focused on these synthetic oxygen transport systems.<sup>19,20</sup> The aim is that these carriers mimic the biological systems in fixation, release, storage and activation of dioxygen. These complexes have been used as models to understand how the proteins behave.<sup>21</sup> The behaviour of these complexes depends on their

physical state. In the solid state, these complexes exhibit spontaneous uptake of dioxygen, but only after an initial activation phase. However, in solution several complexes demonstrate activity towards O<sub>2</sub> spontaneously.<sup>19</sup>

Many investigators have pointed out that in addition to cobalt porphyrins and cobalt phthalocyanines, these compounds would be promising electrocatalysts based on their oxygen-carrying ability.<sup>22</sup>

The first salen-metal complex was prepared by Combes<sup>23</sup> while he was studying the effect of diamines and diketones.<sup>24</sup> Since then, a range of salen derivatives together with their metal complexes have been synthesized and their role as catalysts has increased. It has been discovered by various researchers that cobalt(II) and cobalt(III) Schiff base complexes can be used as catalysts in a variety of reactions, viz., hydroxylation,<sup>25</sup> cyclopropanation,<sup>26</sup> epoxide ring opening<sup>27</sup> and hydrolytic kinetic resolution<sup>28</sup> to name a few.

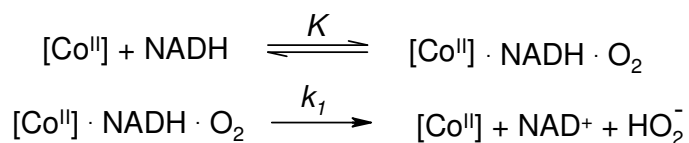
Another area in which cobalt Schiff base complexes find wide application is in the catalytic oxygenation reactions of organic substrates. They are also used in the catalytic oxidative coupling reactions of phenols and in the oxidation of olefins, as well as in epoxidation reactions.<sup>6</sup> Zhang *et al.*<sup>16</sup> have studied their chemical, thermal and electrochemical behaviour. This was stimulated by the stereo isomerism or optical isomerism in Schiff base cobalt complexes on the catalysis of the oxidation of some organic compounds, organic synthesis and the hetero-Diels-Alder reaction.<sup>16</sup>

In recent times, Co(salen) and Co(salophen) have attracted significant interest as catalysts for the electrochemical activation of carbon dioxide<sup>29,30</sup> and the free bases as chelating agents for the extraction of metal species in supercritical CO<sub>2</sub>.<sup>31</sup>

Ion selective electrodes (ISEs) have been the bases of potentiometric determination of small amounts of ionic species. However, the cationic selective electrodes are far more advanced than their anionic counterparts. This is due to the fact that it is difficult to control the selectivity among anions because of low charge to radii ratios, sensitivities to pH and high solvation energies. There have been several literature reports on metalloporphyrins, metallophthalocyanines and some lipophilic organometallic compounds which have been used as the basis for anion selective electrodes. However, with these complexes there has

been strong interaction between the anions and the ionophores used. The anion selectivity behaviour of membrane electrodes based on different transitional metal complexes was shown to be influenced by the properties of the central metal ion and the structure of the ligand. H<sub>2</sub>salophen as a ligand has been shown to form very stable complexes with transition metal ions. However, little is known about their complexes as carriers in ion-selective electrodes. This situation is changing as their use in ion-selective electrodes increases with continued research.<sup>32,33</sup>

Transition-metal complexes have been recognized as active catalysts in many chemical reactions. M. E. Vol'pin and G. N. Novodarova<sup>34</sup> proposed that synthetic metal-catalysts could display their activity in chemical as well as biochemical systems. Their main aim was to find catalysts that were capable of taking part in the main biological redox processes, respiration and photosynthesis. In their search for such catalysts, they turned to redox active transition metal complexes. These catalysts were investigated in terms of chemical, biochemical and biological activity. They found that cobalt chelates with Schiff bases were the most active and promising catalysts.<sup>34</sup> The kinetics of NADH oxidation in the presence of Co(salen) were studied and the catalytic reaction was described as follows:



M. E. Vol'pin and G. N. Novodarova<sup>34</sup> have concluded that Co(II) complexes are promising catalysts as they can be incorporated in the chemical and biochemical redox process. These complexes can stimulate direct electron transfer and bypass the enzymatic process.<sup>34</sup>

### **1.3 Co(II) Schiff Base Complexes**

These complexes have a well known ability to interact with the dioxygen molecule. This ability has resulted in the development of reversible O<sub>2</sub> binding agents (the O<sub>2</sub> molecule forms a co-ordinate bond to the metal centre) and the production of new oxygenation catalysts, particularly since the cobalt(II) complexes activate the O<sub>2</sub> molecule toward

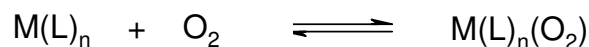
reaction with organic substrates.<sup>35</sup> As a result of this they are being used as models in the study of oxygen's reversible fixation by its natural carriers.<sup>36,37</sup>

In 1933 Pfeiffer was the first to describe a compound having the composition of cobaltous bis-salicylaldehydethylenediimine (salen), which he observed changed colour from a reddish colour to black upon exposure to the air for several days. It was then in 1938 that Tsumaki carried out and reported further studies on this compound.<sup>38</sup> He reported that the blackening was apparently due to the absorption of oxygen from the air. He also stated that this oxygen could be removed by heating the compound in a stream of carbon dioxide.<sup>38-41</sup> During 1944-1945, this compound and those closely related to it was extensively studied by Calvin and his colleagues.<sup>42,43</sup>

Ever since Tsumaki discovered that four-coordinate or five-coordinate cobalt(II) Schiff base complexes are oxygen carriers, there has been increasing interest in these complexes and their properties have been widely investigated.<sup>44-47</sup> These complexes have received wide interest for both heuristic reasons and as a practical means of isolating pure O<sub>2</sub> from the atmosphere.<sup>47</sup>

Naturally occurring dioxygen carriers and storage proteins contain a transitional metal ion to which the dioxygen can bind, e.g. iron (myoglobin, hemoglobin) or copper (hemocyanin).<sup>21</sup>

Some metal-ligand systems afford the delicate balance needed to form a 1:1 dioxygen complex without the metal (M) and/or the ligand (L) being irreversibly oxidized. These systems are called oxygen carriers:



and are used biologically in the transport and storage of molecular oxygen.<sup>45,46</sup>

In order for a complex to be classified as an oxygen carrier it is important that the reverse reaction, i.e., the dissociation of the dioxygen complex to give M(L) and O<sub>2</sub> be observed.<sup>45</sup> In the past, dioxygen carriers included metal complexes of Schiff bases, porphyrins and macrocyclic ligands. The ligands in these carriers are usually tetra- or pentadentate and in the case of Co(II), the resulting complex may have wide variations in structure, composition

and dioxygen affinity. Complexes based on Fe(II), Cu(I), Ni(II) and Mn(II) have been reported but chelates of Co(II) offer the greatest promise for oxygen production because of the wide range of stabilities of cobalt dioxygen complexes and the equally wide range of structures and properties available.<sup>48</sup>

Among these applications and various other applications of Co complexes, they are of fundamental importance for the design of materials in modern communication technology. This is owing to their nonlinear optical properties.<sup>49</sup> Investigations have been carried out by Bella *et al.*<sup>50</sup> to determine the nonlinear optical properties of these complexes. They found that metal complexes, and more specifically metal H<sub>2</sub>salophen complexes including those of cobalt(II), nickel(II) and copper(II), offer a larger variety of structures, better environmental stability and a much greater diversity for the design of materials in modern communication technology because of the coordinated metal centre.<sup>50</sup>

#### **1.4 Co(III) Schiff Base Complexes**

Low-spin d<sup>6</sup> cobalt (III) complexes are known to be hexacoordinate but pentacoordinate complexes are known to exist either as reactive intermediates in ligand-exchange reactions or as relatively stable species.<sup>51</sup> The occurrence of the latter is relatively rare but evidence for such species has been presented for a range of organocobalt(III) B<sub>12</sub> models as well as for cobalamins.<sup>52</sup> Five-coordinate species have been cited in models systems which range from the “electron-deficient” cobaloximes to the “electron-rich” Schiff base complexes, where the corrin ring in cobalamins is replaced by a tetradentate N<sub>2</sub>O<sub>2</sub> Schiff base ligand.

More specifically, the Co(salophen) system contains a Co centre which emulates the Co centre in cobalamins better than other models. Due to the electron-rich phenylene ring, H<sub>2</sub>salophen system reflects the properties of cobalamin more closely than other related systems, e.g. salen. These complexes strongly resemble vitamin B<sub>12</sub> compounds and due to the structural diversity of possible equatorial and axial ligands, these systems provide a powerful means for studying the coordination chemistry of the vitamin itself.<sup>53</sup>

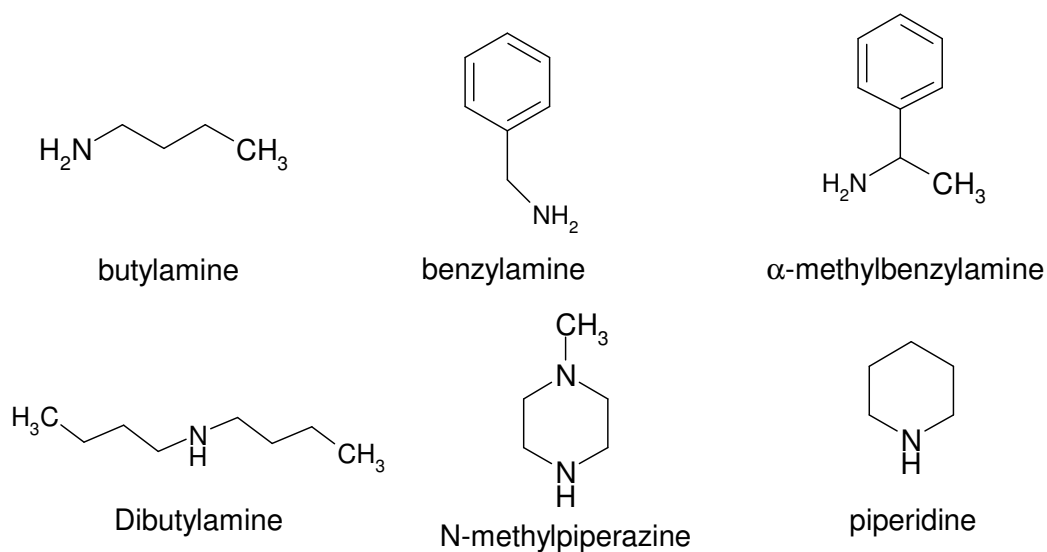
Asbell *et al.* have shown that cobalt(III) Schiff base complexes are potent antiviral drugs.<sup>54</sup> The exact mechanism of this antiviral activity is not yet known but studies have shown that

complexes like  $[\text{Co}(\text{acacen})(\text{NH}_3)_2]^+$  bind to histidine residues of proteins and model peptides.<sup>55,56</sup> The  $^1\text{H}$  NMR spectra of the product from the above reaction reveals that the Co(III) complexes are bound to the nitrogen atom of the imidazole ring of a histidine residue. Takeuchi and coworkers proposed that a possible mechanism for the observed antiviral activity is through inhibition of a histidine containing viral enzyme that is important for replication, since free histidines are essential for the catalytic activity of many enzymes.<sup>57</sup> A number of protein families have histidine residues at or near the active site. Enzymes within these families are of therapeutic significance as anticancer, antithrombolytic, antiparasitic and antiviral targets. As a result of this, the development of cobalt(III) Schiff base complexes as antienzymatic therapeutics is of great importance and interest because of the wide range of potential targets.<sup>57</sup>

The most important objective of cancer therapy is to achieve maximum therapeutic benefit. This means maximum damage to tumor cells with the least damage to the healthy or normal cells. In principle this can be obtained through selective antitumor preparations, by restricting the cytostatic effects within the tumor tissue. Ever since the discovery of the cytostatic effects of platinum complexes, Osinsky *et al.*<sup>58</sup> have been interested in transition metal complexes for their antitumor activities which have been of interest in tumor chemotherapy. In particular, cobalt (III) complexes offer promise because of a high electron affinity of the metal in the trivalent state, the ability to bind to DNA and the ready reducibility of the compounds. More specifically, Osinsky *et al.*<sup>58</sup> focused their studies on the redox-active cobalt complexes, viz., those containing the tetradentate aliphatic Schiff base ligands and nitrogenous axial ligands. Their studies have found that the chosen cobalt complexes affect the tumor tissue with a very high level of selectivity. This supports the feasibility of their role as anticancer agents.<sup>58</sup>

## 1.5 Objectives:

1. To synthesis a range of salen-type ligands.
2. To metallate these ligands with cobalt(II) followed by air-oxidation to afford  $[\text{Co}(\text{L})\text{X}]$ .
3. To fully characterize these complexes using UV-vis, IR,  $^1\text{H}$  NMR,  $^{13}\text{C}$  NMR and  $^{59}\text{Co}$  NMR.
4. To obtain crystal structures of the complexes.
5. To react the metallated complex with the following primary and secondary amines and characterize the new complexes fully.



**Scheme 1.5.1:** Primary and secondary amines used as axial ligands.

6. To obtain crystal structures of the amine complexes.
7. To obtain thermodynamic data by means of spectrophotometric titrations.

## Chapter Two: Experimental

### **2.1 General Procedure**

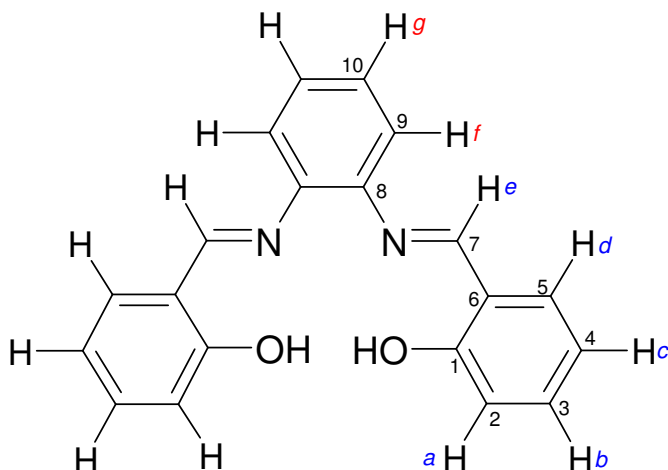
All solvents used were dried and distilled before used. THF was dried over Na/K alloy. Hexane was dried and distilled over sodium wire. Dichloromethane was distilled over CaH<sub>2</sub>. All amines used were dried over CaH<sub>2</sub> with an anhydrous CaCl<sub>2</sub> guard for 1 hour and then distilled. Salicylaldehyde, 1,2-phenylenediamine, 1,3-diamino-2-hydroxypropane, 1,2-diamino-ethane, N-(3-aminopropyl)-1,3-propanediamine, diethylenetriamine, diaminomaleonitrile, 2,2-dimethyl-1,3-propanediamine and 1,3-diaminopropane (Aldrich) were used as received.

### **2.2 Instrumentation**

Electronic spectra were recorded using a Perkin Elmer Lambda 45 double beam scanning spectrophotometer using CH<sub>2</sub>Cl<sub>2</sub> and DMSO solutions in 1.0 cm path length quartz cuvettes. Samples for Infrared spectroscopy were KBr mulls of polycrystalline material. FT-IR spectra were recorded using a Perkin-Elmer Spectrum One spectrometer (4 scans, spectral resolution = 1.0 cm<sup>-1</sup>). <sup>1</sup>H, <sup>13</sup>C and <sup>59</sup>Co NMR spectra of compounds were recorded using saturated solutions in DMSO-d<sub>6</sub> and CDCl<sub>3</sub> with a 500 MHz Varian Unity Inova spectrometer equipped with an Oxford magnet (11.744 T).

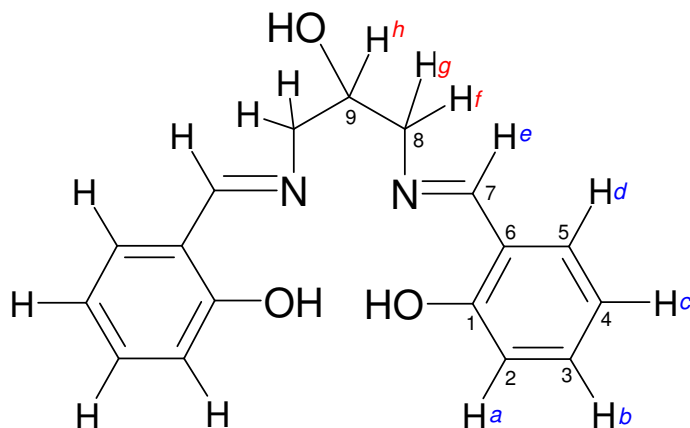
## 2.3 Synthesis of Schiff Base Ligands

### 2.3.1 Synthesis of *N,N*-disalicylidene-1,2-phenylenediamine, (H<sub>2</sub>salophen)



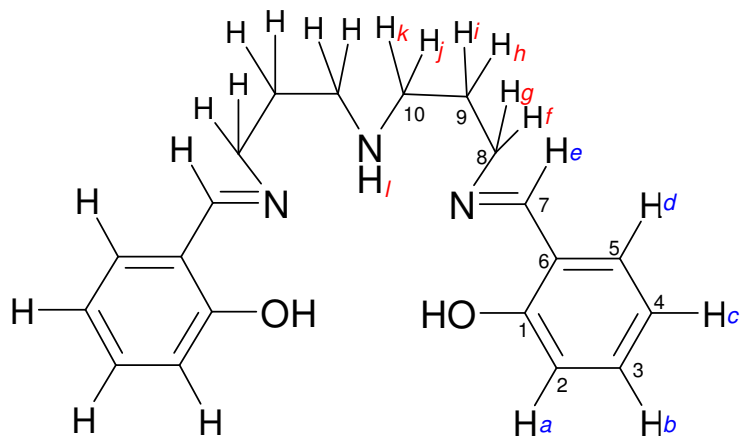
1,2-phenylenediamine (4.0035 g, 37.04 mmol) was dissolved in dry ethanol (35mL) and heated with magnetic stirring. To this solution, salicylaldehyde (8mL, 739.8 mmol) was added slowly. The solution immediately turned from brown to orange. Upon further stirring, a bright orange precipitate was formed. The mixture was stirred for about 30 minutes and then allowed to cool. The solution was filtered by suction. A bright orange powder of the Schiff base was collected (11.1127 g, 94.89 % yield). Anal. Calcd for C<sub>20</sub>H<sub>16</sub>N<sub>2</sub>O<sub>2</sub> : C, 75.93; H, 5.10; N, 8.86; found : C, 76.9; H, 5.08; N, 8.73. UV-vis (CH<sub>2</sub>Cl<sub>2</sub>) [ $\lambda_{\text{max}}$ , nm ( $\epsilon$ , M<sup>-1</sup>cm<sup>-1</sup>): 269.91, 334.03. IR (KBr pellet, cm<sup>-1</sup>): 3423m br  $\nu$ (O-H), 2970m  $\nu$ (C-H), 1611s  $\nu$ (C=N), 1276s  $\nu$ (C-O). <sup>1</sup>H NMR (500MHz, CDCl<sub>3</sub>) [ $\delta$ , ppm]: 13.04 (br s, 2H, OH); 8.64 (s, 2H, CH=N, *e*); 7.38 (m, 2H, Ph H, *b*); 7.35 (m, 2H, Ph H, *d*); 7.27-7.22 (m, 4H, Ph H, *f*, *g*); 7.05 (d, *J* = 8.37 Hz, 2H, Ph H, *a*); 6.93 (m, 2H, Ph H, *c*). <sup>13</sup>C NMR (125 MHz, CDCl<sub>3</sub>) [ $\delta$ , ppm]: 163.72 (C-7); 161.46 (C-1); 142.66 (C-8); 133.47 (C-3); 132.41 (C-5); 127.71 (C-9); 119.80 (C-10); 119.24 (C-6); 119.00 (C-4); 117.57 (C-2). These data are consistent with those reported by Amirnasr *et al.*<sup>59</sup>

### 2.3.2 Synthesis of 2-*{(E)-[(2-hydroxy-3-*{(1E)-(2-hydroxyphenyl)methylene}amino}propyl)imino]methyl}phenol**



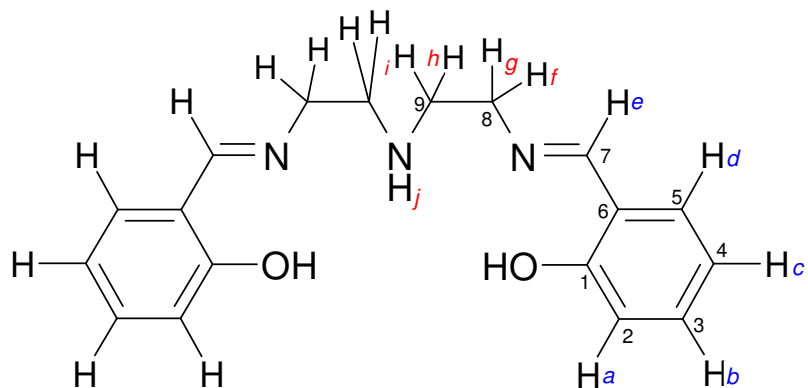
1,3-diamino-2-hydroxypropane (3.9410 g, 43.73 mmol) was dissolved completely in dry ethanol (30 mL) and salicylaldehyde (9.5 mL, 88.77 mmol) was added to the solution. Upon the addition of salicylaldehyde, the solution immediately turned bright yellow. The solution was stirred for 45 minutes. After 45 minutes of stirring, no precipitate was present. The reaction flask was then set aside overnight to allow the precipitation of the Schiff base. The solution was then filtered. Canary yellow crystals were collected (9.8128 g, 13.05 %). Anal. calcd for  $C_{17}H_{18}N_2O_3$ : C, 68.44; H, 6.08; N, 9.39; found : C, 69.04; H, 6.16; N, 9.86. UV-vis ( $CH_2Cl_2$ ) [ $\lambda_{max}$ , nm]: 257.72, 317.73. IR (KBr pellet,  $cm^{-1}$ ): 3418m br  $\nu(O-H)$ , 2897m  $\nu(C-H)$ , 1633s  $\nu(C=N)$ , 1459s  $\nu(CH_2)$ , 1276s  $\nu(C-O)$ .  $^1H$  NMR (500MHz,  $CDCl_3$ ) [ $\delta$ , ppm]: 13.07 (br s, 2H, OH); 8.41 (s, 2H, CH=N, *e*); 7.32 (m, 2H, Ph H, *b*); 7.27 (dd,  $J_1 = 9.51$  Hz,  $J_2 = 6.03$  Hz, 2H, Ph H, *d*); 6.97 (d,  $J = 8.29$  Hz, 2H, Ph H, *a*); 6.89 (m, 2H, Ph H, *c*); 4.27 (t, 1H, CH, *h*); 3.89-3.71 (m, 4H,  $CH_2$ , *f, g*).  $^{13}C$  NMR (125 MHz,  $CDCl_3$ ) [ $\delta$ , ppm]: 167.43 (C-7); 160.98 (C-1); 132.60 (C-3); 131.57 (C-5); 118.78 (C-4); 117.00 (C-2); 76.99 (C-6); 70.48 (C-9); 63.22 (C-8).

**2.3.3 Synthesis of 2-([3-([3-[(2-hydroxybenzylidene)amino]propyl]amino)propyl]imino)methyl)phenol, (H<sub>2</sub>saldiprop)**



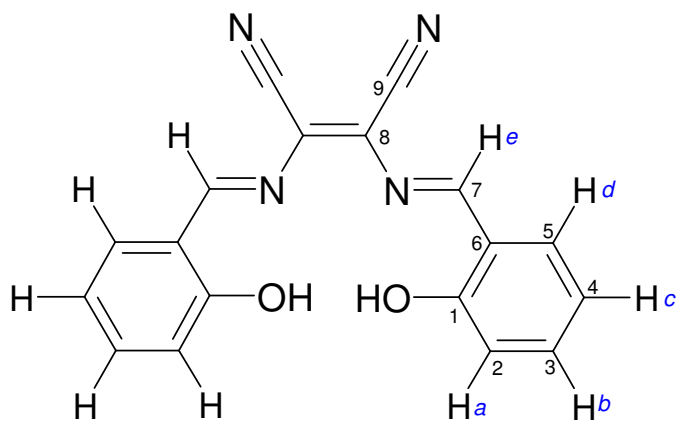
*N*-(3-aminopropyl)-1,3-propanediamine (4 mL, 30.48 mmol) was a colourless liquid which was completely dissolved in dry ethanol (25 mL). Salicylaldehyde (6.5 mL, 60.97 mmol) was slowly added to the solution. Upon this addition, the solution turned yellow. This solution was stirred for 30 minutes. The colour of the solution changed from yellow to a bright orange. The flask was then placed on the rotor evaporator to remove most if not all of the solvent. However, there was no change in the amount of liquid present. It was deduced that this ligand is an oil. UV-vis (CH<sub>2</sub>Cl<sub>2</sub>) [ $\lambda_{\text{max}}$ , nm]: 255.26, 316.00. IR (KBr pellet, cm<sup>-1</sup>): 2933m br  $\nu$ (C-H), 1631s  $\nu$ (C=N), 1460m  $\nu$ (CH<sub>2</sub>), 1278s  $\nu$ (C-O). <sup>1</sup>H and (500MHz, CDCl<sub>3</sub>) [ $\delta$ , ppm] 8.28 (br s, 2H, OH); 7.98 (s, 2H, CH=N, *e*); 7.22 (m, 2H, Ph H, *b*); 7.15 (dd,  $J_1 = 7.63$  Hz,  $J_2 = 7.60$  Hz, 2H, Ph H, *d*); 6.88 (d,  $J = 8.26$  Hz, 2H, Ph H, *a*); 6.79 (m, 2H, Ph H, *c*); 3.62 (m, 4H, CH<sub>2</sub>, *j, k*); 3.50 (s, 1H, NH, *l*); 1.79 (t, 4H, CH<sub>2</sub>, *f, g*); 1.15 (t, 4H, CH<sub>2</sub>, *h, i*). <sup>13</sup>C NMR (125 MHz, CDCl<sub>3</sub>) [ $\delta$ , ppm]: 165.68 (C-7), 160.91 (C-1), 132.03 (C-3), 131.13 (C-5), 118.33 (C-4), 116.69 (C-2), 77.25 (C-6), 61.77 (C-9), 57.32 (C-10), 17.87.

2.3.4                      Synthesis                      of                      2-[(*E*)-{(2-[(2-[(1*E*)-(2-hydroxyphenyl)methylene]amino}ethyl)amino]ethyl)imino)methyl]phenol



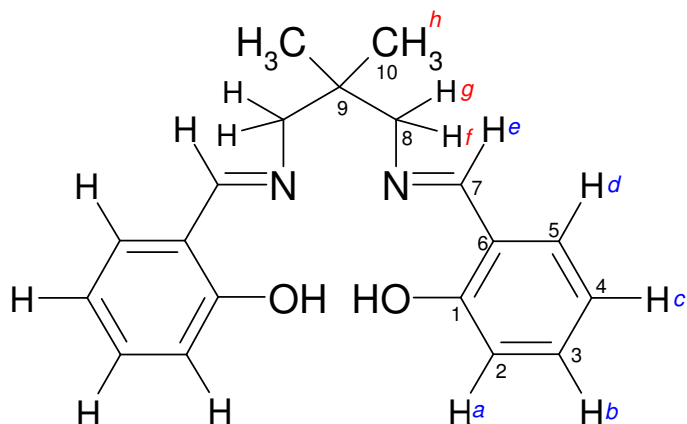
Diethylenetriamine (4 mL, 38.77 mmol) was a colourless liquid, which was completely dissolved, in dry ethanol (30 mL). To this, salicylaldehyde (8 mL, 77.54 mmol) was added slowly. The solution immediately turned colour from colourless to bright yellow. The solution was stirred for 30 minutes. After stirring the colour remained bright yellow. This ligand is also present as an oil. UV-vis (CH<sub>2</sub>Cl<sub>2</sub>) [ $\lambda_{\text{max}}$ , nm]: 255.77, 316.22. IR (KBr pellet, cm<sup>-1</sup>): 3424br  $\nu$ (O-H), 2845m br  $\nu$ (C-H), 1631s  $\nu$ (C=N), 1461m  $\nu$ (CH<sub>2</sub>), 1279s  $\nu$ (C-O). <sup>1</sup>H and (500MHz, CDCl<sub>3</sub>) [ $\delta$ , ppm]: 13.31 (br s, 2H, OH), 8.28 (s, 2H, CH=N, *e*), 7.25 (m, 2H, Ph H, *b*), 7.16 (dd,  $J_1 = 7.63$  Hz,  $J_2 = 7.61$  Hz, 2H, Ph H, *d*), 6.90 (d,  $J = 8.26$  Hz, 2H, Ph H, *a*), 6.81 (m, 2H, Ph H, *c*), 3.64 (s, 4H, CH<sub>2</sub>, *f, g*), 2.93 (s, 1H, NH, *j*), 1.18 (t, 4H, CH<sub>2</sub>, *h, i*). <sup>13</sup>C NMR (125 MHz, CDCl<sub>3</sub>) [ $\delta$ , ppm]: 165.85 (C-7), 160.85 (C-1), 132.00 (C-3), 131.12 (C-5), 118.30 (C-4), 116.68 (C-2), 77.24 (C-6), 59.08 (C-8), 49.35 (C-9).

**2.3.5 Synthesis of (2Z)-2,3-bis{[(1E)-1-(2-hydroxyphenyl)ethylidene]amino}but-2-enitrile, (H<sub>2</sub>salmal)**



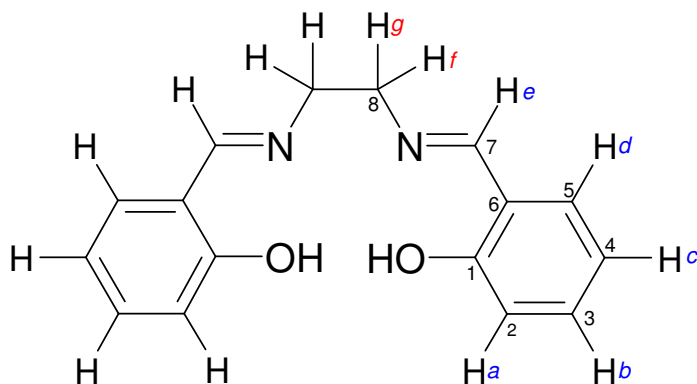
Diaminomaleonitrile (4.0011 g, 37.02 mmol), in the presence of molecular sieves, was completely dissolved in dry ethanol (30 mL) with stirring. Salicylaldehyde (8 mL, 74.00 mmol) a few drops of trifluoroacetic acid was added to the solution. Upon the addition of the acid, a solid began to precipitate out immediately. The solution was filtered by suction. A mustard coloured powder was collected (6.7524 g, 57.33 %). Anal. calcd for C<sub>18</sub>H<sub>12</sub>N<sub>4</sub>O<sub>2</sub> : C, 68.35; H, 3.82; N, 17.71; found : C, 62.72; H, 3.86; N, 26.03. UV-vis (CH<sub>2</sub>Cl<sub>2</sub>) [ $\lambda_{\max}$ , nm]: 255.67, 325.90. IR (KBr pellet, cm<sup>-1</sup>): 3419br  $\nu$ (O-H), 2850m br  $\nu$ (C-H), 2243s  $\nu$ (C≡N), 1625s  $\nu$ (C=N), 1279s  $\nu$ (C-O). <sup>1</sup>H and (500MHz, CD<sub>3</sub>COCD<sub>3</sub>) [ $\delta$ , ppm]: 10.72 (br s, 2H, OH); 8.64 (s, 2H, CH=N, *e*); 7.74 (dd,  $J_1 = 7.80$  Hz,  $J_2 = 7.74$  Hz, 2H, Ph H, *d*); 7.42 (m, 2H, Ph H, *b*); 6.99 (m, 2H, Ph H, *c*); 6.96 (d,  $J = 8.32$  Hz, Ph H, *a*). <sup>13</sup>C NMR (125 MHz, CD<sub>3</sub>COCD<sub>3</sub>) [ $\delta$ , ppm]: 159.61 (C-7); 159.39 (C-1); 133.96 (C-3); 132.57 (C-5); 125.76 (C-8); 120.03 (C-4); 116.85 (C-2); 113.06 (C-9); 104.97 (C-6).

### 2.3.6 Synthesis of 2-[(*E*)-[(3-[(1*E*)-(2-hydroxyphenyl)methylene]amino)-2,2-dimethylpropyl]imino]methyl]phenol, (H<sub>2</sub>saldmprop)



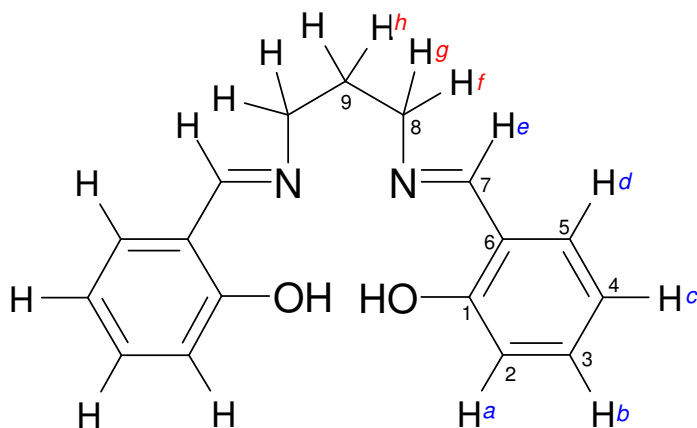
2,2-dimethyl-1,3-propanediamine (4.0 mL, 39.15 mmol) was completely dissolved in dry ethanol (25 mL) with stirring. Upon the addition of salicylaldehyde (8 mL, 78.29 mmol), the solution turned bright yellow in colour. It was left to stir for 30 minutes. At the end of the 30 minutes a bright yellow precipitate was present. This was filtered by suction. A bright yellow microcrystalline product was collected (10.5747 g, 87.02 %). Anal. calcd for C<sub>19</sub>H<sub>22</sub>N<sub>2</sub>O<sub>2</sub> : C, 73.52; H, 7.14; N, 9.02; found : C, 73.85; H, 7.24; N, 9.01. UV-vis (CH<sub>2</sub>Cl<sub>2</sub>) [ $\lambda_{\max}$ , nm]: 256.95, 317.14. IR (KBr pellet, cm<sup>-1</sup>): 2833m br v(C-H), 1635s v(C=N), 1461m v(CH<sub>2</sub>), 1390m br v(CH<sub>3</sub>), 1278s v(C-O). <sup>1</sup>H NMR (500MHz, CDCl<sub>3</sub>) [ $\delta$ , ppm]: 13.55 (br s, 2H, OH); 8.34 (s, 2H, CH=N, *e*); 7.32 (m, 2H, Ph H, *b*) 7.26 (dd, *J*<sub>1</sub> = 9.25 Hz, *J*<sub>2</sub> = 6.01 Hz, 2H, Ph H, *d*); 6.98 (d, *J* = 8.28 Hz, 2H, Ph H, *a*); 6.89 (m, 2H, Ph H, *c*); 3.49 (s, 4H, CH<sub>2</sub>, *f*, *g*); 1.09 (s, 6H, CH<sub>3</sub>, *h*). <sup>13</sup>C NMR (125 MHz, CDCl<sub>3</sub>) [ $\delta$ , ppm]: 165.72 (C-7); 161.19 (C-1); 132.30 (C-3); 131.34 (C-5); 118.62 (C-4); 116.95 (C-2); 76.74 (C-6); 68.15 (C-8); 36.25 (C-9); 24.38 (C-10).

**2.3.7 Synthesis of 2-[(E)-[(2-[(1E)-(2-hydroxyphenyl)methylene]amino)ethyl]imino]methyl]phenol (H<sub>2</sub>salen)**



Ethylenediamine (4.0 mL, 66.56 mmol) was completely dissolved in dry ethanol (30 mL) with stirring. Salicylaldehyde (14.0 mL, 133.1 mmol) was added slowly to the yellow solution. Upon this addition, a bright yellow precipitate began to form immediately. This precipitate was collected by filtration. A bright yellow crystalline powder was collected (17.2448 g, 96.56 %). Anal. calcd for C<sub>16</sub>H<sub>16</sub>N<sub>2</sub>O<sub>2</sub>: C, 71.62; H, 6.01; N, 10.44; found : C, 72.48; H, 6.16; N, 10.44. UV-vis (CH<sub>2</sub>Cl<sub>2</sub>) [ $\lambda_{\max}$ , nm]: 257.13, 318.02. IR (KBr pellet, cm<sup>-1</sup>): 3451br  $\nu$ (O-H), 2869m  $\nu$ (C-H), 1635s  $\nu$ (C=N), 1461m  $\nu$ (CH<sub>2</sub>), 1283s  $\nu$ (C-O). <sup>1</sup>H NMR (500MHz, CDCl<sub>3</sub>) [ $\delta$ , ppm]:13.19 (br s, 2H, OH); 8.36 (s, 2H, CH=N, *e*); 7.29 (m, 2H, Ph H, *b*); 7.22 (d, *J* = 7.62 Hz, 2H, Ph H, *d*); 6.95 (d, *J* = 8.27 Hz, 2H, Ph H, *a*); 6.85 (t, 2H, Ph H, *c*); 3.94 (s, 4H, CH<sub>2</sub>, *f*, *g*). <sup>13</sup>C NMR (125 MHz, CDCl<sub>3</sub>) [ $\delta$ , ppm]: 166.64 (C-7); 160.96 (C-1); 132.36 (C-3); 131.45 (C-5); 118.65 (C-4); 116.92 (C-2); 76.65 (C-6); 59.69 (C-8).

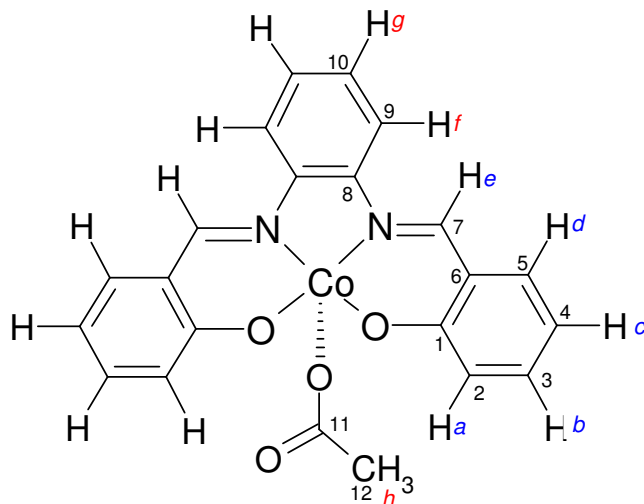
**2.3.8                      Synthesis                      of                      2-*{(E)-[(3-*{[(1E)-(2-hydroxyphenyl)methylene]amino}propyl)imino]methyl}phenol****



1,3-diaminopropane (4.5 mL, 54.00 mmol) was completely dissolved in dry ethanol (25 mL). Upon the addition of salicylaldehyde (11.5 mL, 107.90 mmol), the solution immediately turned bright yellow in colour. This solution was stirred for 15 minutes. Upon stirring a bright yellow precipitate began to form. This precipitate was filtered by suction. A bright yellow powder, which was very crystalline, was collected (15.0089 g, 98.44 %). Anal. calcd for  $C_{17}H_{18}N_2O_2$  : C, 72.32; H, 6.43; N, 9.92; found : C, 71.01; H, 6.43; N, 9.72. UV-vis ( $CH_2Cl_2$ ) [ $\lambda_{max}$ , nm]: 256.40, 316.08. IR (KBr pellet,  $cm^{-1}$ ): 3423br  $\nu(O-H)$ , 2850m  $\nu(C-H)$ , 1630s  $\nu(C=N)$ , 1456m  $\nu(CH_2)$ , 1278s  $\nu(C-O)$ .  $^1H$  and (500MHz,  $CDCl_3$ ) [ $\delta$ , ppm]: 13.43 (br s, 2H, OH); 8.38 (s, 2H, CH=N, *e*); 7.32 (m, 2H, Ph H, *b*); 7.25 (dd,  $J_1 = 7.66$  Hz,  $J_2 = 7.64$  Hz, 2H, Ph H, *d*); 6.97 (d,  $J = 8.23$  Hz, 2H, Ph H, *a*); 6.89 (t, 2H, Ph H, *c*); 3.72 (t, 4H,  $CH_2$ , *f, g*); 2.12 (m, 2H,  $CH_2$ , *h*).  $^{13}C$  NMR (125 MHz,  $CDCl_3$ ) [ $\delta$ , ppm]: 165.41 (C-7); 161.07 (C-1); 132.24 (C-3); 131.23 (C-5); 118.60 (C-4); 116.94 (C-2); 76.99 (C-6) 56.79 (C-8); 31.67 (C-9).

## 2.4 Synthesis of Cobalt Complexes:

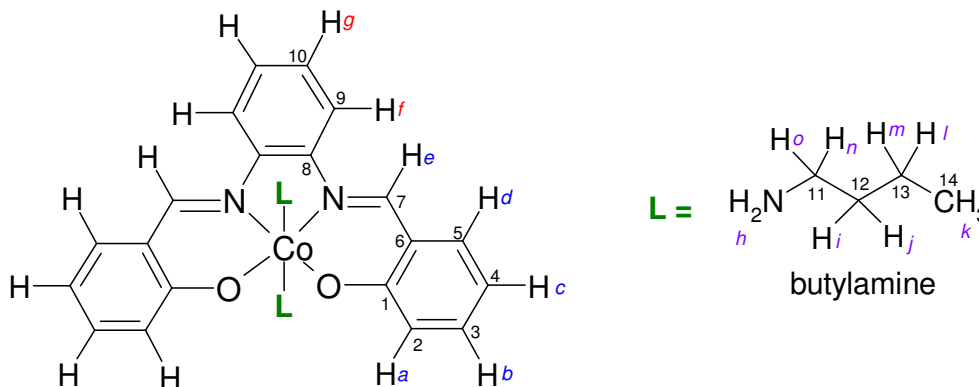
### 2.4.1 Synthesis of [Co(salophen)(OAc)]



*H<sub>2</sub>salophen* (1.0046 g, 3.175 mmol) was completely dissolved in dry THF (14 mL). Cobalt acetate (0.7822 g, 3.140 mmol) was completely dissolved in dry methanol (22 mL) and added slowly to the THF mixture. There was an immediate colour change from yellow to brown. The solution was stirred for approximately 2 hours and then left to stand for one hour. The progress of the reaction was monitored by TLC. The brown solution was then filtered. A reddish brown powder was collected (0.9641 g, 58 %). UV-vis (MeOH) [ $\lambda_{\text{max}}$ , nm ( $\epsilon$ ,  $\text{M}^{-1}\text{cm}^{-1}$ ): 471 ( $1.18 \times 10^4$ ). IR (KBr pellet,  $\text{cm}^{-1}$ ): 1700s  $\nu(\text{C}=\text{O})$ , 1616s  $\nu(\text{C}=\text{N})$ .  $^1\text{H}$  NMR (500MHz,  $\text{CDCl}_3$ ) [ $\delta$ , ppm]: 8.25 (br s, 2H,  $\text{CH}=\text{N}$ , *e*); 7.93 (m, 2H, Ph H, *f*), 7.49 (d,  $J = 8.66$  Hz, 2H, Ph H, *d*); 7.42 (m, 2H, Ph H, *g*); 7.34 (m, 2H, Ph H, *b*) 6.79 (d,  $J = 7.44$  Hz, 2H, Ph H, *a*); 6.61 (t, 2H, Ph H, *c*); 1.50 (s, 3H,  $\text{CH}_3$ , *h*).  $^{13}\text{C}$  NMR (125 MHz,  $\text{CDCl}_3$ ) [ $\delta$ , ppm]: 207.87 (C-11); 168.70 (C-1); 158.88 (C-7); 146.04 (C-8); 135.86 (C-3); 129.08 (C-2); 127.59 (C-10); 124.57 (C-5); 118.65 (C-6); 115.60 (C-4); 115.26 (C-9); 24.16 (C-12).

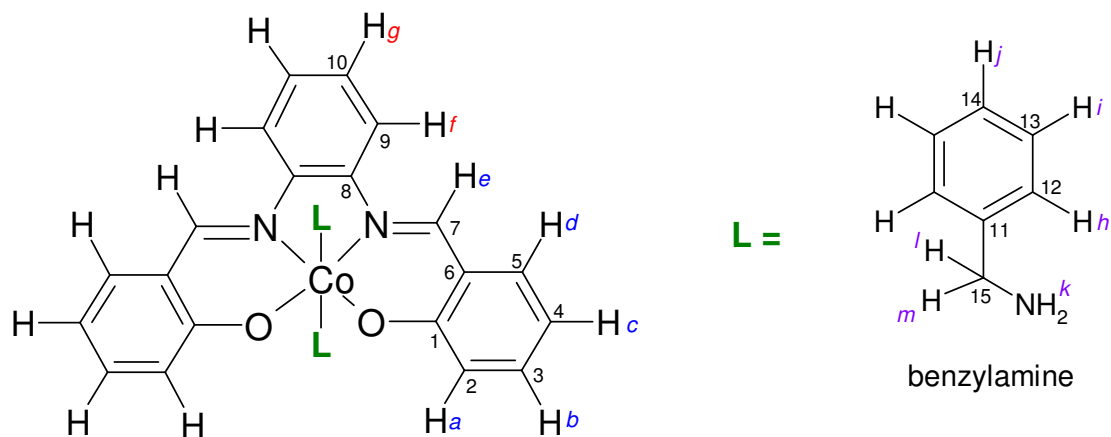
## 2.4.2 Synthesis of [Co(salophen)(L)<sub>2</sub>] Complexes

### 2.4.2.1 Synthesis of [Co(salophen)(BuNH<sub>2</sub>)<sub>2</sub>]<sup>+</sup>Cl<sup>-</sup>



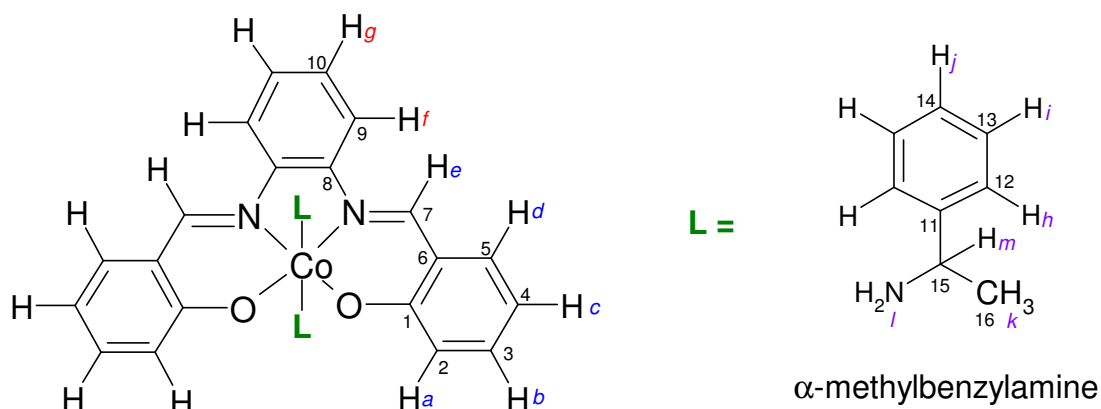
[Co(salophen)(OAc)] (0.1018 g, 0.2727 mmol) was dissolved in dry dichloromethane (20 mL). To this stirring solution, butylamine (79.4  $\mu$ L) was added. The solution immediately changed to a dark red colour. This solution was stirred for a further 30 minutes. On completion of stirring, the flask was set aside to allow for complete precipitation of the solid. However, only a fine powder was obtained the remaining solution was placed on the rotary evaporator to remove all the solvent. A fine textured red-orange powder identified as the Cl<sup>-</sup> salt where Cl<sup>-</sup> is derived from CH<sub>2</sub>Cl<sub>2</sub>, was obtained (0.0491 g, 43 %). UV-vis (DMSO) [ $\lambda_{\text{max}}$ , nm ( $\epsilon$ , M<sup>-1</sup>cm<sup>-1</sup>): 364 (1.37  $\times 10^4$ ), 394 (8.37  $\times 10^3$ ), 470 (9.55  $\times 10^3$ ). IR (KBr pellet, cm<sup>-1</sup>): 3299m  $\nu$ (N-H), 2873m  $\nu$ (C-H), 1609s  $\nu$ (C=N), 1456m  $\nu$ (CH<sub>2</sub>) 1387m br  $\nu$ (CH<sub>3</sub>). <sup>1</sup>H NMR (500MHz, DMSO-d<sub>6</sub>) [ $\delta$ , ppm]: 8.89 (br s, 2H, CH=N, *e*); 8.41 (m, 2H, Ph H, *f*); 7.63 (d, *J* = 7.65 Hz, 2H, Ph H, *d*); 7.50 (m, 2H, Ph H, *g*); 7.34 (t, 2H, Ph H, *b*); 7.19 (d, *J* = 8.44 Hz, 2H, Ph H, *a*); 6.65 (t, 2H, Ph H, *c*); 2.50 (s, 4H, NH<sub>2</sub>, *h*); 1.76 (t, 4H, CH<sub>2</sub>, *o, n*); 1.14 (m, 4H, CH<sub>2</sub>, *i, j*); 0.89 (m, 4H, CH<sub>2</sub>, *m, l*); 0.57 (t, 6H, CH<sub>3</sub>, *k*). <sup>13</sup>C NMR (125 MHz, DMSO-d<sub>6</sub>) [ $\delta$ , ppm]: 167.23 (C-1); 160.97 (C-7); 143.68 (C-8); 135.92 (C-5); 135.60 (C-3); 127.82 (C-10); 122.22 (C-2); 118.31 (C-6); 117.11 (C-9); 114.77 (C-4); 40.97 (C-11); 31.22 (C-12); 19.52 (C-13); 13.31 (C-14).

### 2.4.2.2 Synthesis of [Co(salophen)(BzNH<sub>2</sub>)<sub>2</sub>]<sup>+</sup>Cl<sup>-</sup>



[Co(salophen)(OAc)] (1.0063 g, 2.33 mmols) was dissolved in dry dichloromethane (20 mL) and stirred. Upon the addition of benzylamine (900  $\mu$ L), the solution immediately darkened in colour. This solution was stirred for a further hour and then left to stand overnight. The progress of the reaction was monitored by TLC. All of the solvent had evaporated and a black sticky residue was left behind. This residue was redissolved in dichloromethane and placed on the rotary evaporator, where all of the solvent was removed. The remaining solid which was reddish in colour and was identified as the Cl<sup>-</sup> salt where Cl<sup>-</sup> is derived from CH<sub>2</sub>Cl<sub>2</sub>, was collected (1.0653 g, 78 %). UV-vis (DMSO) [ $\lambda_{\text{max}}$ , nm ( $\epsilon$ , M<sup>-1</sup>cm<sup>-1</sup>): 343 (1.12  $\times 10^4$ ), 362 (1.19  $\times 10^4$ ), 393 (7.86  $\times 10^3$ ), 467 (8.10  $\times 10^3$ ). IR (KBr pellet, cm<sup>-1</sup>): 3280m  $\nu$ (N-H), 2890m  $\nu$ (C-H), 1609s  $\nu$ (C=N), 1456m  $\nu$ (CH<sub>2</sub>). <sup>1</sup>H NMR (500MHz, CDCl<sub>3</sub>) [ $\delta$ , ppm]: 8.40 (br s, 2H, CH=N, *e*); 7.79 (m, 2H, Ph H, *f*); 7.48 (d, 2H, Ph H, *d*); 7.43 (m, 2H, Ph H, *g*); 7.34 (m, 2H, Ph H, *b*); 6.97-7.14 (m, 6H, Ph H, *h, i, j*); 6.79 (d, 2H, Ph H, *a*); 6.61 (t, 2H, Ph H, *c*); 4.83 (s, 4H, CH<sub>2</sub>, *l, m*); 2.02 (s, 4H, NH<sub>2</sub>, *k*). <sup>13</sup>C NMR (125 MHz, CDCl<sub>3</sub>) [ $\delta$ , ppm]: 166.86 (C-1); 161.99 (C-7); 145.91 (C-11); 143.88 (C-8); 136.99 (C-5); 135.87 (C-3); 128.83 (C-9); 128.58 (C-12); 128.26 (C-13); 127.96 (C-14); 126.99 (C-10); 118.64 (C-6); 116.94 (C-2); 115.57 (C-4); 64.88 (C-15).

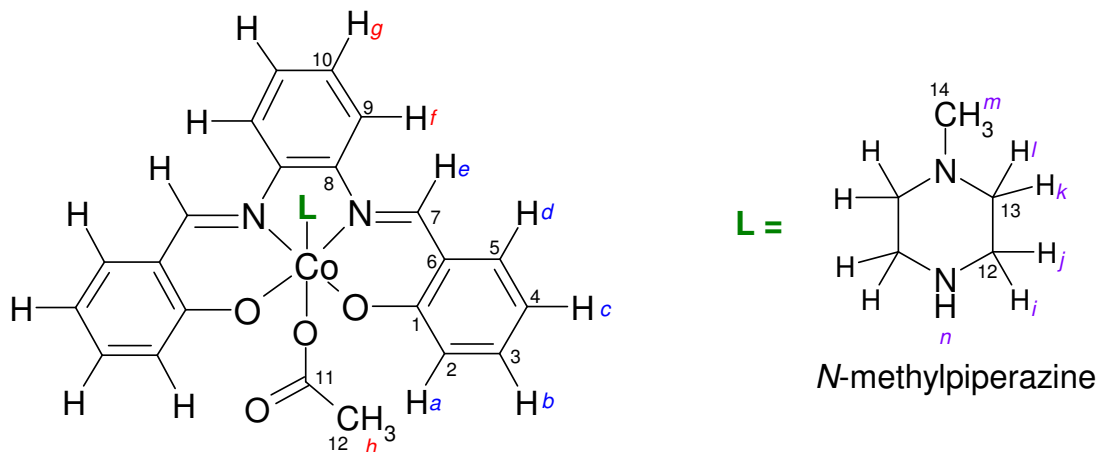
### 2.4.2.3 Synthesis of [Co(salophen)( $\alpha$ -MeBzNH<sub>2</sub>)<sub>2</sub>]Cl



[Co(salophen)(OAc)] (0.1009 g, 0.2334 mmol) was dissolved in dry dichloromethane (25 mL) and the solution was stirred. Upon the addition of  $\alpha$ -methylbenzylamine (104  $\mu$ L), the solution changed colour from brown to a more orange-red colour. The resulting solution was stirred for approximately one hour and then left aside. During this time the formation of a precipitate was evident. A reddish-brown powder which was identified as the Cl<sup>-</sup> salt where Cl<sup>-</sup> is derived from CH<sub>2</sub>Cl<sub>2</sub>, was collected by suction filtration (0.0371 g, 26 %). UV-vis (DMSO) [ $\lambda_{\text{max}}$ , nm ( $\epsilon$ , M<sup>-1</sup>cm<sup>-1</sup>): 392 (1.51  $\times$  10<sup>4</sup>), 476 (1.18  $\times$  10<sup>4</sup>). IR (KBr pellet, cm<sup>-1</sup>): 3445m  $\nu$ (N-H), 2854s  $\nu$ (C-H), 1621s  $\nu$ (C=N), 1464m  $\nu$ (CH<sub>2</sub>), 1382m br  $\nu$ (CH<sub>3</sub>). <sup>1</sup>H NMR (500MHz, DMSO-d<sub>6</sub>) [ $\delta$ , ppm]: 8.69 (br s, 2H, CH=N, *e*); 8.36 (m, 2H, Ph H, *f*); 7.59 (d, *J* = 7.38 Hz, 2H, Ph H, *d*); 7.38 (m, 8H, Ph H, *a, b, c, g*); 6.76 (m, 8H, Ph H, *h, i*); 6.60 (t, 2H, Ph H, *j*); 5.51 (s, 4H, NH<sub>2</sub>, *l*); 1.18 (s, 6H, CH<sub>3</sub>, *k*); -0.16 (m, 2H, CH, *m*). <sup>13</sup>C NMR (125 MHz, DMSO-d<sub>6</sub>) [ $\delta$ , ppm]: 166.34 (C-1); 161.54 (C-7); 146.67 (C-11); 143.28 (C-8); 137.52 (C-5); 135.71 (C-3); 129.26 (C-13); 128.23 (C-14); 126.76 (C-10); 125.91 (C-12); 118.89 (C-6); 117.33 (C-9); 116.92 (C-2); 115.77 (C-4); 50.64 (C-15); 25.04 (C-16).

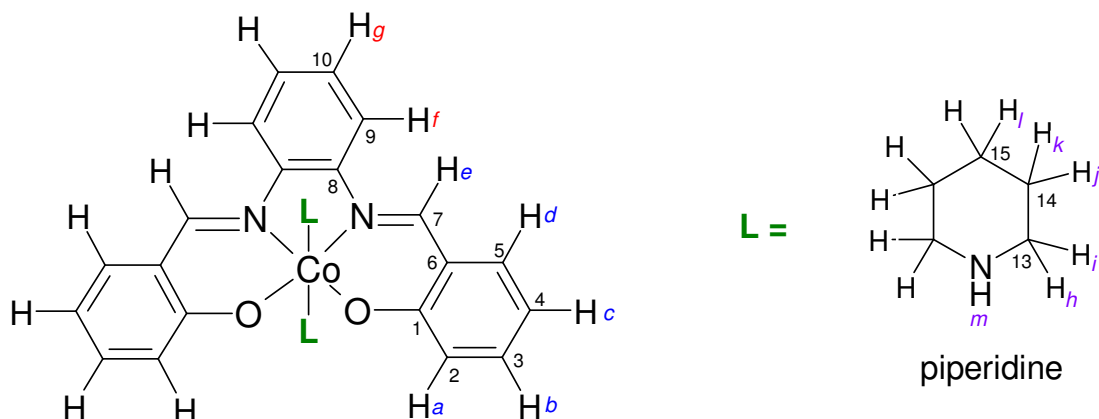


### 2.4.2.5 Synthesis of [Co(salophen)(*N*-MePipz)<sub>2</sub>]Cl



[Co(salophen)(OAc)] (0.1017 g, 0.2352 mmol) was dissolved in dry dichloromethane (20 mL) with stirring. To this solution, *N*-methylpiperazine (89  $\mu$ L) was added. Upon this addition, there was a colour change from brown to red-orange. This solution was stirred for 30 minutes and left aside. Initially there was no sign of a precipitate. A fine reddish-orange powder identified as the Cl<sup>-</sup> salt where Cl<sup>-</sup> is derived from CH<sub>2</sub>Cl<sub>2</sub>, was collected by suction filtration after prolonged standing (0.0231 g, 18 %). UV-vis (DMSO) [ $\lambda_{\text{max}}$ , nm ( $\epsilon$ , M<sup>-1</sup>cm<sup>-1</sup>): 372 (1.51  $\times 10^4$ ), 390 (1.45  $\times 10^4$ ), 477 (1.13  $\times 10^3$ ). IR (KBr pellet, cm<sup>-1</sup>): 3022br  $\nu$ (N-H), 1622s  $\nu$ (C=N), 1465m  $\nu$ (CH<sub>2</sub>), 1383m br  $\nu$ (CH<sub>3</sub>). Due to poor solubility, we were not able to obtain NMR data for this complex.

### 2.4.2.6 Synthesis of [Co(salophen)(Pip)<sub>2</sub>]<sup>+</sup>Cl<sup>-</sup>



[Co(salophen)(OAc)] (0.1005 g, 0.2325 mmol) was dissolved in dry dichloromethane (30 mL) and stirred. To the stirring solution, piperidine (80  $\mu$ L) was added. A colour change from brown to reddish-orange was observed. This solution was stirred for an hour and then left aside. A fine reddish-orange powder identified as the Cl<sup>-</sup> salt where Cl<sup>-</sup> is derived from CH<sub>2</sub>Cl<sub>2</sub>, was collected by suction filtration (0.0038 g, 3.02 %). UV-vis (CH<sub>2</sub>Cl<sub>2</sub>) [ $\lambda_{\text{max}}$ , nm ( $\epsilon$ , M<sup>-1</sup>cm<sup>-1</sup>): 378 (5.54  $\times$  10<sup>3</sup>), 405 (4.83  $\times$  10<sup>3</sup>), 494 (4.83  $\times$  10<sup>3</sup>). IR (KBr pellet, cm<sup>-1</sup>): 3023br  $\nu$ (N-H), 1613s  $\nu$ (C=N), 1462m (CH<sub>2</sub>). <sup>1</sup>H NMR (500MHz, CDCl<sub>3</sub>) [ $\delta$ , ppm]: 8.62 (br s, 2H, CH=N, *e*); 8.24 (m, 2H, Ph H, *f*); 7.98 (d, 2H, Ph H, *d*); 7.33 (m, 4H, Ph H, *b*, *g*); 6.78 (d, 2H, Ph H, *a*); 6.59 (t, 2H, Ph H, *c*); 3.02 (m, 8H, CH<sub>2</sub>, *h*, *i*); 2.37 (t, 2H, NH, *m*); 1.71 (m, 8H, CH<sub>2</sub>, *j*, *k*); 1.24 (m, 4H, CH<sub>2</sub>, *l*). <sup>13</sup>C NMR (125 MHz, CDCl<sub>3</sub>) [ $\delta$ , ppm]: 166.34 (C-1); 161.54 (C-7); 143.28 (C-8); 135.73 (C-5); 135.12 (C-3); 128.03 (C-10); 123.43 (C-2); 118.91 (C-6); 117.49 (C-9); 114.25 (C-4); 47.80 (C-13); 27.62 (C-14); 25.70 (C-15).

## Chapter Three: Synthesis of Cobalt(III) complexes

### 3.1 Ligand Synthesis

During this project, eight ligands with  $N_2O_2$  donor atom sets were synthesised. These ligands all belong to the salen-type group. **Figure 3.1.1** illustrates the structures of the ligands synthesised. The ligands were synthesised according to the literature method<sup>59</sup> by condensation of the appropriate diamine with salicylaldehyde, in a 1:2 mol ratio, in ethanol at room temperature. The product was then purified from a mixture of dichloromethane and hexane.<sup>59</sup> While the synthesis of every ligand proved successful,  $H_2salophen$  was our choice of ligand due to its rigidity and thus the simplicity of the system as far as conformational isomerism and / or other dynamic exchange phenomena are concerned.

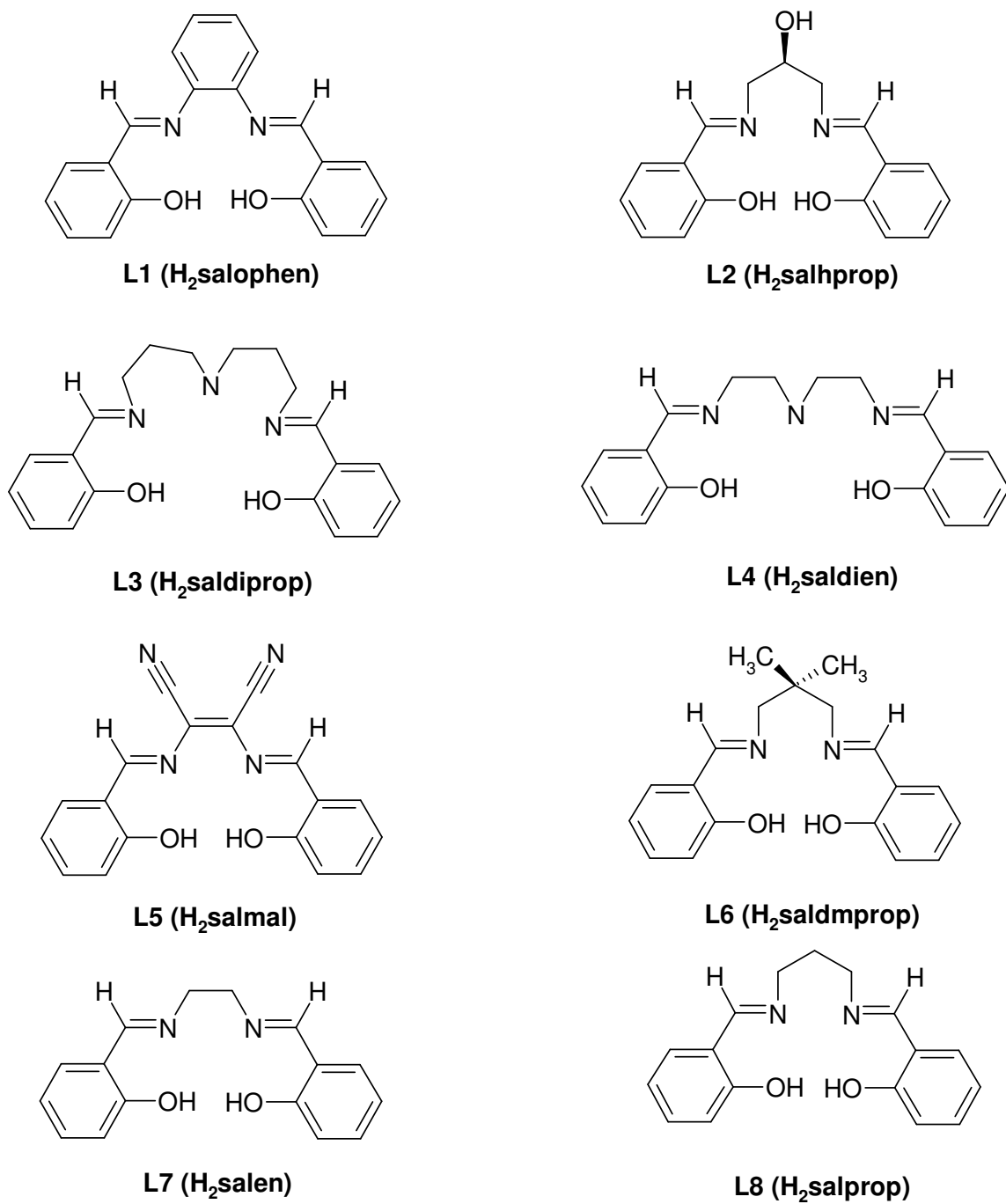


**Figure 3.1.1:** Salen-type ligands that were synthesized during this project.

### 3.1.1 Synthesis of Hsalmal

In our first attempt to synthesise H<sub>2</sub>salmal, we crystallised and obtained the X-ray structure of a novel Schiff base that had only one addition of salicylaldehyde. This half-reacted product was a light yellow powder with only one ionisable proton, Hsalmal.

Hsalmal crystallised in the monoclinic space group  $P2_1/a$ . The asymmetric unit consists of the neutral, planar half-reacted ligand.

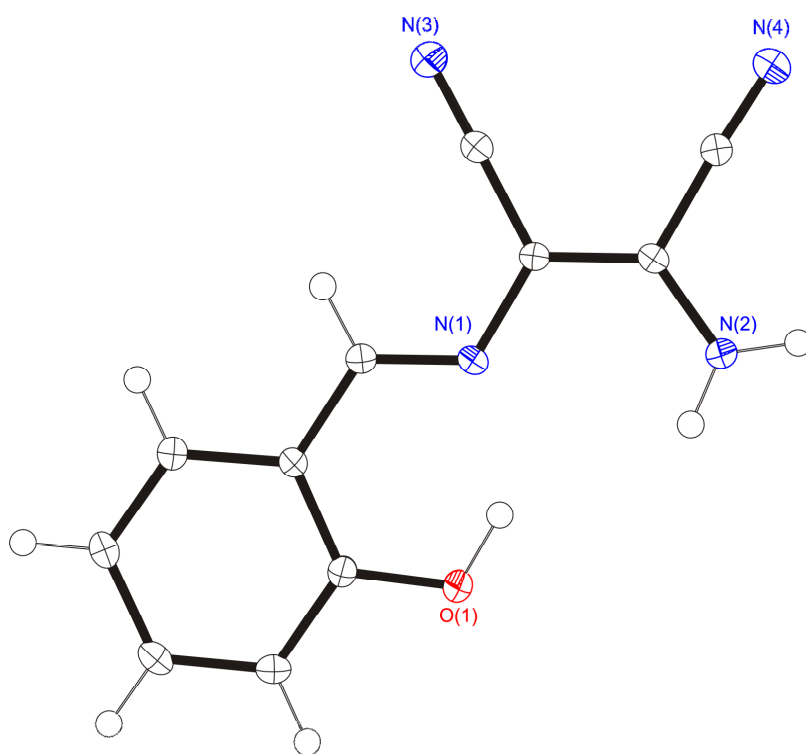


**Figure 3.1.1.1:** Partially labelled ORTEP<sup>60</sup> diagram of Hsalmal. Thermal ellipsoids are drawn at the 50% probability level with isotropic hydrogen atoms of arbitrary radii.

A summary of the crystallographic details for Hsalmal is given in **Table 3.1.1.1**. **Appendices A.1** and **E.1** contain more detailed crystallographic data including atom coordinates, bond angles, bond lengths and an IUCR<sup>61</sup> CIF check report.

**Table 3.1.1.1:** Crystal data and structure refinement details for Hsalmal.

Chemical formula	$C_{11}H_8N_4O$
$M_r$	212.21
Cell setting	Monoclinic
Space group	$P 2_1/a$
Unit cell dimensions:	
$a / \text{\AA}$	6.883(4)
$b / \text{\AA}$	11.434(5)
$c / \text{\AA}$	12.818(7)
$\beta / ^\circ$	96.02(5)
Volume / $\text{\AA}^3$	1003.2(9)
Z	4
$\mu / \text{mm}^{-1}$	0.097
T / K	100(2)
Total reflections	8815
Independent reflections	3128
Observed reflections [ $I > 2\sigma(I)$ ]	2379
$R_{\text{int}}$	0.0377
$R[F^2 > 2\sigma(F^2)]$	0.0464
$wR(F^2)$	0.1409

The unit cell packing consists of four Hsalmal molecules. This can be seen in the packing diagram as viewed along the  $a$ -axis overleaf (**Figure 3.1.1.2**).

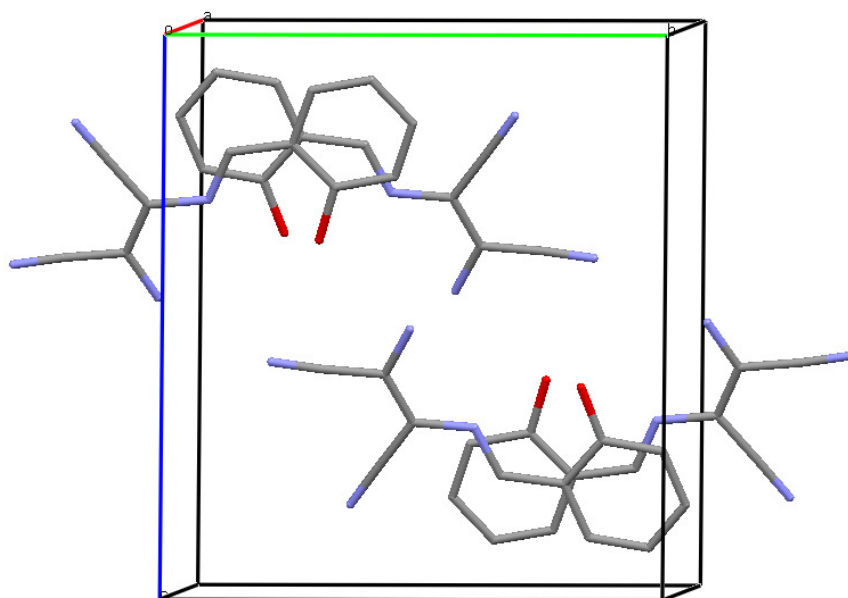


**Figure 3.1.1.2:** Packing diagram for the unit cell of Hsalmal viewed along the *a*-axis. H atoms have been omitted for clarity.

Hydrogen-bonding between the hydroxyl hydrogen atom and the imine nitrogen atom was observed. This is illustrated in **Figure 3.1.1.3**.

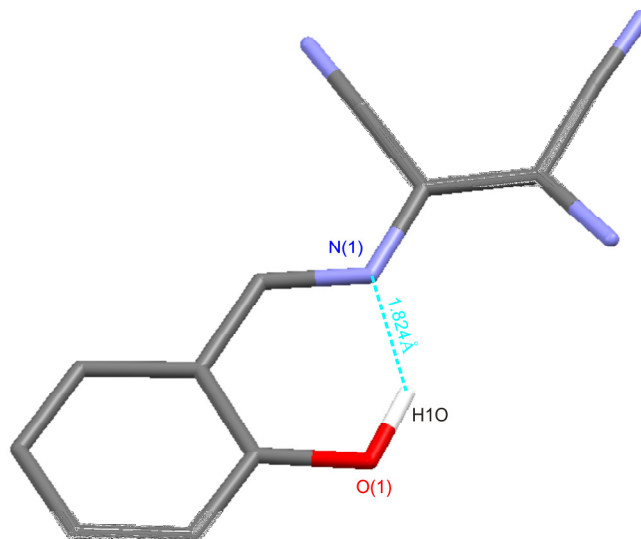


**Figure 3.1.1.3:** Hydrogen-bonding between the hydroxyl atom and the imine nitrogen.

### 3.1.2 Synthesis of H<sub>2</sub>salmal

To prevent the formation of Hsalmal, trifluoroacetic acid was added to the reaction flask. A novel X-ray structure of H<sub>2</sub>salmal was obtained confirming successful acid-catalysed condensation. H<sub>2</sub>salmal crystallised in the monoclinic space group,  $P2_1/n$ . The asymmetric unit consists of the neutral H<sub>2</sub>salmal ligand. The main difference between Hsalmal and H<sub>2</sub>salmal, is that Hsalmal is planar while H<sub>2</sub>salmal is distorted from planarity.

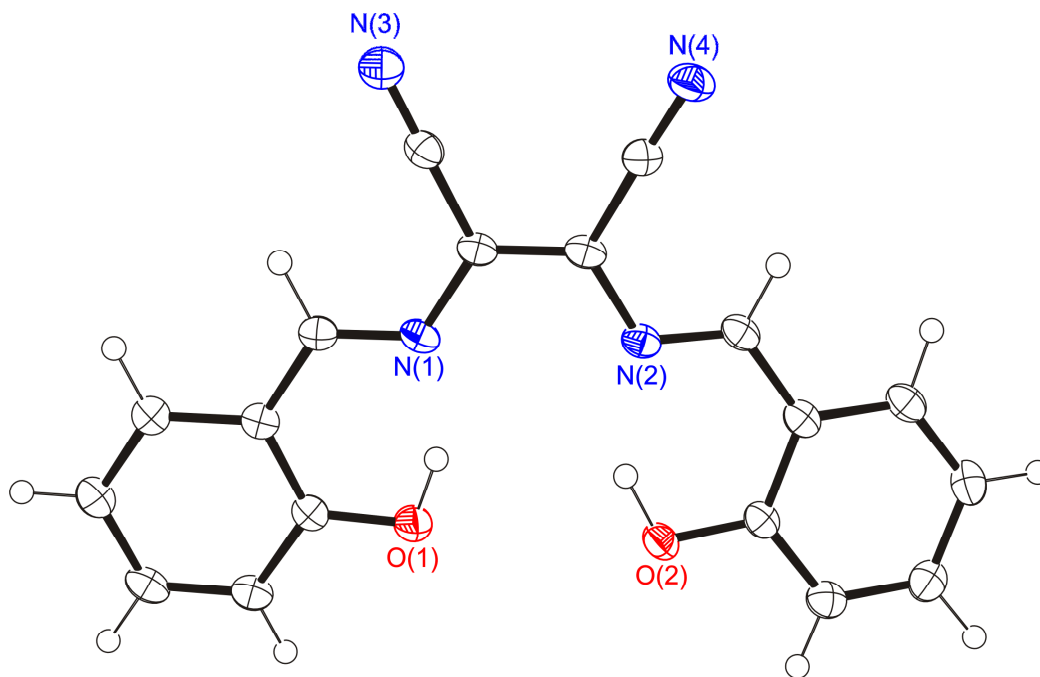


**Figure 3.1.1.4:** Partially labelled ORTEP<sup>60</sup> diagram of H<sub>2</sub>salmal. Thermal ellipsoids are drawn at the 50% probability level with isotropic hydrogen atoms of arbitrary radii.

A summary of the crystallographic details for H<sub>2</sub>salmal is given in **Table 3.1.1.2**. **Appendices A.2** and **E.2** contain more detailed crystallographic data including atom coordinates, bond angles, bond lengths and the IUCR<sup>61</sup> CIF check report.

**Table 3.1.1.2:** Crystal data and structure refinement details of H<sub>2</sub>salmal.

Chemical formula	C <sub>18</sub> H <sub>12</sub> N <sub>4</sub> O <sub>2</sub>
$M_r$	316.32
Temperature	100(2) K
Cell setting	Monoclinic
Space group	$P 2_1/n$
Unit cell dimensions:	
$a / \text{\AA}$	7.297(3)
$b / \text{\AA}$	19.158(3)
$c / \text{\AA}$	10.7922(15)
$\beta / ^\circ$	98.53(2)
Volume / $\text{\AA}^3$	1492.0(7)
Z	4
$\mu / \text{mm}^{-1}$	0.096
T / K	100(2)
Total reflections	8968
Independent reflections	2635
Observed reflections [ $I > 2\sigma(I)$ ]	2199
$R_{\text{int}}$	0.0590
$R[F^2 > 2\sigma(F^2)]$	0.0528
$wR(F^2)$	0.1528

The unit cell packing consists of four H<sub>2</sub>salmal molecules as seen in the packing diagram in **Figure 3.1.1.5** viewed along the  $b$ -axis.

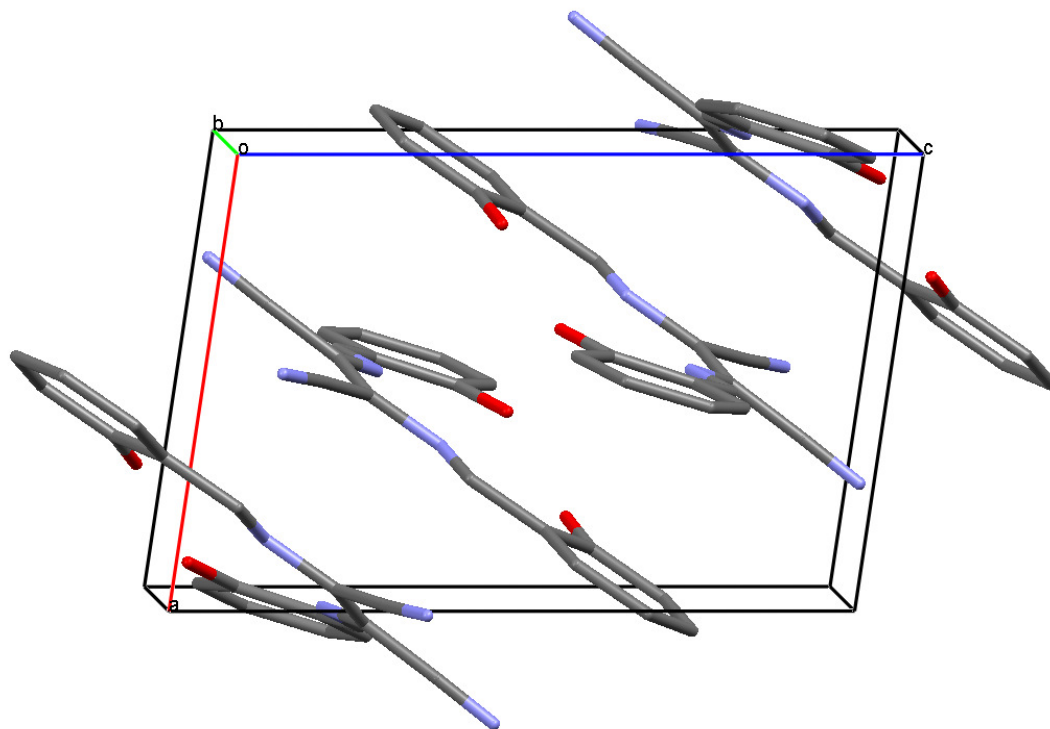


**Figure 3.1.1.5:** Packing diagram of H<sub>2</sub>salmal viewed along the *b*-axis. H atoms have been omitted for clarity.

Short contact interactions exist between the imine carbon (C(7)) and the phenoxy oxygen (O(2)) of adjacent H<sub>2</sub>salmal molecules which suggest  $\pi$ - $\pi$  stacking of adjacent molecules. This is illustrated in **Figure 3.1.1.6**.

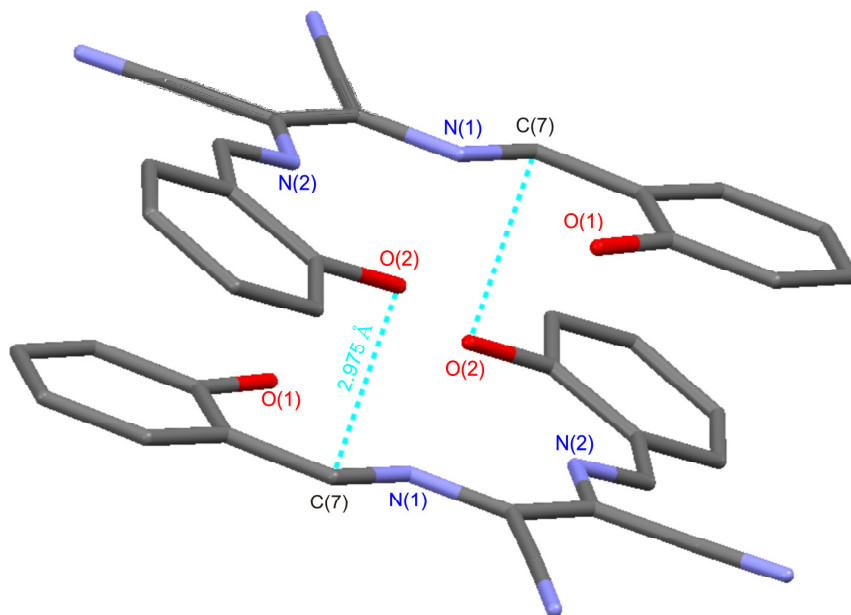


**Figure 3.1.1.6:** Short contact interactions for H<sub>2</sub>salmal. H atoms have been omitted for clarity.

As observed with Hsalmal, hydrogen-bonding between the hydroxyl hydrogen atoms and the imine nitrogen atoms is observed. These intramolecular hydrogen bonds between the nitrogen and oxygen pairs of atoms were also observed in the X-ray structure of H<sub>2</sub>salophen by Pahor *et al.*<sup>71</sup> This can be seen in **Figure 3.1.1.7**.

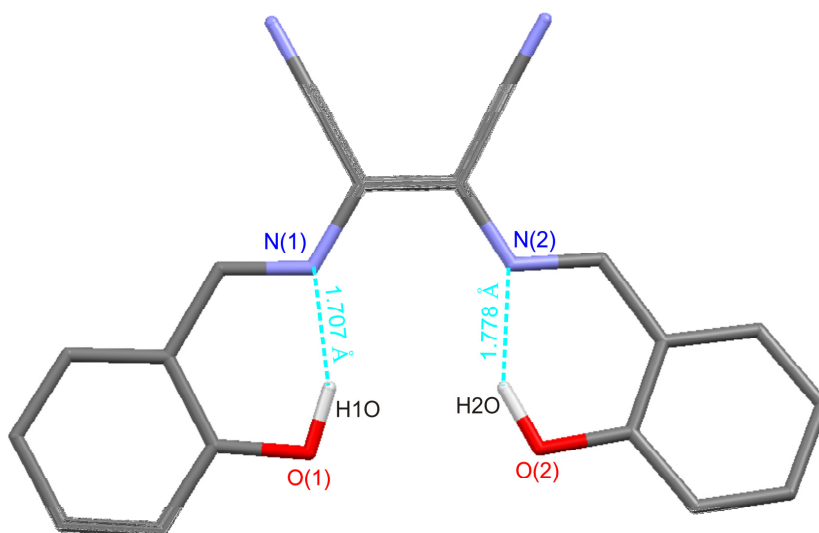


**Figure 3.1.1.7:** Hydrogen-bonding between hydroxyl hydrogen atoms and the imine nitrogen atoms.

### **3.2 Synthesis of [Co(L)(OAc)]**

The cobalt metallation reaction with the each ligand L1 - L7 was carried out according to the literature.<sup>2,42,62</sup> The ligand was dissolved in THF. Cobalt acetate dissolved in methanol was added to the ligand. The solution was air oxidised but the product was found to contain traces (1 – 2%) of the cobalt(II) complex with the bulk material being the cobalt(III) complex.

It must be mentioned that every ligand synthesised was metallated with cobalt acetate according to the literature.<sup>42,62</sup> In most cases, the product formed was that of the cobalt(II) complex. The solution containing the [Co<sup>II</sup>(salophen)] was oxidised by allowing the solution to stir while being open to the atmosphere and this afforded [Co<sup>III</sup>(salophen)(OAc)].

### 3.2.1 Synthesis of [Co(saldiprop)(OAc)]

This complex was synthesised according to the procedure used for the metallation of H<sub>2</sub>salophen with cobalt(II) acetate. We crystallised and obtained the X-ray structure of a new polymorph of the [Co<sup>III</sup>(saldiprop)(OAc)] complex. [Co(saldiprop)(OAc)] crystallised in the monoclinic space group *P*2<sub>1</sub>/*n*. The asymmetric unit consists of the neutral solvent-free complex, [Co(saldiprop)(OAc)]. (See **Appendix A.3.4** for published work on this complex).

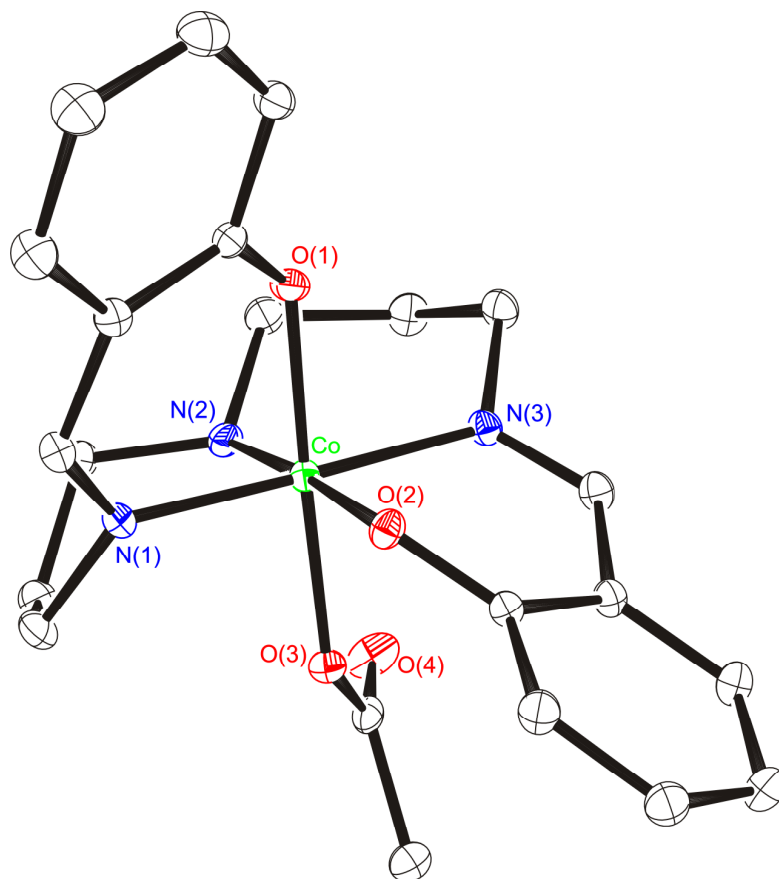


**Figure 3.2.1.1:** Partially labelled ORTEP<sup>60</sup> diagram of the X-ray structure of the [Co(saldiprop)(OAc)]. Thermal ellipsoids are drawn at the 50% probability level with isotropic hydrogen atoms of arbitrary radius. H atoms have been omitted for clarity.

A summary of the crystallographic details are tabulated in **Table 3.2.1.1**. **Appendices A.3** and **E.3** contain more detailed crystallographic data including atom coordinates, bond angles,

bond lengths and the IUCR<sup>61</sup> CIF check report. It also includes published work on this structure.

**Table 3.2.1.1:** Crystal data and structure refinement details for [Co(saldiprop)(OAc)].

Chemical formula	C <sub>22</sub> H <sub>26</sub> CoN <sub>3</sub> O <sub>4</sub>
$M_r$	455.39
Cell setting	Monoclinic
Space group	$P2_1/c$
Unit cell dimensions:	
$a / \text{\AA}$	7.730(2)
$b / \text{\AA}$	20.439(3)
$c / \text{\AA}$	13.321(2)
$\beta / ^\circ$	104.169(18)
Volume / $\text{\AA}^3$	2040.6(7)
$Z$	4
$\mu / \text{mm}^{-1}$	0.876
T / K	100(2)
Total reflections	18148
Independent reflections	6468
Observed reflections [ $I > 2\sigma(I)$ ]	5817
$R_{\text{int}}$	0.0186
$R[F^2 > 2\sigma(F^2)]$	0.0332
$wR(F^2)$	0.0819

The unit cell consists of four [Co(saldiprop)(OAc)] molecules. This can be seen in the packing diagram as viewed along the  $a$ -axis.

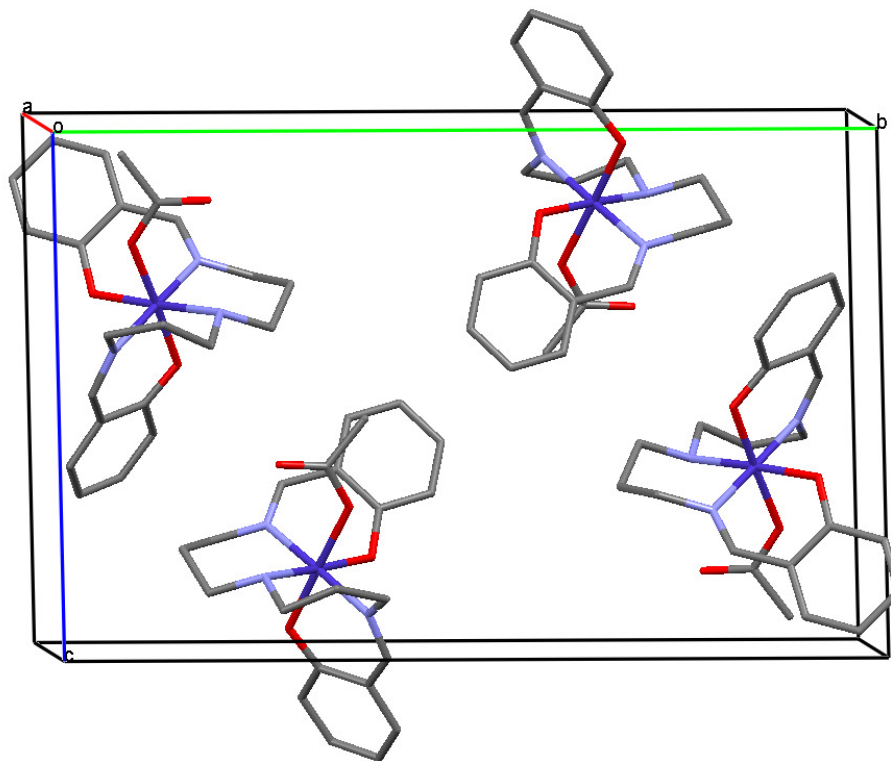


**Figure 3.2.1.2:** Packing diagram for the unit cell of [Co(saldiprop)(OAc)] viewed along the  $a$ -axis. H atoms have been omitted for clarity.

The cobalt(III) ion is six-coordinate with inequivalent Co-O<sub>phenolate</sub> distances and somewhat more equivalent Co-N<sub>imine</sub> distances. The acetate ion occupies the sixth coordination site and forms an intramolecular hydrogen bond with the cobalt-bound NH group of the pentadentate chelate as illustrated in **Figure 3.2.1.3**.

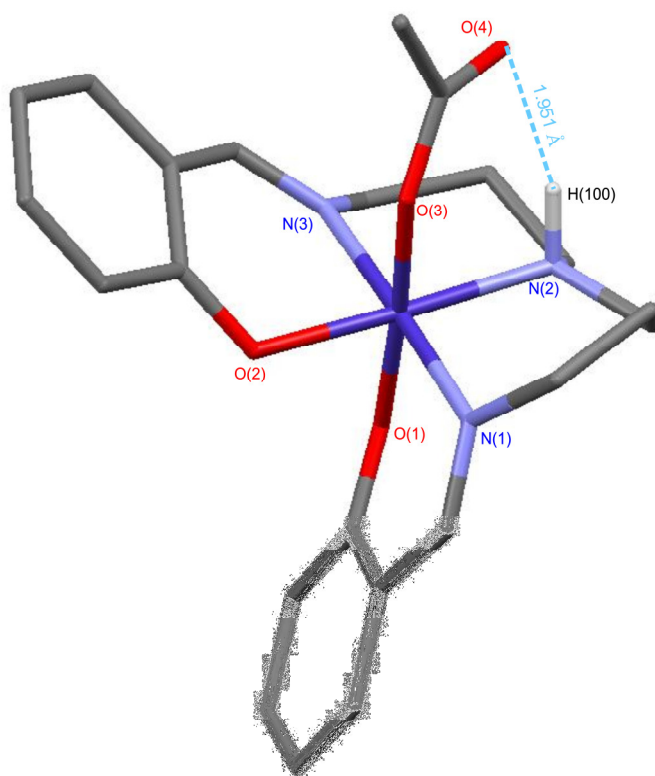


**Figure 3.2.1.3:** Hydrogen-bonding between the oxygen atom of the acetate ion and the hydrogen bound to the nitrogen of the chelate.

The first structure of [Co(saldiprop)(OAc)] was reported by Matsumoto *et al.*<sup>63</sup> in 1983. The cell constants for this complex were found to be  $a = 16.846(4) \text{ \AA}$ ,  $b = 9.417(2) \text{ \AA}$ ,  $c = 14.032(4) \text{ \AA}$  and  $\beta = 111.29(1)^\circ$ .<sup>63</sup> Our structure of [Co(saldiprop)(OAc)] has a unique set of cell constants and is thus a new polymorph.

The average Co-O<sub>chelate</sub> bond distance was found to be  $1.908(10) \text{ \AA}$  and the Co-N<sub>chelate</sub> bond distance was  $1.950(11) \text{ \AA}$ . The Co-O<sub>axial</sub> distance was found to be  $1.924(10) \text{ \AA}$ .

### **3.3 Synthesis of [Co(salophen)(L)<sub>2</sub>](OAc)**

The reaction of [Co(salophen)(L)<sub>2</sub>], where L =  $\alpha$ -methylbenzylamine, benzylamine, butylamine, dibutylamine, *N*-methylpiperazine and piperidine, was successful and resulted in the formation of the cobalt(III) complex in each case. However, the <sup>1</sup>H NMR spectra of these complexes suggested there was evidence of the cobalt(II) complex being present. Amirnasr<sup>59</sup> and colleagues synthesised [Co<sup>III</sup>(salophen)(amine)<sub>2</sub>]ClO<sub>4</sub>, where amine = morpholine, pyrrolidine and piperidine. The main difference in their synthesis and our synthesis is that the metallation of the ligand and the reaction of the axial ligand with the cobalt complex, was carried out in a one pot synthesis and air was bubbled through their reaction mixture once the amine was added. We attempted the metallation of the H<sub>2</sub>salophen and the reaction with the amines according to the method employed by Amirnasr *et al.*<sup>59</sup> but we were unsuccessful.

#### **3.3.1 Synthesis of [Co(saldmprop)(*N*-MePipz)(OAc)]CH<sub>2</sub>Cl<sub>2</sub>**

In our attempt to add axial ligands to the [Co(saldmprop)(OAc)] complex, we were able to crystallise and obtain the X-ray structure of the novel complex [Co(saldmprop)(*N*-MePipz)(OAc)]CH<sub>2</sub>Cl<sub>2</sub>. [Co(saldmprop)(*N*-MePipz)(OAc)]CH<sub>2</sub>Cl<sub>2</sub> crystallised in the monoclinic space group *P*2<sub>1</sub>/*c*. The asymmetric unit consists of the [Co(saldmprop)(*N*-MePipz)(OAc)] complex and a CH<sub>2</sub>Cl<sub>2</sub> molecule.

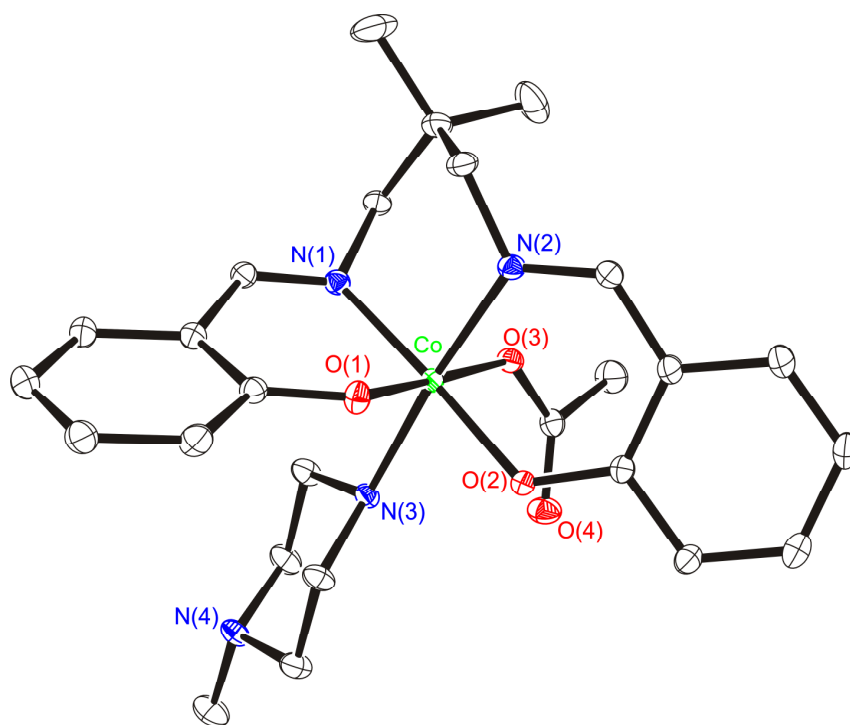


**Figure 3.3.1.1:** Partially labelled ORTEP<sup>60</sup> diagram of the X-ray structure of [Co(saldmprop)(*N*-MePipz)(OAc)]CH<sub>2</sub>Cl<sub>2</sub>. Thermal ellipsoids are drawn at the 50% probability level with isotropic hydrogen atoms of arbitrary radius. H atoms and solvent molecules have been omitted for clarity.

A summary of the crystallographic details is given in **Table 3.3.1.1**. **Appendices A.4** and **E.4** contain more detailed crystallographic data including atom coordinates, bond angles, bond lengths and an IUCR<sup>61</sup> CIF check report.

**Table 3.3.1.1:** Crystal data and structure refinement details for [Co(saldmpop)(*N*-MePipz)(OAc)]CH<sub>2</sub>Cl<sub>2</sub>.

Chemical formula	C <sub>27</sub> H <sub>37</sub> Cl <sub>2</sub> CoN <sub>4</sub> O <sub>4</sub>
$M_r$	611.44
Cell setting	Monoclinic
Space group	$P 2_1/c$
Unit cell dimensions:	
$a / \text{\AA}$	8.9911(4)
$b / \text{\AA}$	25.2721(9)
$c / \text{\AA}$	12.9328(5)
$\beta / ^\circ$	99.353(3)
Volume / $\text{\AA}^3$	2899.6(2)
$Z$	4
$\mu / \text{mm}^{-1}$	0.815
$T / \text{K}$	100(2)
Reflections collected	46550
Independent reflections	10605
Observed reflections [ $I > 2\sigma(I)$ ]	9907
$R_{\text{int}}$	0.0293
$R[F^2 > 2\sigma(F^2)]$	0.0482
$wR(F^2)$	0.101

The unit cell consists of four [Co(saldmpop)(*N*-MePipz)(OAc)] molecules and four CH<sub>2</sub>Cl<sub>2</sub> molecules. This is illustrated in the packing diagram viewed along the  $a$ -axis (**Figure 3.3.1.2**).

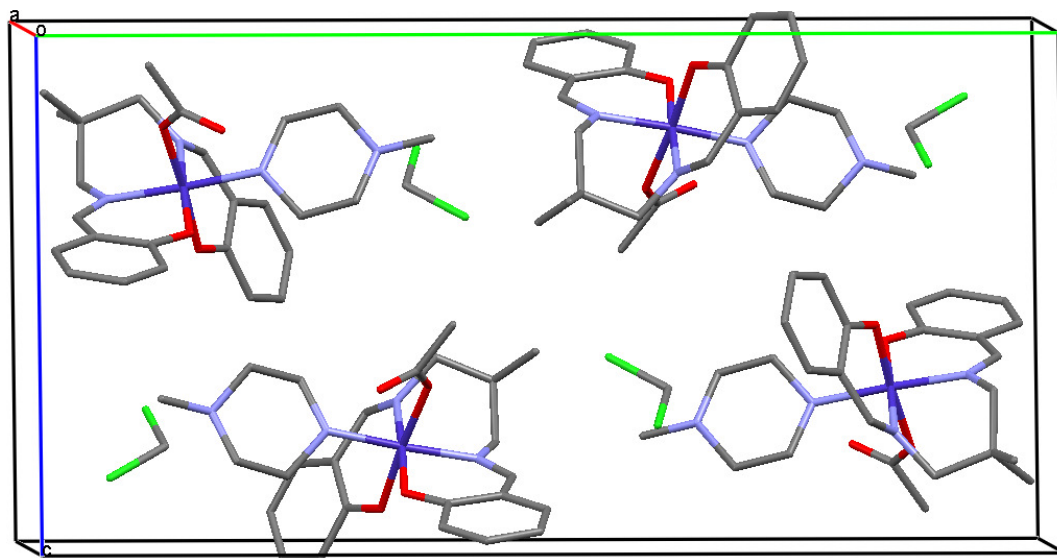


**Figure 3.3.1.2:** Packing diagram for the unit cell of [Co(saldmprop)(N-MePipz)(OAc)]CH<sub>2</sub>Cl<sub>2</sub> viewed along the *a*-axis. H atoms have been omitted for clarity.

**Figure 3.3.1.3** illustrates the hydrogen-bonding that exists between the oxygen atom of the acetate ion and the hydrogen of the axially bound nitrogen.

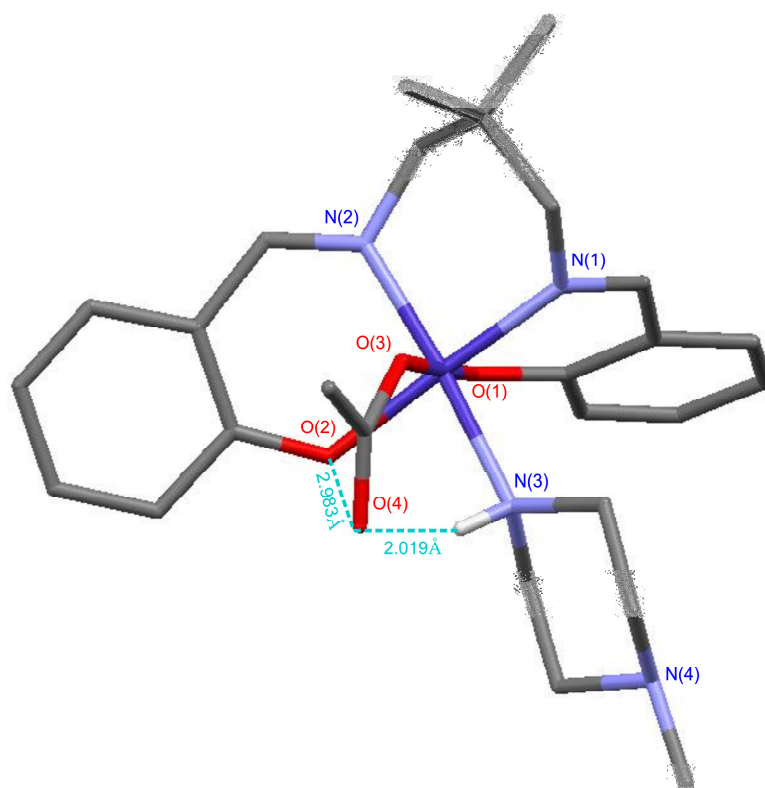


**Figure 3.3.1.3:** Hydrogen-bonding between the oxygen atom of the acetate ion and the hydrogen atom of the axially bound nitrogen atom.

The average  $\text{Co-N}_{\text{chelate}}$  bond distance was  $1.931(12)$  Å and the average  $\text{Co-O}_{\text{chelate}}$  bond distance was  $1.889(11)$  Å. The  $\text{Co-N}_{\text{axial}}$  bond distance was found to be  $2.008(12)$  Å and the  $\text{Co-O}_{\text{axial}}$  bond distance was  $1.935(11)$  Å. The average  $\text{Co-N}_{\text{chelate}}$  bond distance for  $[\text{Co}(\text{saldmprop})(N\text{-MePipz})(\text{OAc})]$  was found to be longer than the average  $\text{Co-N}_{\text{chelate}}$  bond distance for  $[\text{Co}(\text{salophen})(N\text{-MePipz})(\text{OAc})]$  by  $\sim 0.044$  Å. The  $\text{Co-N}_{\text{axial}}$  bond distance for  $[\text{Co}(\text{saldmprop})(N\text{-MePipz})(\text{OAc})]$  is longer than the  $\text{Co-N}_{\text{axial}}$  bond distance for  $[\text{Co}(\text{salophen})(N\text{-MePipz})(\text{OAc})]$  by  $\sim 0.003$  Å. The selected bond lengths for these two complexes are presented in **Table 3.3.1.2** for comparison.

In  $[\text{Co}(\text{saldmprop})(N\text{-MePipz})(\text{OAc})]\text{CH}_2\text{Cl}_2$ , the acetate and *N*-methylpiperazine ligands can be cis and can engage in hydrogen-bonding because of the flexibility in the ligand

backbone. This is not observed in [Co(salophen)(*N*-MePipz)(OAc)] because the salophen ligand is rigid.

**Table 3.3.1.2:** Summary of relevant bond lengths for [Co(saldmprop)(*N*-MePipz)(OAc)] and [Co(salophen)(*N*-MePipz)(OAc)].

<b>Bond lengths</b>	<b>[Co(saldmprop)(<i>N</i>-MePipz)(OAc)]</b>	<b>[Co(salophen)(<i>N</i>-MePipz)(OAc)]</b>
Co-N <sub>axial</sub> / Å	2.0078 (12)	2.005 (3)
Co-N <sub>chelate ave</sub> / Å	1.9305 (12)	1.887 (3)
Co-O <sub>chelate ave</sub> / Å	1.8893 (11)	1.900 (3)
Co-O <sub>axial</sub> / Å	1.9354 (11)	1.944 (3)

In [Co(saldmprop)(*N*-MePipz)(OAc)]CH<sub>2</sub>Cl<sub>2</sub> the axial ligands are trans to each other as compared to the [Co(salophen)(*N*-MePipz)(OAc)] complex in which the axial ligands are cis.

## Chapter Four: Spectroscopy

### 4.1 Infrared Spectroscopy

#### 4.1.1. Introduction

The energy of a molecule can be separated into three additive components. These energies are associated with (1) the rotation of the molecule, (2) the vibrations of each atom in the molecule, and (3) the movement of the electrons in the molecule:

$$E_{total} = E_{el} + E_{vib} + E_{rot}$$

The foundation of the separation lies in the fact that electronic transitions occur on a shorter time scale and rotational transitions occur on a much longer time scale as compared to vibrational transitions. Vibrational transitions occur at high frequencies ( $10^2 \text{ cm}^{-1}$  to  $10^4 \text{ cm}^{-1}$ ) and are due to vibrations of the nuclei that make up the molecule. These transitions are observed in the infrared region of the spectrum. Rotational energy levels are relatively close to each other and as a result rotational transitions occur at low frequencies ( $1 \text{ cm}^{-1}$  to  $10^2 \text{ cm}^{-1}$ ) and can be observed in the microwave and far-infrared regions. The energy levels of the electronic transitions are far apart and the transition frequencies ( $10^4 \text{ cm}^{-1}$  to  $10^6 \text{ cm}^{-1}$ ) can be observed in the visible and ultraviolet region of the spectrum. Infrared spectra originate as a result of photons in the infrared region being absorbed by transitions between two vibrational levels of the molecule in the ground state.<sup>64</sup>

H<sub>2</sub>salophen has characteristic absorption bands due to the most important functional groups. According to the literature,<sup>59</sup> H<sub>2</sub>salophen exhibits a broad band absorption between 3300-3400  $\text{cm}^{-1}$  due to the phenolic OH group. The  $\nu(\text{C}=\text{N})$  band is observed at 1615  $\text{cm}^{-1}$ . The bands corresponding to the axial amine N-H stretching vibrations appear in the 3500-3300  $\text{cm}^{-1}$  region.<sup>65</sup>

The IR spectra of the Schiff base ligands and the complexes studied in this project show absorptions from 4000 to 400  $\text{cm}^{-1}$ . As a result, only the most characteristic absorption bands in the IR spectra were assigned in this project.

#### 4.1.2. Results and Discussion

The most characteristic band in Schiff base ligands is the absorption at 1631  $\text{cm}^{-1}$  due to the imine group (1611-1635  $\text{cm}^{-1}$ ). Another predominant band is due to the absorption of the phenolic OH. The spectra obtained from the ligands synthesised are summarised in **Table 4.1.2.1**.

**Table 4.1.2.1:** Observed frequencies (KBr matrix) for the absorption bands in the IR spectra of the ligands and the Co(III) complex synthesised.

No	Ligand	$\nu(\text{C}=\text{N})/\text{cm}^{-1}$	$\nu(\text{C}-\text{O})/\text{cm}^{-1}$	$\nu(\text{O}-\text{H})/\text{cm}^{-1}$
1	L1(H <sub>2</sub> salophen)	1611	1276	3423
2	L2(H <sub>2</sub> salhprop)	1635	1276	3451
3	L3(H <sub>2</sub> saldiprop)	1631	1278	3418
4	L4(H <sub>2</sub> sadien)	1631	1279	3424
5	L5(H <sub>2</sub> salmal)	1625	1279	3419
6	L6(H <sub>2</sub> saldmprop)	1635	1278	3420
7	L7(H <sub>2</sub> salen)	1635	1283	3451
8	L8(H <sub>2</sub> salprop)	1630	1278	3423
9	[Co(salophen)(OAc)]	1611		-

**Table 4.1.2.2:** Selected frequencies (KBr matrix) for the absorption bands in the IR spectra of cobalt complexes prepared in this work.

No	Complex	$\nu(\text{C}=\text{N})/\text{cm}^{-1}$	$\nu(\text{N}-\text{H})/\text{cm}^{-1}$
1	[Co(salophen)(BuNH <sub>2</sub> ) <sub>2</sub> ]Cl	1609	3299
2	[Co(salophen)(BzNH <sub>2</sub> ) <sub>2</sub> ]Cl	1609	3280
3	[Co(salophen)( $\alpha$ -MeBzNH <sub>2</sub> ) <sub>2</sub> ]Cl	1621	3445
4	[Co(salophen)(Pip) <sub>2</sub> ]Cl	1613	3023
5	[Co(salophen)(Bu <sub>2</sub> NH) <sub>2</sub> ]Cl	1623	3022
6	[Co(salophen)( <i>N</i> -MePipz) <sub>2</sub> ]Cl	1622	3022

In the spectra of the ligands, the broad bands of medium intensity in the 2500-3360 cm<sup>-1</sup> region are assigned to the intramolecular H-bonding vibration (O-H...N).<sup>66</sup> This band is not observed in the spectra of the corresponding cobalt complex which suggests that the salophen ligand is coordinated to the metal ion (phenol groups deprotonated). The vibrations of the azomethine group of the free ligand are observed in the 1610-1640 cm<sup>-1</sup> region. In the complexes, this band is shifted to a higher frequency ( $\Delta\nu = 5 \text{ cm}^{-1}$ ) which indicates that the nitrogen atom of the azomethine is coordinated to the cobalt ion.<sup>66</sup> This corresponds to the loss of hydrogen bonding and the formation of a new chelate ring between the imine nitrogens and the cobalt atom. The presence of an absorption band at 1700 cm<sup>-1</sup> confirms the presence of a carbonyl group. This belongs to the acetate which is bound to the cobalt atom in the axial position. In the ligands, the bands in the 1275-1280 region can be assigned to the phenolic (C-O) group vibrations. In the metal complex, this band is displaced to higher or lower frequencies, indicating chelation of oxygen to the cobalt.<sup>66</sup>

## 4.2 NMR Spectroscopy

### 4.2.1. Introduction

The nuclei of all elements have a charge. Furthermore, atomic nuclei possess a property called spin. For every nucleus with spin, the number of allowed spin states it may adopt is quantized and is determined by its nuclear spin quantum number,  $I$ . The number  $I$  is a physical constant and there are  $2I + 1$  allowed spin states.<sup>65</sup>

In an applied magnetic field, spin states are not of equivalent energy because the nucleus is a charged particle and any moving charge generates a magnetic field of its own. As a result, the nucleus has a magnetic moment,  $\mu$ , generated by its charge and spin. In an applied magnetic field, all protons have their magnetic moments aligned with the field or opposed to it.<sup>65</sup>

The hydrogen nuclei can only adopt one of these orientations with respect to the field. The spin state  $+1/2$  is of lower energy as it is aligned with the field, while the spin state  $-1/2$  is of higher energy as it is opposed to the field.

Nuclear magnetic resonance is of great effectiveness because not all the protons in a molecule resonate at the same frequency. This inconsistency is as a result of the protons in the molecule being surrounded by electrons and the protons exist in a slightly different electronic environment than one another. The protons are shielded by the electrons that surround them.

## 4.2.2. Results and Discussion

Here a brief discussion of some of the salient features of the NMR spectra of compounds prepared in this work will be given. Only selected spectra have been presented. Full characterization data are given in Chapter Two.

The sharp singlet in the  $^1\text{H}$  NMR spectrum of  $\text{H}_2\text{salophen}$  at 13.04 ppm corresponds to the hydroxyl protons and integrates for 2 protons. The other sharp singlet is at 8.64 ppm and was assigned to the imine ( $\text{CH}=\text{N}$ ) protons which also integrate for 2 protons. The signals between 6.8 and 7.6 ppm have been assigned to the phenyl protons of the ligand (**Figure 4.2.2.1**). The  $^{13}\text{C}$  spectrum of  $\text{H}_2\text{salophen}$  is consistent with that reported by Ware *et al.*<sup>67</sup>

The 13.04 ppm singlet observed in the  $^1\text{H}$  spectrum of  $\text{H}_2\text{salophen}$  (**Figure 4.2.2.1**), disappears upon coordination of the salophen dianion to cobalt (Refer to **Appendix B.1**). The aromatic protons are observed between 6.4 and 8.0 ppm. This suggests that the aromatic protons have been shifted to a lower field on coordination of the ligand to  $\text{Co(III)}$ . The singlet at 1.50 ppm was assigned to the methyl protons of the acetate ion of  $[\text{Co}(\text{salophen})(\text{OAc})]$ .

For  $[\text{Co}(\text{salophen})(\text{BuNH}_2)_2]\text{Cl}$ , the singlet observed at 8.89 ppm corresponds to the imine ( $\text{CH}=\text{N}$ ) protons. The aromatic region is observed from 6.65 to 8.41 ppm (see **Figure 4.2.2.2**). The aromatic protons have been shifted to a lower field compared to  $[\text{Co}(\text{salophen})(\text{OAc})]$ . The aromatic region of the  $^1\text{H}$  spectrum of  $[\text{Co}(\text{salophen})(\text{BuNH}_2)_2]\text{Cl}$  is consistent with that reported by Amirnashir *et al.*<sup>59</sup> For this complex, we were able to obtain a  $^{59}\text{Co}$  NMR signal as shown in **Figure 4.2.2.3**. The spectrum exhibits a single line at 8504 ppm. This chemical shift is similar to that reported previously for the complex  $[\text{Co}(\text{TPP})(\text{BuNH}_2)_2]\text{Cl}$ .<sup>68</sup>

It was not possible to detect a  $^{59}\text{Co}$  NMR signal for the other  $\text{Co}^{\text{III}}$  complexes. This could be as a result of infinitely large line widths presumably as a result of large electric field gradients at the nuclei of these derivatives. Another possible reason is the contamination of  $\text{Co}^{\text{II}}$  which could also lead to the infinite broadening of signals.

Note that in **Figure 4.2.2.2** the BuNH<sub>2</sub> axial ligands exhibit <sup>1</sup>H NMR signals that are slightly shielded relative to the free ligand. This indicates a weak “ring current” or magnetic anisotropic effect from the π-electron system of the salophen ligand.

The aromatic region for all complexes has the same pattern. For the benzylamine, α-methylbenzylamine, dibutylamine, *N*-methylpiperazine and piperidine complexes, the axial ligands produced broad low intensity signals with immeasurable coupling constants. The broad lines reflect rotation and / or exchange of the axial ligands.

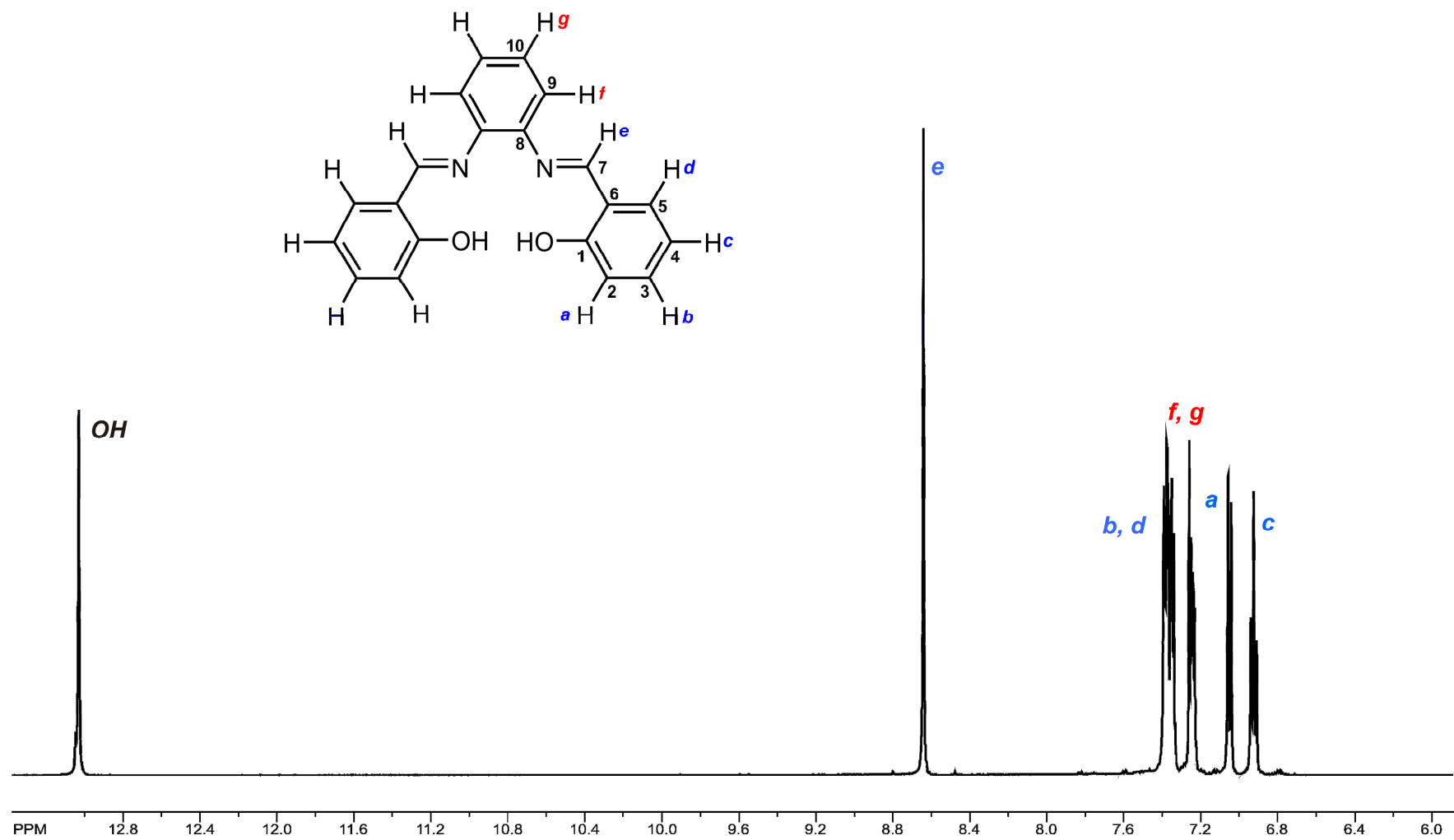


**Figure 4.2.2.1:**  $^1H$  NMR spectrum of  $H_2salophen$  in  $CDCl_3$  at  $25^\circ C$ .

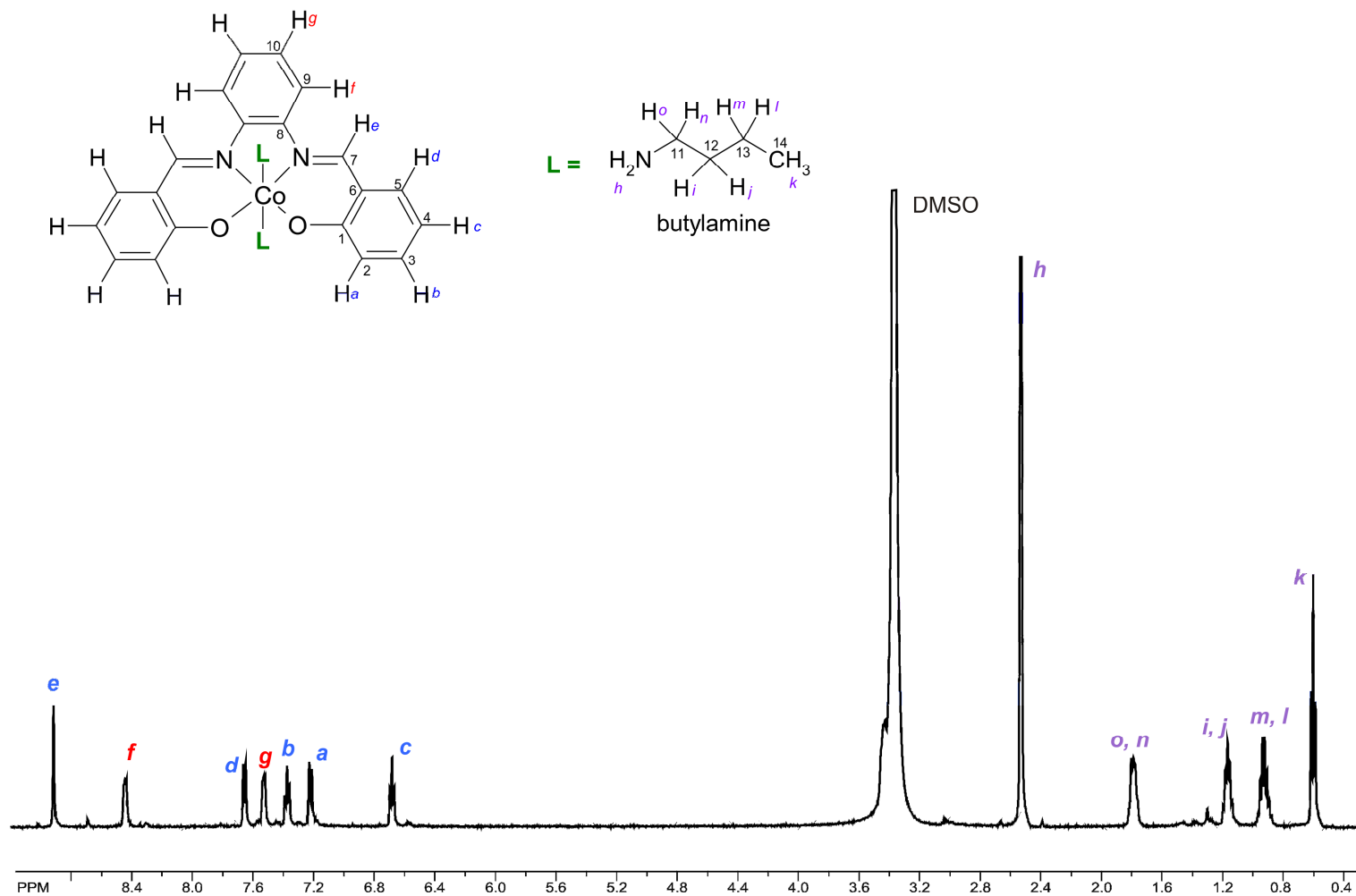


**Figure 4.2.2.2:**  $^1\text{H}$  NMR spectrum of  $[\text{Co}(\text{salophen})(\text{BuNH}_2)_2]\text{Cl}$  in  $\text{DMSO-d}_6$  at  $25^\circ\text{C}$ .

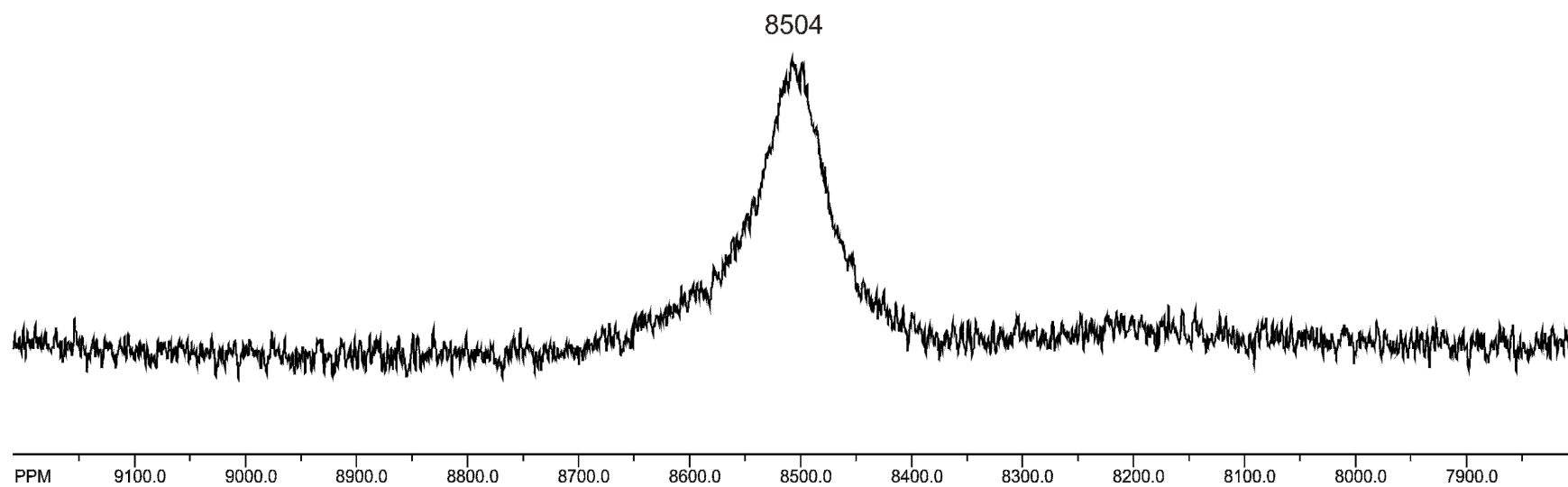


**Figure 4.2.2.3:**  $^{59}\text{Co}$  NMR Spectrum of  $[\text{Co}(\text{BuNH}_2)_2]\text{Cl}$  in DMSO- $d_6$  at 25°C.

## 4.3 UV-vis Spectroscopy

### 4.3.1 Introduction

When continuous radiation is passed through a transparent material, a portion of the radiation is absorbed. When passed through a prism, the remaining radiation yields a spectrum with breaks in it. This is called an absorption spectrum. Due to the absorption of energy, atoms or molecules move from a state of low energy (the ground state) to a state of higher energy (the excited state). This is illustrated by **Figure 4.3.1.1**.<sup>65</sup>

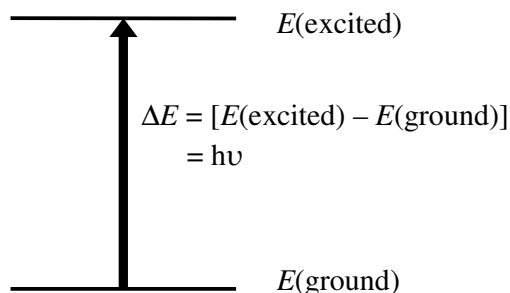


**Figure 4.3.1.1:** The excitation process.

In ultraviolet and visible spectroscopy, it is the transitions between electronic energy levels that result in the absorption of electromagnetic radiation in this region. As energy is absorbed by a molecule, an electron moves from an occupied orbital to an unoccupied orbital of greater potential energy. The most probable transition is from the highest occupied molecular orbital (**HOMO**) to the lowest unoccupied molecular orbital (**LUMO**).<sup>65</sup>

The  $\sigma$  orbital which corresponds to  $\sigma$  bonds are the lowest-energy occupied molecular orbitals. The  $\pi$  orbitals which correspond to  $\pi$  bonds lie at a slightly higher energy level and the nonbonding ( $n$ ) orbitals, the orbitals that hold the unshared electron pairs, lie at even

higher energy levels. The unoccupied or antibonding orbitals ( $\pi^*$  and  $\sigma^*$ ), are the orbitals of the highest energy levels.<sup>65</sup>

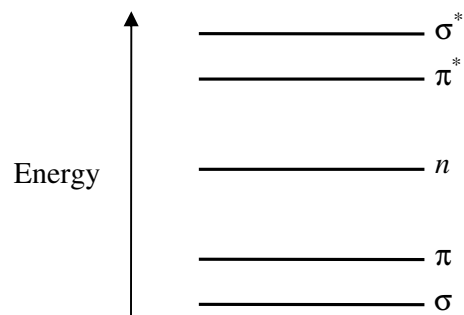


**Figure 4.3.1.2:** Electronic energy levels.<sup>65</sup>

#### 4.3.2 Results and Discussion

**Table 4.3.2.1** shows the absorption data obtained for the ligands synthesised.

**Table 4.3.2.1:** UV-visible absorption data for the ligands synthesised.

No.	Ligand	$\lambda_{\max} / \text{nm} (\epsilon \times 10^3 / \text{M}^{-1} \text{cm}^{-1})$	
1	L1	269(23)	334(18)
2	L2	257(22)	317(7.9)
3	L3	255(13)	314(5.3)
4	L4	255(11)	316(4.2)
5	L5	258(7.3)	326(10)
6	L6	256(20)	317(7.5)
7	L7	257(18)	318(7.1)
8	L8	256(19)	316(7.0)

**Table 4.3.2.2** shows the absorption data for the [Co(salophen)(L)<sub>2</sub>]Cl complexes.

[Co(salophen)L <sub>2</sub> ]Cl, L =	$\lambda_{\text{max}} / \text{nm} (\epsilon \times 10^3 / \text{M}^{-1} \text{cm}^{-1})$		
BuNH <sub>2</sub>	364 (14)	394 (8.4)	470 (9.6)
BzNH <sub>2</sub>	362 (12)	393 (7.9)	467 (8.1)
$\alpha$ -MeBzNH <sub>2</sub>	373(16)	392(15)	476(12)
N-MePipz	372(15)	390(15)	477(1.1)
Bu <sub>2</sub> NH	390(15)	445(10)	477(9.9)
Pip	378(5.5)	405(4.8)	494(4.8)

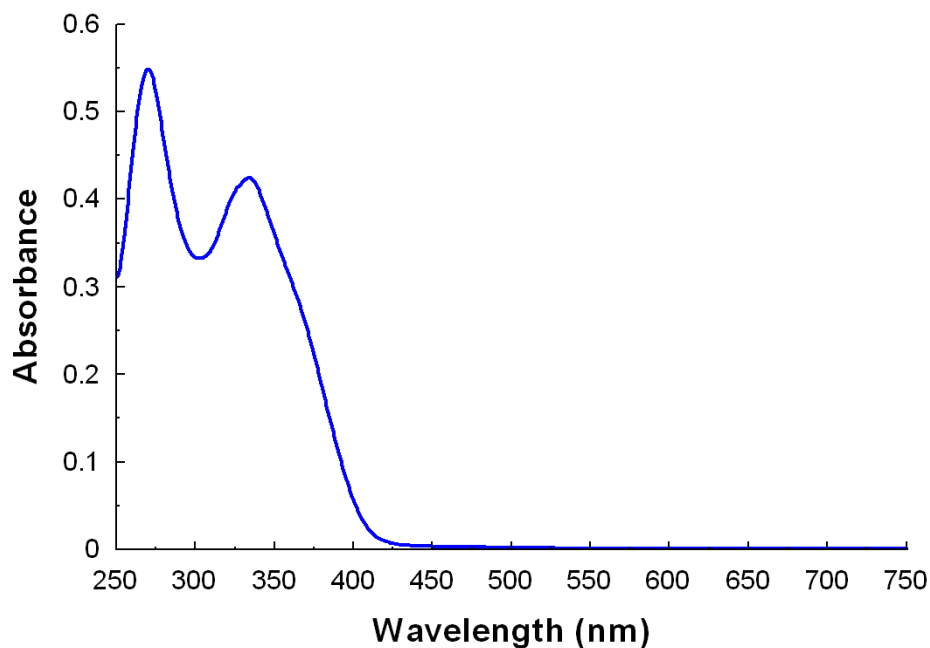


**Figure 4.3.2.1:** Electronic spectrum of H<sub>2</sub>salophen in dichloromethane at 25 °C.

The general UV-vis spectrum for the ligands synthesised is represented by two bands. For H<sub>2</sub>salophen these two bands occur at 269 nm and 334 nm (see **Figure 4.3.2.1**). El-Medani *et al.*<sup>6</sup> attributed the first band at 269 nm, to a  $\pi$ - $\pi^*$  electronic transition and the second band at 334 nm to  $n$ - $\pi^*$  electronic transitions.<sup>6</sup> The first band is due to the transition of the azomethine chromophore and the second band is a result of the transition of the phenol rings.<sup>16</sup> This band is absent in the cobalt complex. Upon metallation, the band at 334 nm

disappears and a new band at 471 nm appears (**Figure 4.3.2.2**). Upon complexation with the amines, an intense band appears in the 440-500 nm region of the spectrum. Amirnasr *et al.*<sup>59</sup> have assigned this band to  $d-\pi^*$  transfers (**Figure 4.3.2.3**).

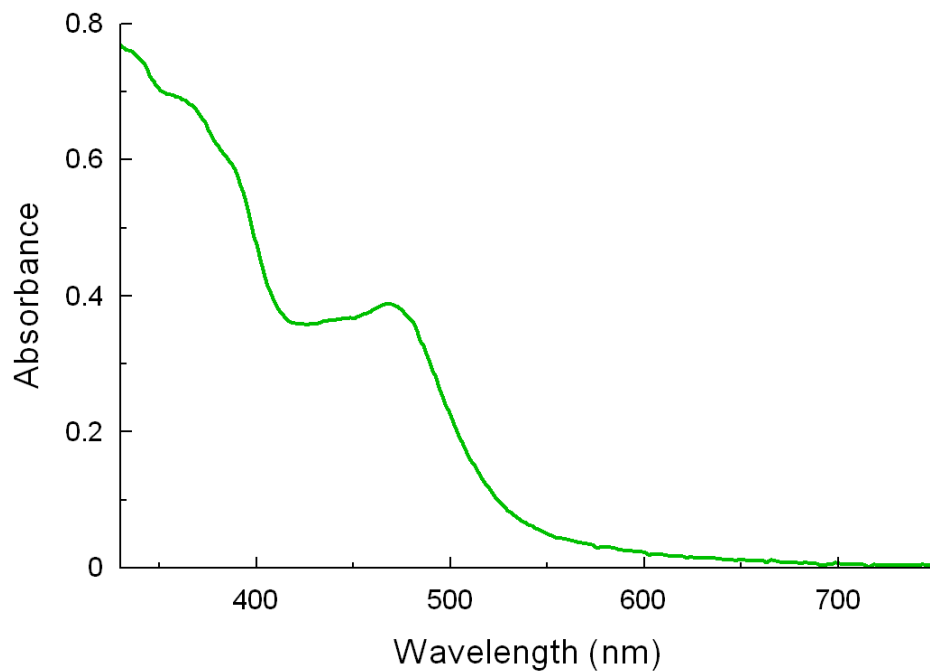


**Figure 4.3.2.2:** Electronic spectrum of [Co(salophen)(OAc)] in DMSO at 25°C.

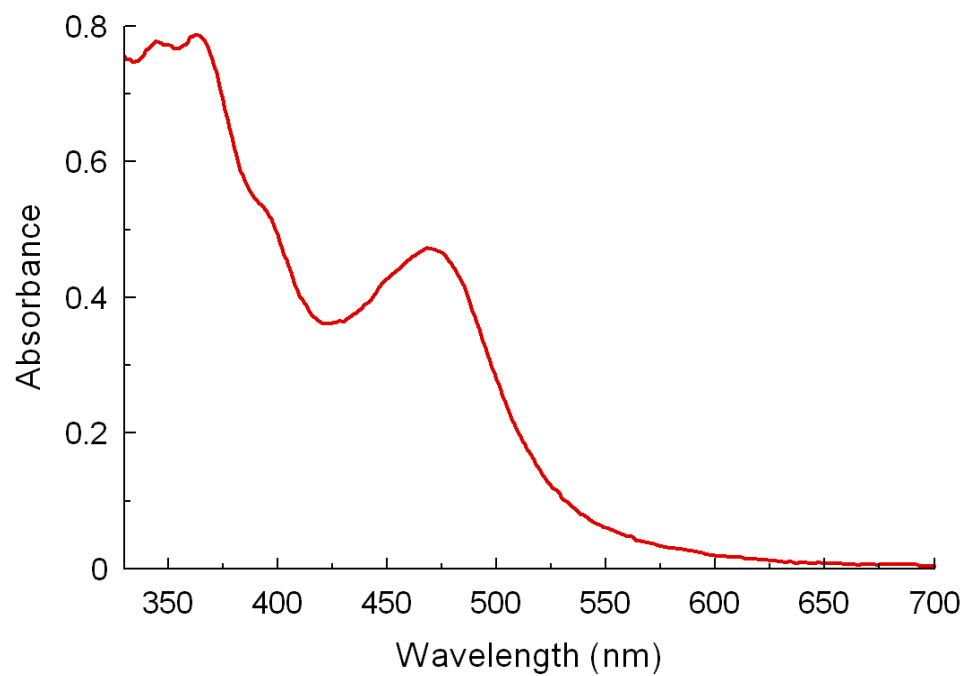


**Figure 4.3.2.3:** Electronic spectrum of [Co(salophen)(α-MeBzNH<sub>2</sub>)<sub>2</sub>]Cl in DMSO at 25°C.

## Chapter Five: X-ray Crystal Structures of Co(III) Schiff Base Complexes

### 5.1 Introduction

A survey of the published crystal structures of H<sub>2</sub>salophen and metal complexes of this ligand using the Cambridge Structural Database (CSD)<sup>69</sup> was performed to collect and illustrate structural and conformational trends. While a number of structures were found, only those that are most relevant to this project will be included in this study.

**Table 5.1.1:** Reported X-ray crystal structures of ligands containing the H<sub>2</sub>salophen backbone.

CSD <sup>69</sup> Reference Code	Complex Name	Literature Reference
OPHSAL01	H <sub>2</sub> salophen	70
OPHSAL10	H <sub>2</sub> salophen	71
MOQCIE	Bis- <i>N,N'</i> - <i>p</i> -bromo-salicylideneamine-1,2-diaminobenzene	72
SAJMIA	<i>N,N'</i> -bis(3,5-di- <i>t</i> -butylsalicylidene)-4,5-dimethyl-1,2-phenylenediamine	73
WUKYAC	<i>N,N'</i> -bis(4-hydroxysalicylidene)-1,2-phenylenediimine	74

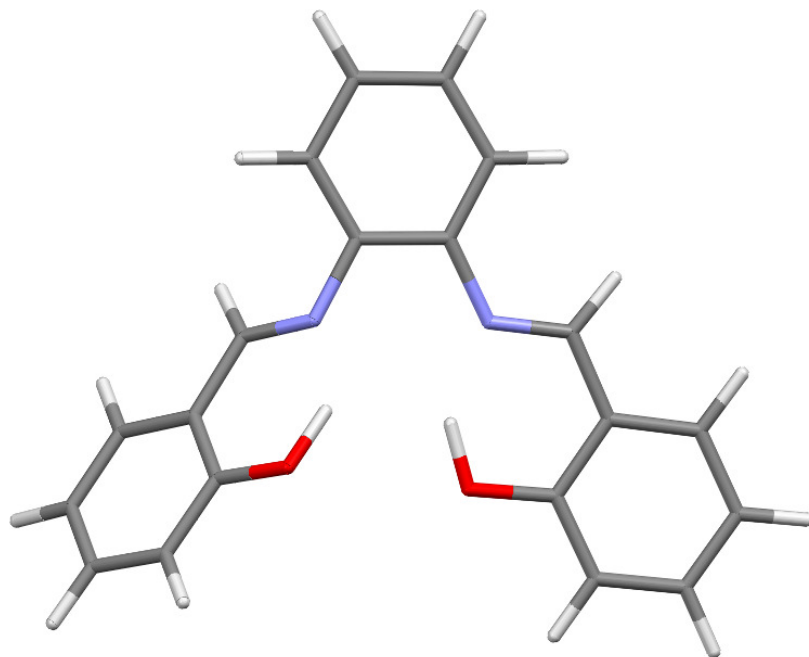


**Figure 5.1.1:** OPHSAL10<sup>71</sup>

The H<sub>2</sub>salophen was crystallised by Pahor *et al.*<sup>71</sup> It was found that the molecules in the crystal lattice were held together by van der Waals forces. Intramolecular hydrogen bonds were found to exist between the nitrogen and oxygen pairs of atoms.<sup>71</sup>

A literature survey of metal complexes containing H<sub>2</sub>salophen crystallized to date reveals a large number of complexes with a wide range of transition metals. These complexes include various axial ligands.

**Table 5.1.2:** Reported X-ray crystal structures of metal complexes containing H<sub>2</sub>salophen.

CSD <sup>69</sup> Reference Code	Complex Name	Metal Centre	Axial Ligand	Oxidation State	Literature Reference
ADIBEU	Salomphen( <i>t</i> Bu)AlMe	Al	Me	+3	75
BANFOM	[Mn(salophen)(N <sub>3</sub> )(CH <sub>3</sub> OH)]	Mn	N <sub>3</sub> <sup>-</sup> and CH <sub>3</sub> OH	+3	76
BEVWEF	[Cu(H <sub>2</sub> salphdc)]·H <sub>2</sub> O	Cu	-	+2	77
BILQAP	[Mn(salophen)(ImzH) <sub>2</sub> ](ClO <sub>4</sub> )	Mn	ImzH <sup>a</sup>	+3	78
COXGIF	[Cu(salophen)]CHCl <sub>3</sub>	Cu	-	+2	79
COXGOL	[Cu(salophen)(py)]	Cu	pyridine	+2	79
FEWVUY	[Fe(salophen)(Him) <sub>2</sub> ]	Fe	HIm <sup>a</sup>	+3	80
HITWAI	[CrN(salophen)]	Cr	N <sup>3-</sup>	+5	81
IGAFOL	[Ru( <sup>t</sup> Bu <sub>2</sub> salophen)(Cl)(NO)]	Ru	Cl <sup>-</sup> and NO	+2	82
KAKZOM	[Mn(salophen)(NCS)]	Mn	NCS <sup>-</sup>	+3	83
KAKZUS	[Mn(salophen)(ClO <sub>4</sub> )(H <sub>2</sub> O)]	Mn	ClO <sub>4</sub> <sup>-</sup> and H <sub>2</sub> O	+3	83
NANNEV	[Mn(salophen)(py)]	Mn	pyridine	+2	84
OKOYIW	[Mn(salophen)(CH <sub>3</sub> OH)(NO <sub>3</sub> )]	Mn	CH <sub>3</sub> OH and NO <sub>3</sub> <sup>-</sup>	+3	85
PAYDIC	[Cu(salophen)]	Cu	-	+2	86
PUKTOE	[Ni(sal-3,4-toluen)·1.5CHCl <sub>3</sub> ]	Ni	-	+2	87
QUBJAY	[In(salophen)(Me)]	In	Me	-	88

<sup>a</sup>ImzH and HIm = Imidazole

**Table 5.1.3:** Reported X-ray crystal structures of [Co(salophen)] complexes.

No.	Complex	Axial Ligands	Ref Code <sup>[Ref]</sup>
1	{[(THF)(salophen)Co-S <sub>2</sub> -Co(salophen)][Na(THF)]} <sup>+</sup>	THF and S <sup>2-</sup>	BENEGEG <sup>89</sup>
2	{[Co(salophen)] <sub>2</sub> (μ-S <sub>2</sub> )Na(THF) <sub>2</sub> } <sup>+</sup>	THF and S <sup>2-</sup>	BENEGEG10 <sup>90</sup>
3	[Co <sup>III</sup> (salophen)(dbm)]	dbm <sup>a</sup>	BZMPSC10 <sup>91</sup>
4	[Co <sup>II</sup> (salophen)(2-MeIm)]	2-MeIm <sup>b</sup>	CEYZUB <sup>92</sup>
5	[Co <sup>III</sup> (salophen)(C <sub>2</sub> H <sub>5</sub> )(py)]·H <sub>2</sub> O	py <sup>c</sup> and C <sub>2</sub> H <sub>5</sub>	CORHOG <sup>93</sup>
6	[Co <sup>III</sup> (salophen)(CH <sub>2</sub> CN)(py)]·H <sub>2</sub> O	py and CH <sub>2</sub> CN	CORHUM <sup>93</sup>
7	[Co <sup>II</sup> (salophen)]	-	COSALP10 <sup>71</sup>
8	[Co <sup>II</sup> (salophen)]	-	COSALP11 <sup>71</sup>
9	[Co(salophen)- <i>i</i> -C <sub>3</sub> H <sub>7</sub> ]·1.5H <sub>2</sub> O	C <sub>3</sub> H <sub>7</sub>	DIDKIK <sup>51</sup>
10	[Co(salophen)CH <sub>3</sub> ]·0.5H <sub>2</sub> O	CH <sub>3</sub>	DIDKOQ <sup>51</sup>
11	[Co(salophen)(CH <sub>2</sub> CF <sub>3</sub> )(py)]	py and CH <sub>2</sub> CF <sub>3</sub>	DIDKUW <sup>51</sup>
12	[Co <sup>III</sup> (salophen)(mrpln) <sub>2</sub> ]ClO <sub>4</sub>	morpholine	XEZQOI <sup>59</sup>
13	[Co <sup>III</sup> (salophen)(prldn) <sub>2</sub> ]ClO <sub>4</sub>	pyrrolidine	XEZQUO <sup>59</sup>

<sup>a</sup>dbm = dibenzoylmethanate<sup>b</sup>2-MeIm = 2-methylimidazole<sup>c</sup>py = pyridine

From the literature, two crystal structures have been reported for [Co(salophen)] COSALP10<sup>71</sup> and COSALP11.<sup>71</sup> The main difference between these two structures is in their space groups and in their unit cell parameters. These structures, together with the most relevant crystal structures from the preceding tables, are illustrated in **Table 5.1.4**.

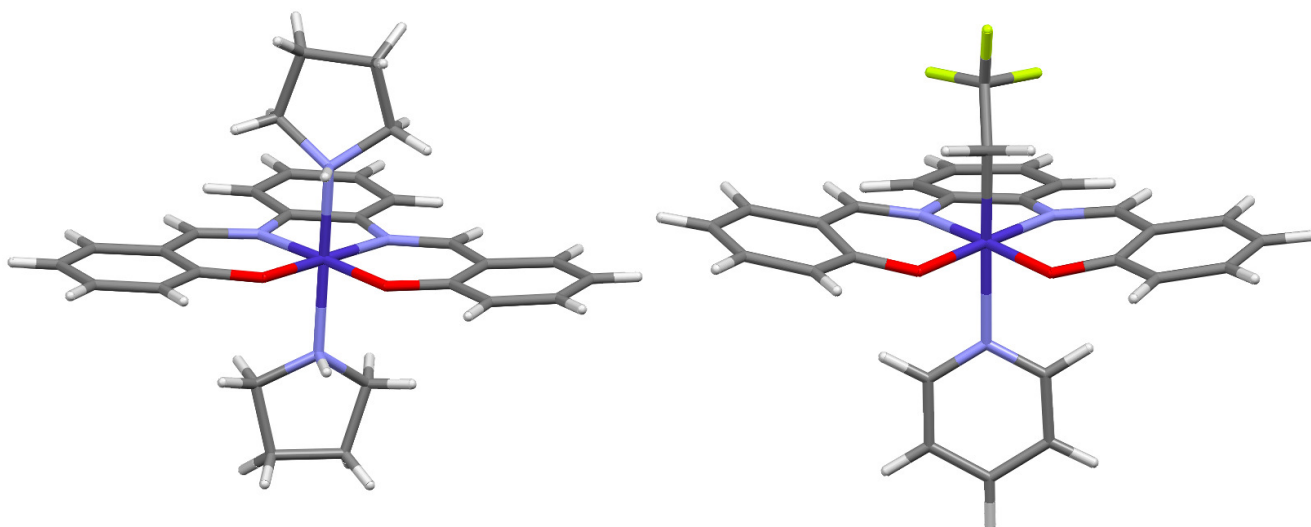


**Figure 5.1.1** XEZQUO<sup>59</sup> and DIDKUW<sup>51</sup>

In  $[\text{Co}(\text{salophen})(\text{prldn})_2]$ , XEZQUO<sup>59</sup> (**Figure 5.1.1**), the cobalt ion is six-coordinate and has an octahedral geometry. The Co-N distances are equivalent at 1.888(14) Å. The Co-O distances are inequivalent 1.881(12) Å and 1.889(12) Å, respectively. The Co-N distances to the axial ligands are 2.004(2) Å and 2.006(2) Å.

For the complex  $[\text{Co}(\text{salophen})(\text{CH}_2\text{CF}_3)(\text{py})]$ , DIDKUW,<sup>51</sup> (**Figure 5.1.1**), the cobalt ion is six-coordinate and has a distorted octahedral geometry with the four H<sub>2</sub>salophen donor atoms at the equatorial positions. The Co-N distances are 1.870(8) Å and 1.899(7) Å. The Co-O distances are more equivalent at 1.894(6) Å and 1.898(7) Å. The Co-N and Co-C distances to the axial ligands were found to be 2.121(9) Å and 2.001(11), respectively.<sup>51</sup>

**Table 5.1.4:** Relevant crystal data and bond lengths of published [Co(salophen)Y<sub>1</sub>Y<sub>2</sub>] complexes, where Y<sub>1</sub> = Y<sub>2</sub>, Y<sub>1</sub> ≠ Y<sub>2</sub> and Y<sub>1</sub> = Y<sub>2</sub> = 0

Structure	[Co(salophen)Y <sub>1</sub> Y <sub>2</sub> ]										
	DBM <sup>a</sup>	2-MeIm	Py and C <sub>2</sub> H <sub>5</sub>	Py and CH <sub>2</sub> CN			C <sub>3</sub> H <sub>7</sub>	CH <sub>3</sub>	Py and CH <sub>2</sub> CF <sub>3</sub>	Mrpln <sup>b</sup>	Prldn <sup>c</sup>
CSD											
Ref.	BZMPSC10	CEYZUB	CORHOG	CORHUM	COSALP10	COSALP11	DIDKIK	DIDKOQ	DIDKUW	XEZQOI	XEZQUO
Code											
Space Group Setting	Monoclinic	Monoclinic	Monoclinic	Monoclinic	Monoclinic	Orthorhombic	Orthorhombic	Triclinic	Monoclinic	Triclinic	Tetragonal
Space Group	<i>P2<sub>1</sub>/n</i>	<i>P2<sub>1</sub>/n</i>	<i>P2<sub>1</sub>/c</i>	<i>P2<sub>1</sub>/n</i>	<i>P2<sub>1</sub>/n</i>	<i>P2<sub>1</sub>2<sub>1</sub>2<sub>1</sub></i>	<i>Pbcn</i>	<i>P<math>\bar{1}</math></i>	<i>P2<sub>1</sub>/c</i>	<i>P<math>\bar{1}</math></i>	<i>I4<sub>1</sub>/a</i>
Z	4	4	4	4	4	4	8	4	8	2	16
Co-N ave/Å	1.904(4)	2.080(4)	1.892(3)	1.891(4)	1.872 <sup>d</sup>	1.875 <sup>d</sup>	1.878(5)	1.877(5)	1.891(8)	1.893(2)	1.888(14)
Co-O ave/Å	1.900(4)	1.975(3)	1.902(3)	1.899(4)	1.841 <sup>d</sup>	1.845 <sup>d</sup>	1.877(4)	1.873(6)	1.905(6)	1.881(2)	1.885(12)

<sup>a</sup>DBM = dibenzoylmethanate

<sup>b</sup>Mrpln = morpholine

<sup>c</sup>Prldn = pyrrolidine

<sup>d</sup>Esd's not reported

## 5.2 Experimental: X-ray structure determinations

### General

X-ray diffraction data were collected on an Oxford Diffraction Xcalibur2 CCD 4-circle diffractometer equipped with an Oxford Instruments Cryojet operating at 100(2) K, unless otherwise specified. The data were collected with Mo K $\alpha$  ( $\lambda = 0.71073$  Å) radiation at a crystal-to-detector distance of 50 mm using omega scans at  $\theta = 29.389^\circ$  with 20-35 s exposures taken at 2.00 kW X-ray power with  $0.75^\circ$  frame widths. The data were reduced with the program CrysAlis RED<sup>69</sup> using outlier rejection, scan speed scaling, as well as standard Lorentz and polarization correction factors. Unless otherwise stated, direct methods (SHELXS-97, WinGX32)<sup>94,95</sup> were used to solve the structures. All non-H atoms were located in the E-map and refined anisotropically with SHELXL-97.<sup>96</sup> All hydrogen atoms in each of the structures were included as idealized contributors in the least-squares process with standard SHELXL-97<sup>96</sup> parameters, unless otherwise stated.

### 5.2.1 X-ray structure determination of [Co(salophen)(CH<sub>2</sub>CH<sub>2</sub>CH<sub>2</sub>OCHO)]

C<sub>24</sub>H<sub>21</sub>N<sub>2</sub>O<sub>4</sub>Co, fw = 460.36 amu,  $a = 7.2668(5)$  Å,  $b = 11.5154(8)$  Å,  $c = 12.7925(9)$  Å,  $\beta = 93.297(6)^\circ$ ,  $V = 696.88(12)$  Å<sup>3</sup>, triclinic,  $P-1$ ,  $Z = 2$ ,  $D_c = 1.576$  g cm<sup>-3</sup>,  $\mu = 0.921$  mm<sup>-1</sup>,  $T = 100(2)$  K,  $R_1 (wR_2) = 0.0404 (0.1097)$  for 5493 unique data with  $I > 2\sigma(I)$ ,  $R_1 (wR_2) = 0.043 (0.110)$  for all 5866 data ( $R_{\text{int}} = 0.0342$ ).

The data yielded a two-molecule triclinic unit cell. The final  $R_1$  was 0.0404 and  $wR_2$  was 0.1097. A numeric analytical absorption correction was applied to the data using CrysAlis RED 170.<sup>69</sup> The maximum and minimum electron densities on the final difference Fourier map were 0.66 (0.93 Å from O(4)) and -0.86 (0.72 Å from Co) e/Å<sup>3</sup>, respectively. Atomic coordinates, crystal data and structure refinement tables as well as the IUCR<sup>61</sup> CIF check report is available in **Appendix C.1**. Full crystallographic data tables can be found in **Appendix F.1**.

### 5.2.2 X-ray structure determination of [Co(salophen)(BuNH<sub>2</sub>)<sub>2</sub>]Cl·1.5 CH<sub>2</sub>Cl<sub>2</sub>

C<sub>29.50</sub>H<sub>39</sub>Cl<sub>4</sub>CoN<sub>4</sub>O<sub>2</sub>, fw = 682.38 amu,  $a = 17.284(2)$  Å,  $b = 19.3302(13)$  Å,  $c = 19.138(2)$  Å,  $\beta = 97.390(10)^\circ$ ,  $V = 6341.1(11)$  Å<sup>3</sup>, monoclinic,  $C2/c$ ,  $Z = 8$ ,  $D_c = 1.430$  g cm<sup>-3</sup>,  $\mu = 0.912$  mm<sup>-1</sup>,  $T = 100(2)$  K,  $R_1 (wR_2) = 0.0475 (0.1271)$  for 8572 unique data with  $I > 2\sigma(I)$ ,  $R_1 (wR_2) = 0.0549 (0.1312)$  for all 10034 data ( $R_{\text{int}} = 0.0230$ ).

The data yielded an eight-molecule monoclinic unit cell. The final value of  $R_1$  was 0.0475 and  $wR_2$  was 0.1271. A numeric analytical absorption correction was applied to the data using CrysAlis RED 170.<sup>69</sup> The maximum and minimum electron densities on the final difference Fourier map were 1.13 (1.07 Å from Cl2s) and -1.34 (0.51 from Cl3s) e/Å<sup>3</sup>, respectively. Atomic coordinates, crystal data and the structure refinement tables plus the IUCR<sup>61</sup> CIF check report is available in **Appendix C.2**. Full crystallographic data tables can be found in **Appendix F.2**.

### 5.2.3 X-ray structure determination of [Co(salophen)(BzNH<sub>2</sub>)<sub>2</sub>]Cl·CH<sub>2</sub>Cl<sub>2</sub>

C<sub>35</sub>H<sub>34</sub>Cl<sub>3</sub>CoN<sub>4</sub>O<sub>2</sub>, fw = 707.94 amu,  $a = 11.172(16)$  Å,  $b = 11.564(16)$  Å,  $c = 12.859(4)$  Å,  $\alpha = 76.485(18)^\circ$ ,  $\beta = 84.583(18)^\circ$ ,  $\gamma = 83.213(12)^\circ$ ,  $V = 1600.2(5)$  Å<sup>3</sup>, triclinic,  $P-1$ ,  $Z = 2$ ,  $D_c = 1.469$  g cm<sup>-3</sup>,  $\mu = 0.826$  mm<sup>-1</sup>,  $T = 100(2)$  K,  $R_1 (wR_2) = 0.0694 (0.2036)$ , for unique 4365 data with  $I > 2\sigma(I)$ ,  $R_1 (wR_2) = 0.0826 (0.2156)$  for all 5629 data ( $R_{\text{int}} = 0.0394$ ).

The data yielded a two molecule triclinic unit cell. The final value of  $R_1$  was 0.0694 and  $wR_2$  was 0.2036. A numeric analytical absorption correction was applied to the data using CrysAlis RED 170.<sup>69</sup> The maximum and minimum electron densities on the final difference Fourier map were 1.30 (0.04 Å from Co) and -1.38 (0.65 Å from Cl2s) e/Å<sup>3</sup>, respectively. Atomic coordinates, crystal data and structure refinement tables together with the IUCR<sup>61</sup> CIF check report is available in **Appendix C.3**. Full crystallographic data tables can be found in **Appendix F.3**.

## 5.2.4 X-ray structure determination of [Co(salophen)(*N*-Me-Pipz)(OAc)]

$C_{27}H_{31}CoN_4O_6$ , fw = 566.49 amu,  $a = 9.428(2)$  Å,  $b = 15.263(4)$  Å,  $c = 17.778(3)$  Å,  $\beta = 98.744(15)^\circ$ ,  $V = 2528.7(9)$  Å<sup>3</sup>, monoclinic,  $P2_1/a$ ,  $Z = 4$ ,  $D_c = 1.488$  g cm<sup>-3</sup>,  $\mu = 0.730$  mm<sup>-1</sup>,  $T = 100(2)$  K,  $R_1$  ( $wR_2$ ) = 0.0521 (0.1157) for 2877 unique data with  $I > 2\sigma(I)$ ,  $R_1$  ( $wR_2$ ) = 0.0888 (0.1276) for all 4468 data ( $R_{int} = 0.0540$ ).

The data yielded a 4-molecule monoclinic unit cell. The final value of  $R_1$  was 0.0521 and  $wR_2$  was 0.1157. The maximum and minimum electron densities on the final difference Fourier map were 0.49 (0.57 Å from H(25A)) and -0.59 (0.55 Å from O2s) e/Å<sup>3</sup>, respectively. Atomic coordinates, crystal data and structure refinement tables as well as the IUCR<sup>61</sup> CIF check report is available in **Appendix C.4**. Full crystallographic data tables can be found in **Appendix F.4**.

## 5.2.5 X-ray structure determination of [Co(salophen)(Pip)<sub>2</sub>](OAc)

$C_{32}H_{39}CoN_4O_4$ , fw = 602.60 amu,  $a = 16.1010(16)$  Å,  $b = 10.1199(5)$  Å,  $c = 19.7187(7)$  Å,  $\beta = 112.750(3)^\circ$ ,  $V = 2963.0(2)$  Å<sup>3</sup>, monoclinic,  $P2/c$ ,  $Z = 4$ ,  $D_c = 1.351$  g cm<sup>-3</sup>,  $\mu = 0.622$  mm<sup>-1</sup>,  $T = 100(2)$  K,  $R_1$  ( $wR_2$ ) = 0.0584 (0.1694) for 4145 unique data with  $I > 2\sigma(I)$ ,  $R_1$  ( $wR_2$ ) = 0.0865 (0.1823) for all 6514 data ( $R_{int} = 0.0388$ ).

The data yielded a 4-molecule unit cell. The final  $R_1$  was 0.0584 and  $wR_2$  was 0.1694. An empirical Multiscan<sup>97</sup> absorption correction was applied to the data. Platon's Squeeze<sup>98</sup> algorithm was used to eliminate a disordered solvent molecule within the lattice. The maximum and minimum electron densities on the final difference Fourier map were 2.21 (0.90 Å from O2S) and -1.97 (0.26 Å from O2S) e/Å<sup>3</sup>, respectively. Atomic coordinates, crystal data and structure refinement tables as well as the IUCR<sup>61</sup> CIF check report is available in **Appendix C.5**. Full crystallographic data tables can be found in **Appendix F.5**.

### 5.3 Results and Discussion

#### X-ray structure analysis of [Co(salophen)(CH<sub>2</sub>CH<sub>2</sub>CH<sub>2</sub>OCHO)]

[Co(salophen)(CH<sub>2</sub>CH<sub>2</sub>CH<sub>2</sub>OCHO)] crystallised in the triclinic space group, P-1. The asymmetric unit consists of the neutral solvent-free complex [Co(salophen)(CH<sub>2</sub>CH<sub>2</sub>CH<sub>2</sub>OCHO)]. Although crystal structures have been reported for [Co(salophen)], (COSALP10<sup>71</sup> and COSALP11<sup>71</sup>, with space groups  $P21/n$  and  $P2_12_12_1$  respectively), none have been reported for this system.

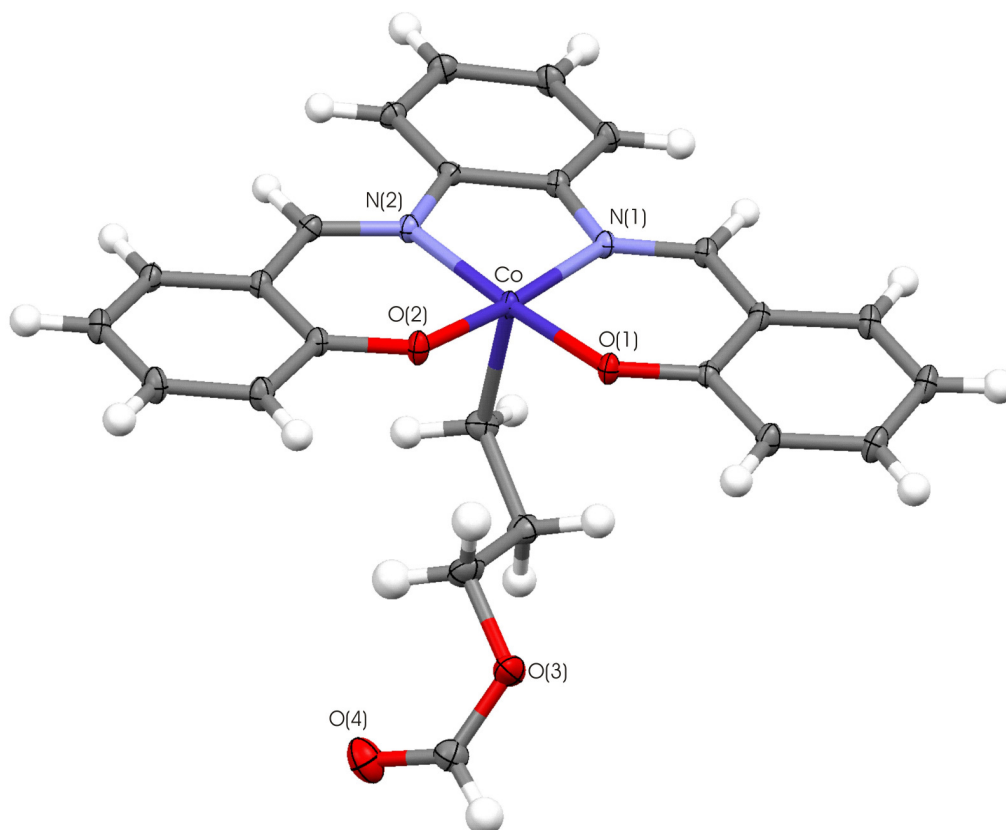


**Figure 5.3.1:** Partially labelled thermal ellipsoid plot of the X-ray structure of [Co(salophen)(CH<sub>2</sub>CH<sub>2</sub>CH<sub>2</sub>OCHO)]. Thermal ellipsoids are drawn at the 50% probability level with isotropic hydrogen atoms.

The unit cell packing consists of two [Co(salophen)(CH<sub>2</sub>CH<sub>2</sub>CH<sub>2</sub>OCHO)] molecules which are situated opposite to each other. This can be seen in the packing diagram as viewed along the *a*-axis.

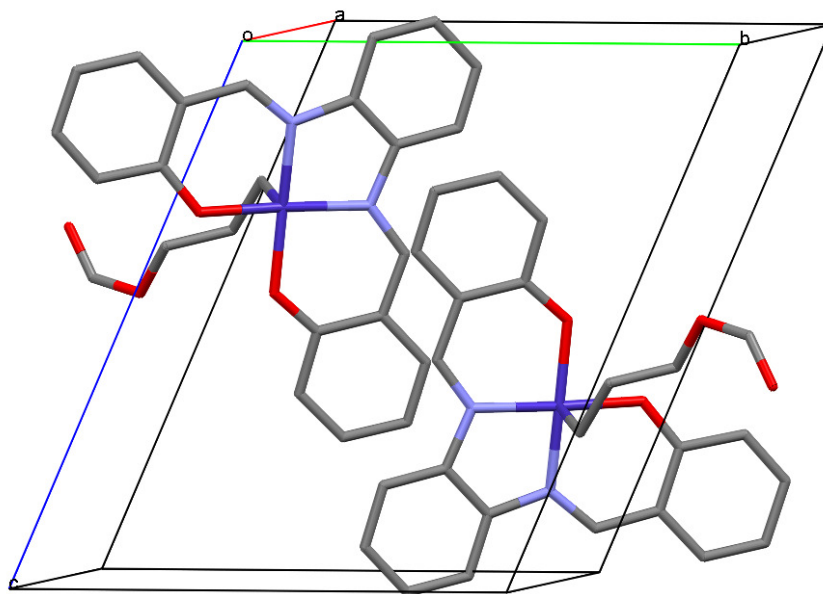


**Figure 5.3.2:** Packing diagram for the unit cell of [Co(salophen)(CH<sub>2</sub>CH<sub>2</sub>CH<sub>2</sub>OCHO)] viewed along the *a*-axis. H atoms have been omitted for clarity.

The molecules of [Co(salophen)(CH<sub>2</sub>CH<sub>2</sub>CH<sub>2</sub>OCHO)] form a dimer through Co- $\pi$  interactions.

The unusual axial ligand of the complex is presumably derived from a radical-mediated cleavage of THF in which O<sub>2</sub> plays a role and affords the aldehyde carbonyl group in the structure. This reaction is known for Co<sup>II</sup> porphyrins.<sup>99</sup>

### **X-ray structure analysis of [Co(salophen)(BuNH<sub>2</sub>)<sub>2</sub>]Cl·1.5CH<sub>2</sub>Cl<sub>2</sub>**

[Co(salophen)(BuNH<sub>2</sub>)<sub>2</sub>]Cl crystallised in the monoclinic space group *C2/c*. The asymmetric unit consists of the [Co(salophen)(BuNH<sub>2</sub>)<sub>2</sub>]<sup>+</sup> cation, a Cl<sup>-</sup> anion and 1.5 CH<sub>2</sub>Cl<sub>2</sub> molecules. One of the CH<sub>2</sub>Cl<sub>2</sub> molecules is located on a special position, accounting for the non-integer solvation number.

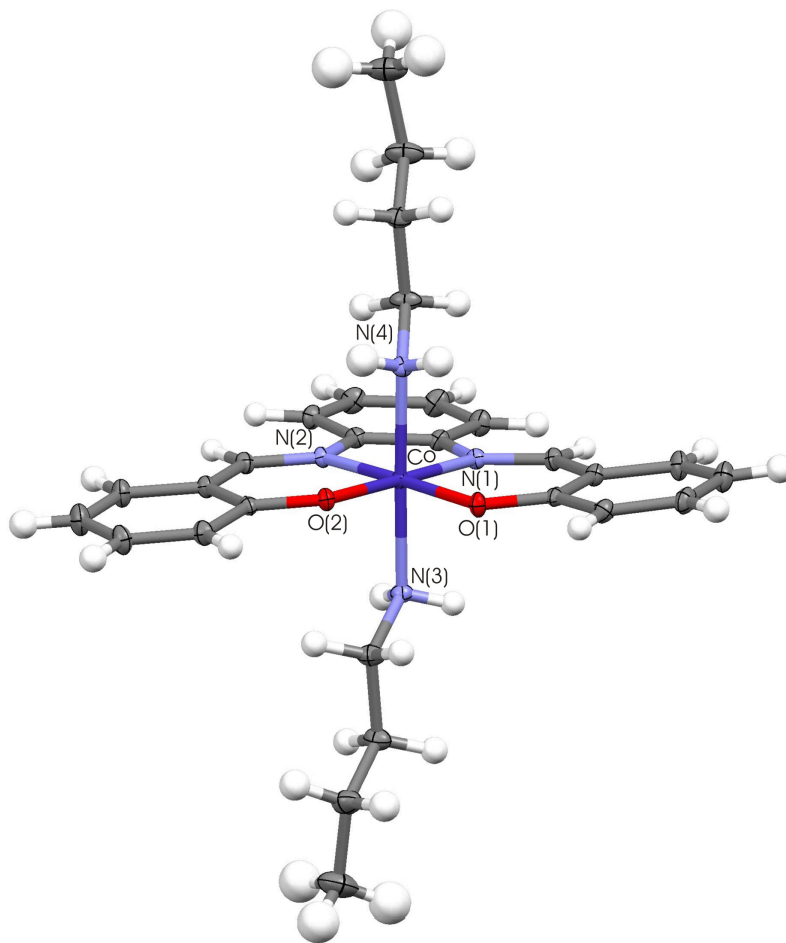


**Figure 5.3.3:** Partially labelled thermal ellipsoid plot of the X-ray structure of the  $[\text{Co}(\text{salophen})(\text{BuNH}_2)_2]^+$  cation. The solvent molecules and  $\text{Cl}^-$  ion have been omitted for clarity. Thermal ellipsoids are drawn at the 50% probability level with isotropic H atoms.

The unit cell packing consists of eight  $[\text{Co}(\text{salophen})(\text{BuNH}_2)_2]^+$  cations, four  $\text{CH}_2\text{Cl}_2$  molecules occupying special positions and eight  $\text{CH}_2\text{Cl}_2$  molecules and eight  $\text{Cl}^-$  anions in general positions.

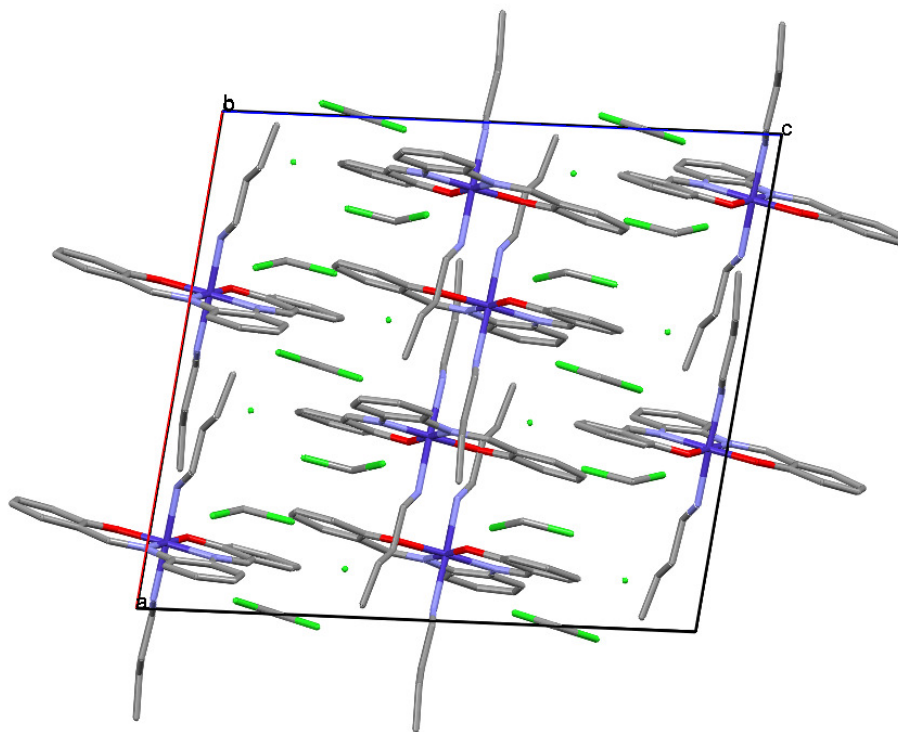


**Figure 5.3.4:** Packing diagram for the unit cell of  $[\text{Co}(\text{salophen})(\text{BuNH}_2)_2]\text{Cl}\cdot 1.5\text{CH}_2\text{Cl}_2$  viewed along the  $b$ -axis, illustrating the position of the solvent molecules. H atoms have been omitted for clarity.

As illustrated in **Figure 5.3.5**, complimentary H-bonding exists between the oxygen atom of  $\text{H}_2\text{salophen}$  and the NH of the axial bound ligand. This H-bonding holds the two monomers together to give an H-bonded dimer.

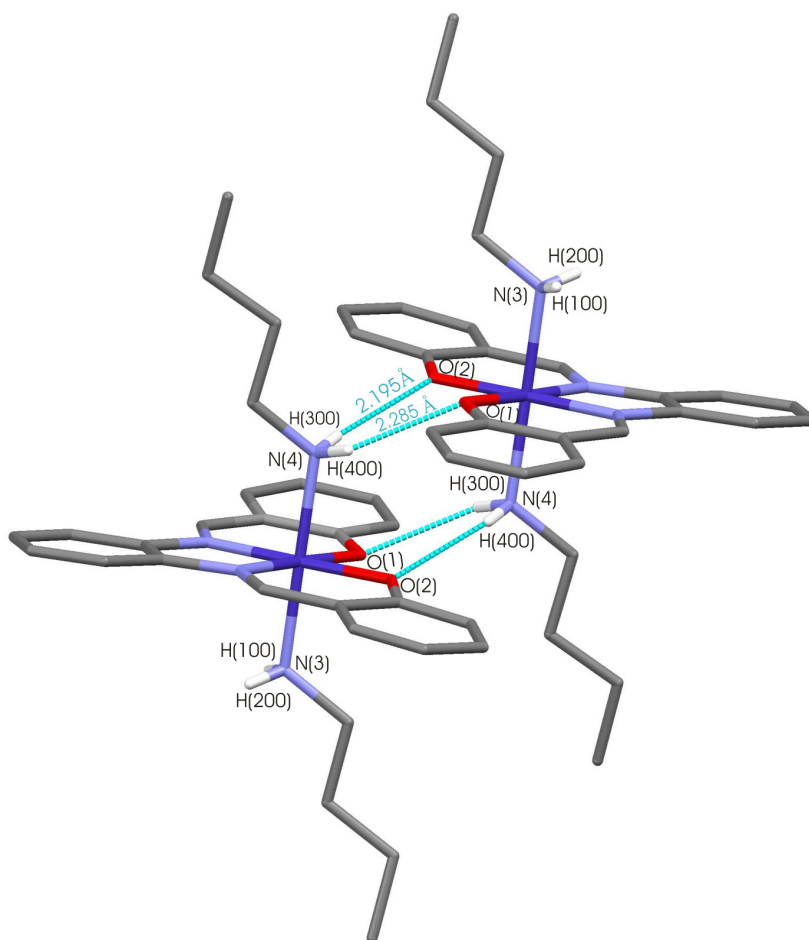


**Figure 5.3.5:** Hydrogen-bonding between adjacent [Co(salophen)(BuNH<sub>2</sub>)<sub>2</sub>]<sup>+</sup> cations.

Short contact interactions exist between the chloride ion and H(9) on the phenyl ring of H<sub>2</sub>salophen as well as between H(7) on the imine carbon and the chloride ion. There also exists a short contact interaction between H(200) on the axial bound ligand and the chloride ion and between Cl1S (chloride ion) and H1S1 on the dichloromethane solvent molecule (**Figure 5.3.6**).

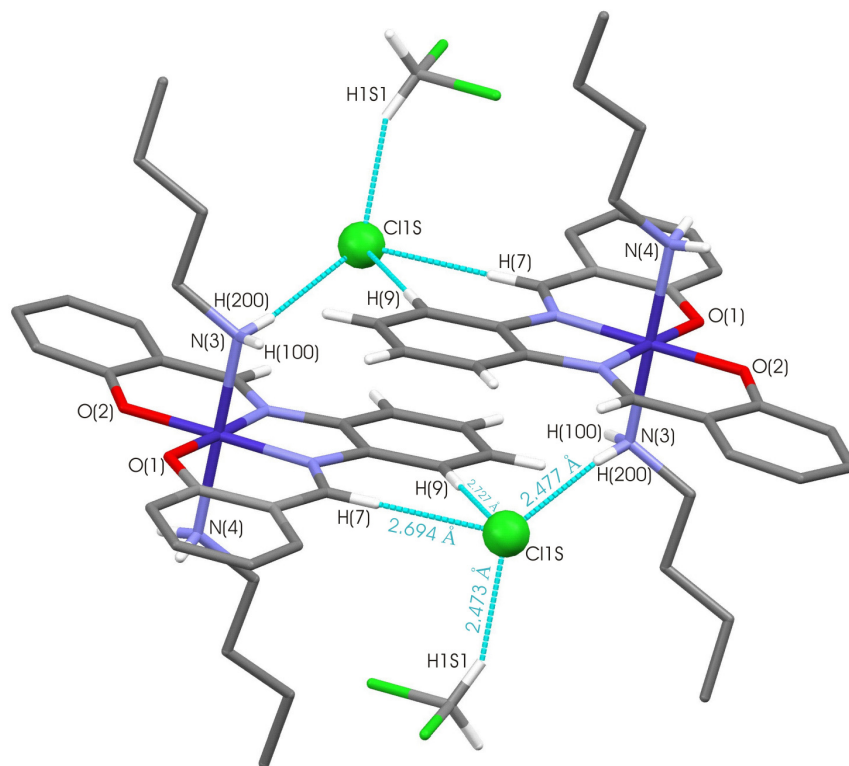


**Figure 5.3.6:** Short contact interactions for  $[\text{Co}(\text{salophen})(\text{BuNH}_2)_2]\text{Cl}\cdot 1.5\text{CH}_2\text{Cl}_2$ . H atoms not involved in the interactions have been omitted for clarity.

### X-ray structure analysis of $[\text{Co}(\text{salophen})(\text{BzNH}_2)_2]\text{Cl}\cdot \text{CH}_2\text{Cl}_2$

$[\text{Co}(\text{salophen})(\text{BzNH}_2)_2]\text{Cl}$  crystallised in the triclinic space group  $P-1$ . The asymmetric unit consists of the  $[\text{Co}(\text{salophen})(\text{BzNH}_2)_2]^+$  cation, one  $\text{Cl}^-$  ion and a  $\text{CH}_2\text{Cl}_2$  molecule.

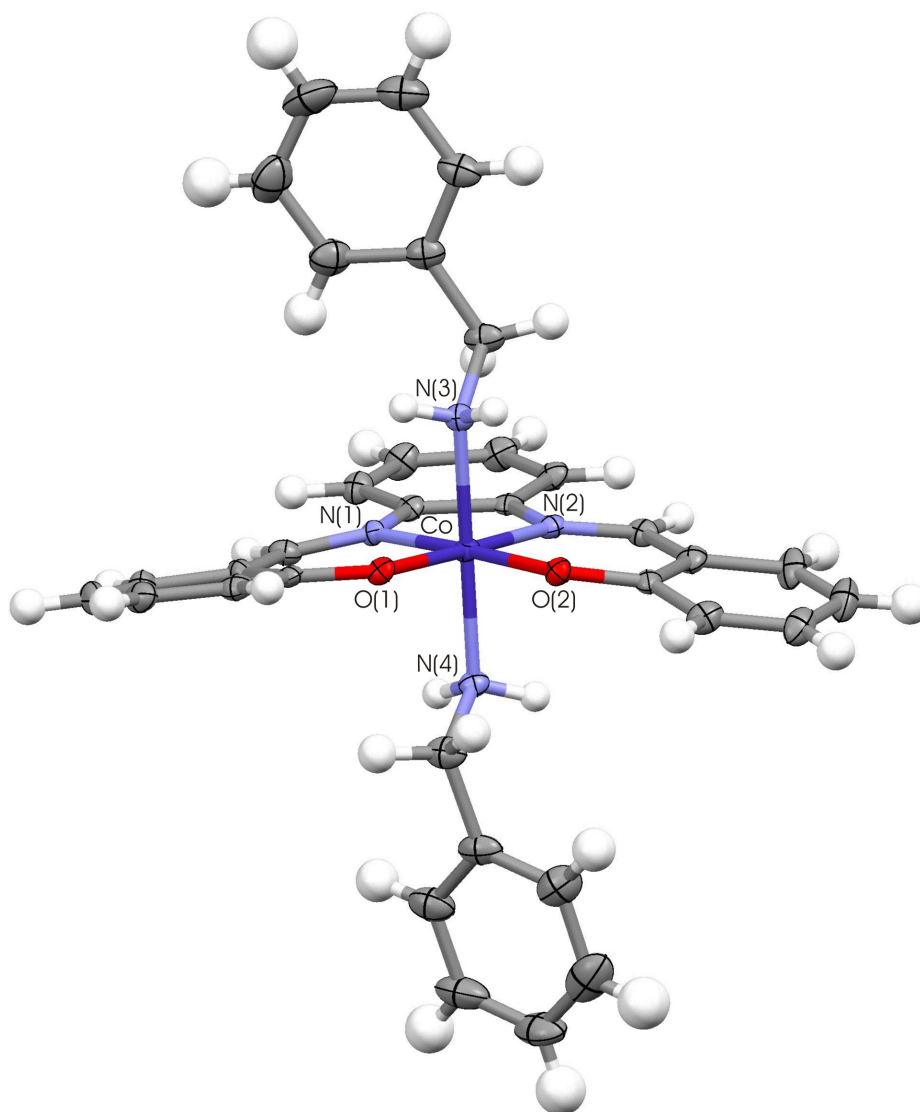


**Figure 5.3.7:** Partially labelled thermal ellipsoid plot of the X-ray structure of  $[\text{Co}(\text{salophen})(\text{BzNH}_2)_2]\text{Cl}\cdot\text{CH}_2\text{Cl}_2$ . Solvent molecules have been omitted for clarity. Thermal ellipsoids are drawn at the 50% probability level with isotropic H atoms.

As with the butylamine derivative, two cations of  $[\text{Co}(\text{salophen})(\text{BzNH}_2)_2]^+$  are held together by complimentary H-bonding (to give a dimer) which occurs between the oxygen atom of  $\text{H}_2\text{salophen}$  and the NH on the axial bound ligand. There is also H-bonding between H(19) of the phenyl ring of  $\text{H}_2\text{salophen}$  and C(27) of the phenyl ring of the axial ligand (**Figure 5.3.8**). This type of interaction, an (aryl)C-H $\cdots\pi$  hydrogen bond, is well described by Steiner<sup>100</sup> and Nishio.<sup>101</sup>

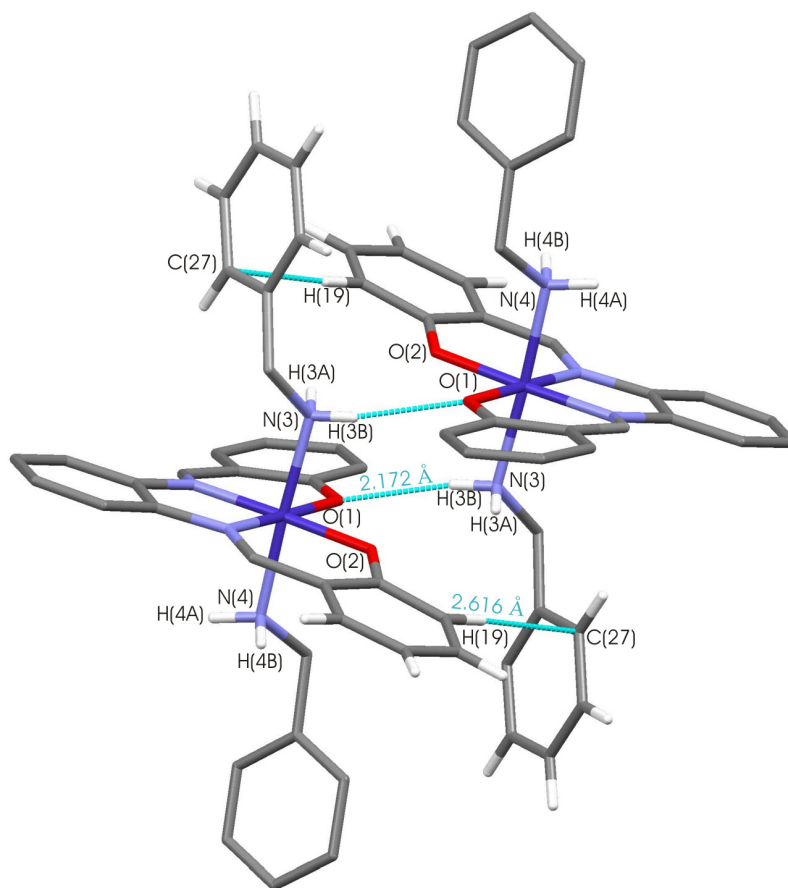


**Figure 5.3.8:** Hydrogen bonding between adjacent [Co(salophen)(BzNH<sub>2</sub>)<sub>2</sub>]<sup>+</sup> cations.

For [Co(salophen)(BzNH<sub>2</sub>)<sub>2</sub>]Cl·CH<sub>2</sub>Cl<sub>2</sub>, short contacts were found between H(4A) on the axial bound ligand and Cl1S of the chloride ion as well as between H(14) on the imine carbon and Cl1S of the chloride ion. Short contact interactions were also found between H(35B) on the methylene chloride molecule and Cl1S of the chloride ion (**Figure 5.3.9**).

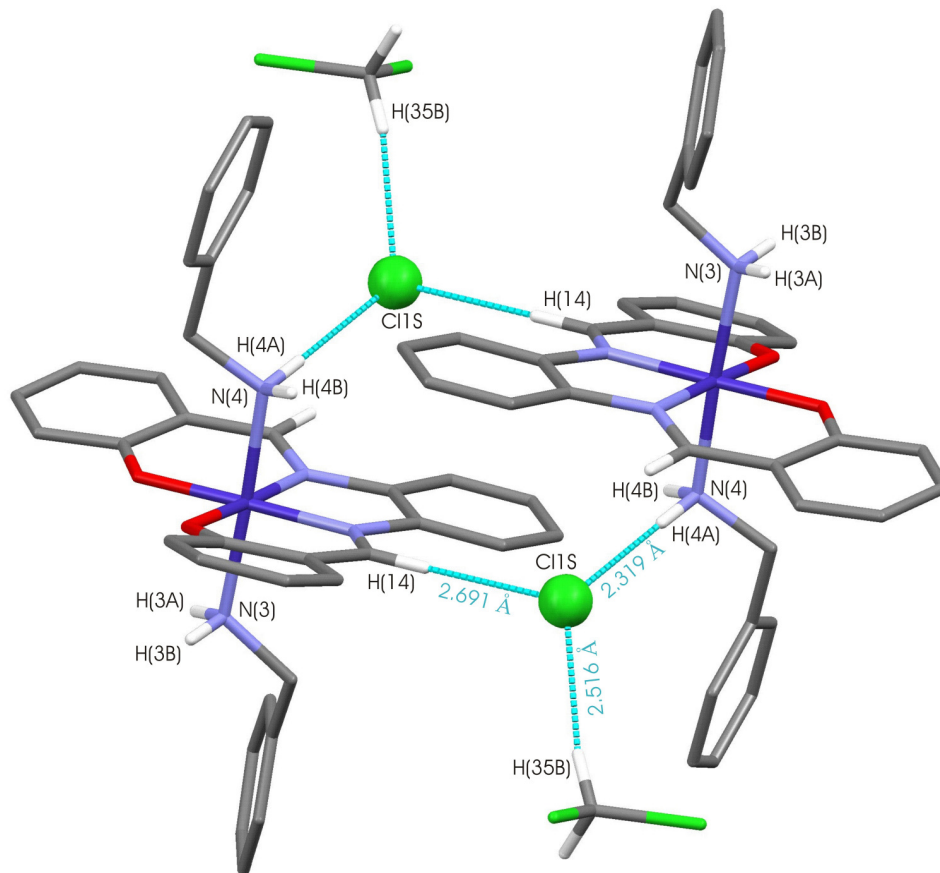


**Figure 5.3.9:** Short contact interactions between adjacent  $[\text{Co}(\text{salophen})(\text{BzNH}_2)_2]\text{Cl}\cdot\text{CH}_2\text{Cl}_2$  molecules. H atoms not involved in the interactions have been omitted for clarity.

The average  $\text{Co}-\text{N}_{\text{axial}}$  bond distance for  $[\text{Co}(\text{salophen})(\text{BuNH}_2)_2]^+$  is longer than the average  $\text{Co}-\text{N}_{\text{axial}}$  bond distance for  $[\text{Co}(\text{salophen})(\text{BzNH}_2)_2]^+$  by  $\sim 0.007 \text{ \AA}$ . The average  $\text{Co}-\text{N}_{\text{chelate}}$  bond distance for  $[\text{Co}(\text{salophen})(\text{BzNH}_2)_2]^+$  is longer than the average  $\text{Co}-\text{N}_{\text{chelate}}$  bond distance for  $[\text{Co}(\text{salophen})(\text{BuNH}_2)_2]^+$  by  $\sim 0.005 \text{ \AA}$ . These bonds are, within a standard error limit of  $4\sigma$ , equivalent for the cations, as might be expected for two primary amine derivatives.

The structure data details for  $[\text{Co}(\text{salophen})(\text{BuNH}_2)_2]^+$  and  $[\text{Co}(\text{salophen})(\text{BzNH}_2)_2]^+$  are presented in **Table 5.3.1** for comparison.

**Table 5.3.1:** Summary of the crystal data of  $[\text{Co}(\text{salophen})(\text{BuNH}_2)_2]^+$  and  $[\text{Co}(\text{salophen})(\text{BzNH}_2)_2]^+$ .

Crystal data	$[\text{Co}(\text{salophen})(\text{BuNH}_2)_2]^+$	$[\text{Co}(\text{salophen})(\text{BzNH}_2)_2]^+$
Chemical formula	$\text{C}_{29.50}\text{H}_{39}\text{Cl}_4\text{CoN}_4\text{O}_2$	$\text{C}_{35}\text{H}_{34}\text{Cl}_3\text{CoN}_4\text{O}_2$
Cell setting	monoclinic	triclinic
Space group	$C2/c$	$P-1$
$a / \text{\AA}$	17.284(2)	11.172(16)
$b / \text{\AA}$	19.330(13)	11.564(16)
$c / \text{\AA}$	19.138(2)	12.859(4)
$\alpha / ^\circ$	90	76.485(18)
$\beta / ^\circ$	97.390(10)	84.583(18)
$\gamma / ^\circ$	90	83.213(12)
$T / \text{K}$	100(2)	100(2)
$Z$	8	2
$V / \text{\AA}^3$	6341.1(11)	1600.2(5)
$R_1$	0.0475	0.0694

**Table 5.3.2:** Selected bond lengths for  $[\text{Co}(\text{salophen})(\text{BuNH}_2)_2]^+$  and  $[\text{Co}(\text{salophen})(\text{BzNH}_2)_2]^+$ .<sup>a</sup>

Bond	$[\text{Co}(\text{salophen})(\text{BuNH}_2)_2]^+$	$[\text{Co}(\text{salophen})(\text{BzNH}_2)_2]^+$
	Length / $\text{\AA}$	Length / $\text{\AA}$
Co-N(1)	1.9029(15)	1.907(4)
Co-N(2)	1.8953(15)	1.901(4)
Co-N(3)	1.9803(16)	1.972(4)
Co-N(4)	1.9757(16)	1.971(4)
Co-O(1)	1.9044(13)	1.916(3)
Co-O(2)	1.8989(13)	1.887(3)

<sup>a</sup>Distance esd's are given in parenthesis.

## X-ray structure analysis of [Co(salophen)(*N*-Me-Pipz)(OAc)]

[Co(salophen)(*N*-Me-Pipz)(OAc)] crystallised in the monoclinic space group  $P2_1/a$ . The asymmetric unit consists of the [Co(salophen)(*N*-Me-Pipz)(OAc)] molecule, a H<sub>2</sub>O molecule and an oxygen atom belonging to a second water molecule; we were unable to locate clearly the H atoms of this solvent molecule in the 3D difference Fourier map.

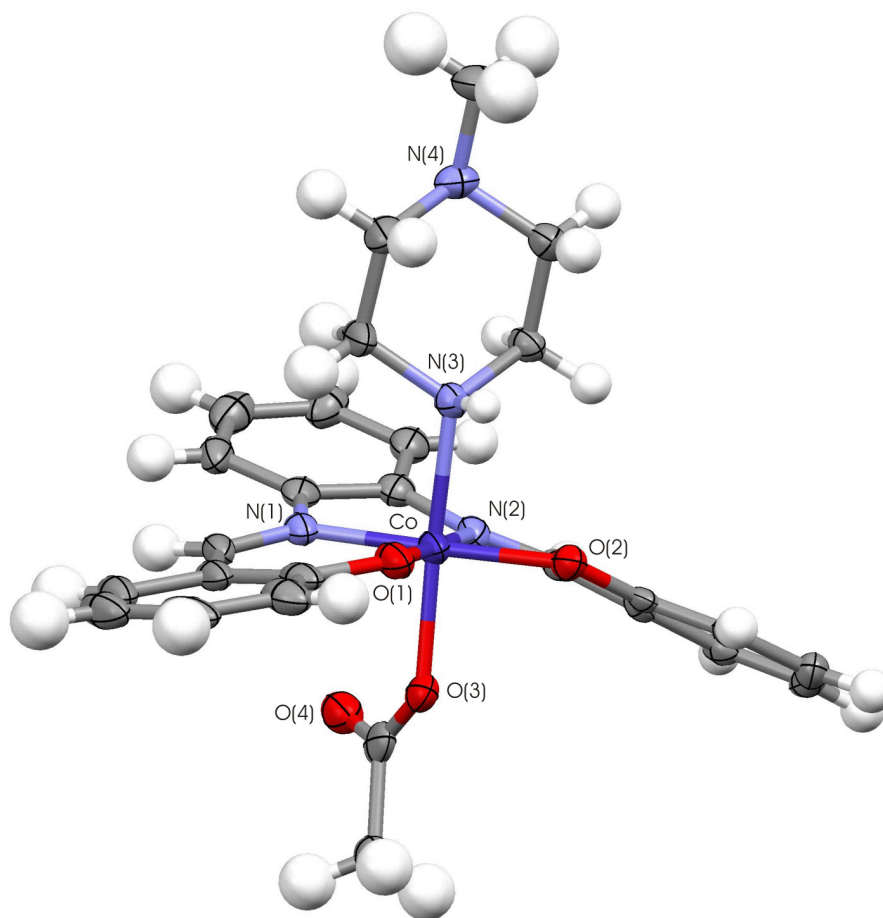


**Figure 5.3.10:** Partially labelled thermal ellipsoid plot of the X-ray structure of [Co(salophen)(*N*-Me-Pipz)(OAc)]. Solvent molecules have been omitted for clarity. Thermal ellipsoids are drawn at the 50% probability level with isotropic H atoms.

The salophen ligand has a highly non-planar conformation in this complex, a structural hallmark that reflects coordination of one bulky 2° amine ligand trans to a small acetate ion.

The phenoxy phenyl rings clearly tip away from the  $\alpha$ -CH<sub>2</sub> groups of the axial *N*-MePipz ligand to eliminate undue steric strain between the equatorial and axial ligands.

The unit cell packing consists of four [Co(salophen)(*N*-Me-Pipz)(OAc)] molecules.

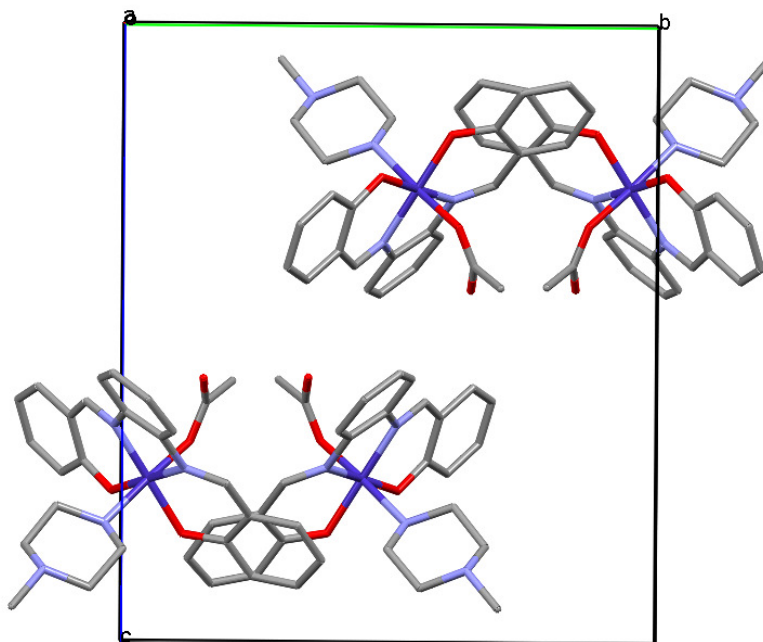


**Figure 5.3.11:** Packing diagram for the unit cell of [Co(salophen)(*N*-Me-Pipz)(OAc)] viewed along the *a*-axis. H atoms and solvent molecules have been omitted for clarity.

Short contacts exist between N(1) and N(2) of H<sub>2</sub>salophen and O(4) of the acetate ligand. There are also short contact interactions between O1S of the water molecule and O(2) of H<sub>2</sub>salophen as well as between O2S and O1S of the solvent water molecules (**Figure 5.3.12**). These interactions are consistent with hydrogen bonding.

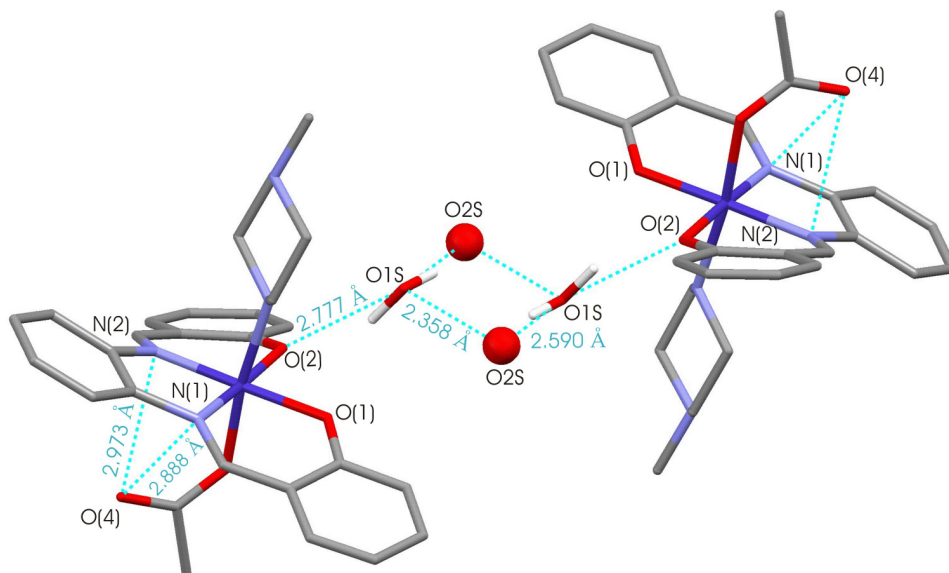


**Figure 5.3.12:** Short contacts between neighbouring  $[\text{Co}(\text{salophen})(N\text{-Me-Pipz})(\text{OAc})]$  molecules and solvent water molecules as well as within the molecule itself.

### X-ray structure analysis of $[\text{Co}(\text{salophen})(\text{Pip})_2](\text{OAc})$

$[\text{Co}(\text{salophen})(\text{Pip})_2](\text{OAc})$  crystallised in the monoclinic space group  $P2_1/c$ . the asymmetric unit consists of the  $[\text{Co}(\text{salophen})(\text{Pip})_2]^+$  cation and an acetate ion as the counter ion.

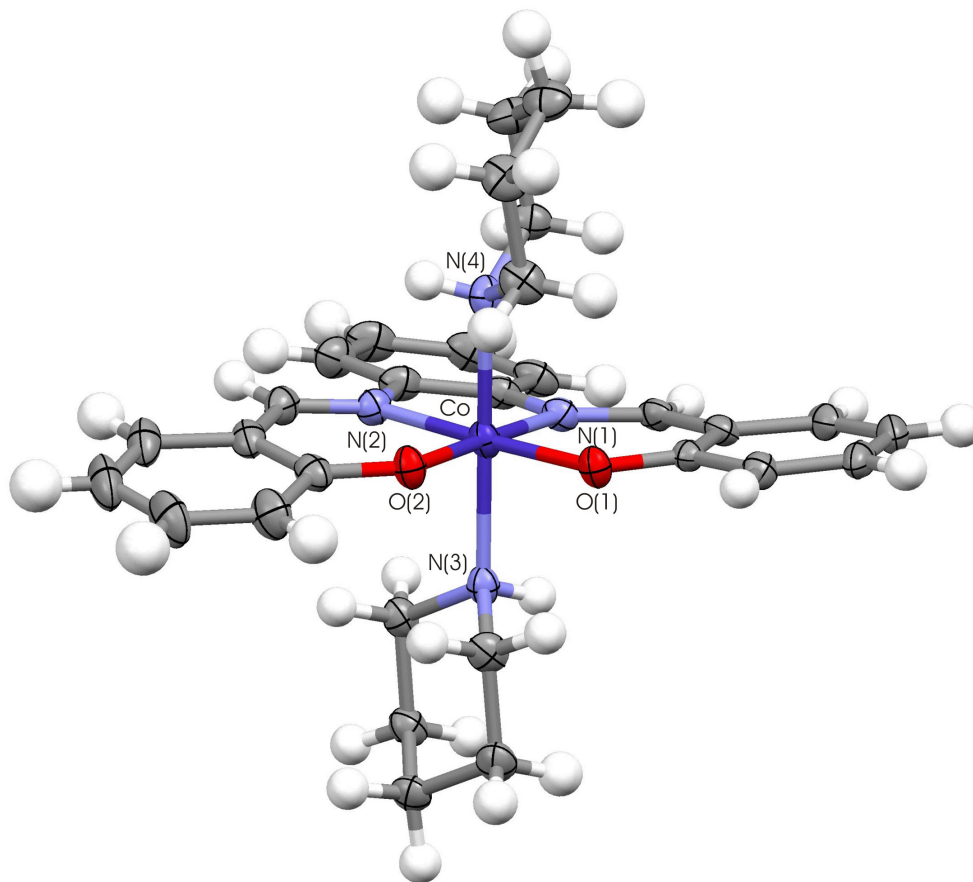


**Figure 5.3.13:** Partially labelled thermal ellipsoid plot of the X-ray structure of  $[\text{Co}(\text{salophen})(\text{Pip})_2](\text{OAc})$ . The acetate ion has been omitted for clarity. Thermal ellipsoids are drawn at the 50% probability level with isotropic H atoms.

The  $\text{H}_2\text{salophen}$  conformation is clearly non-planar; however, the degree of distortion of the ligand is noticeably smaller than in the mixed ligand complex  $[\text{Co}(\text{salophen})(N\text{-MePipz})(\text{OAc})]$ . Steric effects between the bulky secondary amine ligands and  $\text{H}_2\text{salophen}$  chelate appear to be more balanced when two bulky axial ligands are coordinated to the metal.

The unit cell packing consists of four  $[\text{Co}(\text{salophen})(\text{Pip})_2]^+$  cations and four acetate ions.

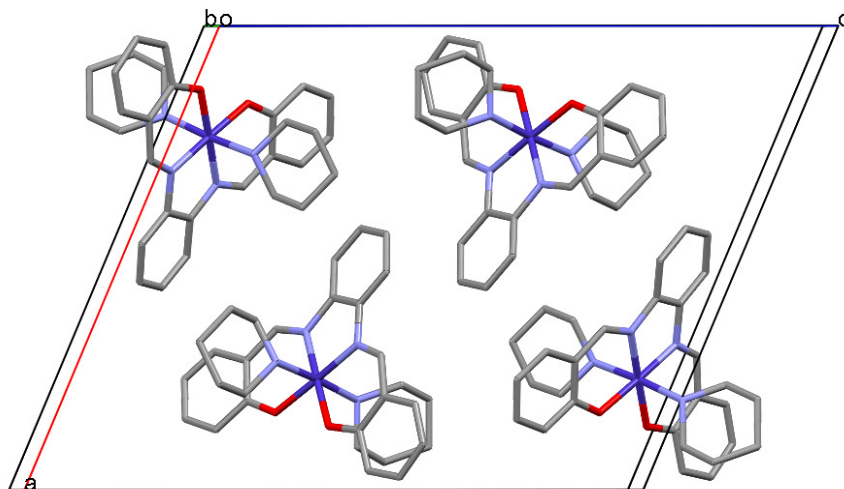


**Figure 5.3.14:** Packing diagram for the unit cell for  $[\text{Co}(\text{salophen})(\text{Pip})_2](\text{OAc})$  viewed along the  $b$ -axis. The acetate ions and H atoms are omitted for clarity.

There are short contact interactions between H(400) on the nitrogen atom of piperidine and O2S of the acetate ion as well as between H(29A) on the piperidine group and H31S on the methyl group of the acetate ion. There is also a short contact interaction between O1S on the acetate ion and C(7) of the imine carbon. Between H(300) on the nitrogen atom of the piperidine and O1S on the acetate molecule, there exists a hydrogen bond. The interaction distance is short at 2.19 Å. Although the H(400)⋯O2S distance is considerably longer (2.45 Å), this is clearly also a N-H⋯O hydrogen bond.<sup>100</sup>

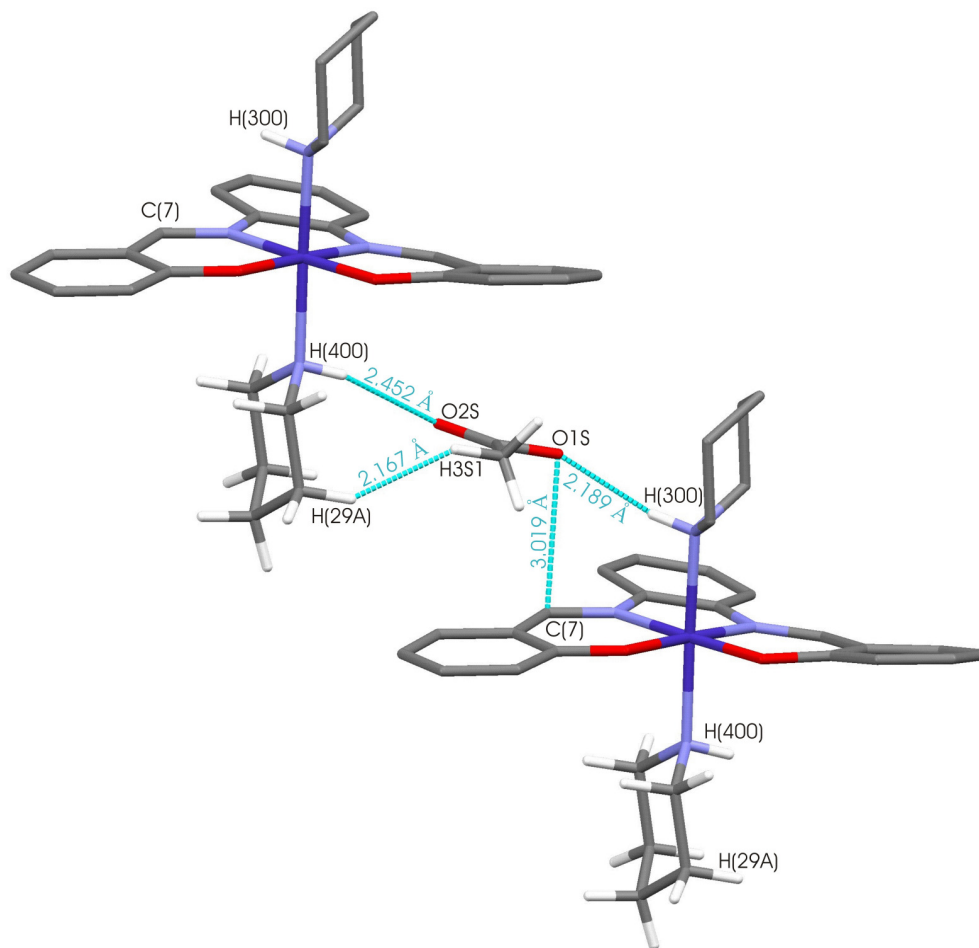


**Figure 5.3.15:** Short contact interactions between the acetate counterion and adjacent [Co(salophen)(Pip)<sub>2</sub>]<sup>+</sup> cations.

Amirnasr *et al.* were able to obtain crystal structures of [Co(salophen)(morpholine)<sub>2</sub>]ClO<sub>4</sub> (XEZQOI<sup>59</sup>) and [Co(salophen)(pyrrolidine)<sub>2</sub>]ClO<sub>4</sub> (XEZQUO<sup>59</sup>) but were unable to obtain a crystal structure of [Co(salophen)(piperidine)<sub>2</sub>]ClO<sub>4</sub>. The structural details of these complexes as well as that of [Co(salophen)(Pip)<sub>2</sub>](OAc) are presented in **Table 5.3.3** for comparison.

**Table 5.3.3:** Summary of key crystallographic data of XEZQOI<sup>59</sup>, XEZQUO<sup>59</sup> and our structure of [Co(salophen)(Pip)<sub>2</sub>](OAc).

Crystal data	XEZQOI <sup>59</sup>	XEZQUO <sup>59</sup>	[Co(salophen)(Pip) <sub>2</sub> ]
Chemical formula	C <sub>28</sub> H <sub>32</sub> ClCoN <sub>4</sub> O <sub>8</sub>	C <sub>28</sub> H <sub>32</sub> ClCoN <sub>4</sub> O <sub>6</sub>	C <sub>32</sub> H <sub>39</sub> CoN <sub>4</sub> O <sub>4</sub>
Cell setting	triclinic	tetragonal	monoclinic
Space group	<i>P</i> -1	<i>I</i> 4 <sub>1</sub> / <i>a</i>	<i>P</i> 2/ <i>c</i>
<i>a</i> / Å	9.4474(8)	31.713(2)	16.1010(6)
<i>b</i> / Å	10.2805(9)	31.713(2)	10.1199(5)
<i>c</i> / Å	15.0018(13)	10.7501(8)	19.7187(7)
$\alpha$ / °	106.492(2)	90	90
$\beta$ / °	91.190(2)	90	112.750(3)
$\gamma$ / °	98.732(2)	90	90
<i>T</i> / K	293(2)	293(2)	100(2)
<i>Z</i>	2	16	4
<i>V</i> / Å <sup>3</sup>	1377.8(2)	10811.7(11)	2963.0(2)
<i>R</i> <sub>1</sub>	0.0457	0.0498	0.0584

**Table 5.3.4:** Summary of relevant bond lengths of XEZQOI<sup>59</sup>, XEZQUO<sup>59</sup> and [Co(salophen)(Pip)<sub>2</sub>](OAc).

Bond lengths	XEZQOI <sup>59</sup>	XEZQUO <sup>59</sup>	[Co(salophen)(Pip) <sub>2</sub> ] <sup>+</sup>
Co-N <sub>axial</sub> ave / Å	2.031(2)	2.005(2)	2.024(3)
Co-N <sub>chelate</sub> ave / Å	1.893(2)	1.8878(14)	1.898(3)
Co-O ave / Å	1.882(2)	1.8847(12)	1.878(2)

The selected bond lengths presented in **Table 5.3.4** are similar for all three complexes, despite having different space group settings. In all three complexes, H<sub>2</sub>salophen is not planar. The mean Co-N<sub>axial</sub> distance for the morpholine derivative is closest to that of the piperidine complex since the axial ligands are both 6-membered rings. The pyrrolidine analogue, in contrast, shows a markedly shorter Co-N<sub>axial</sub> distance due to the fact that the 5-membered heterocycle is sterically less encumbered than a 6-membered heterocycle.

The average Co-N bond distance for  $[\text{Co}(\text{salophen})(\text{Pip})_2]$  is longer than the  $\text{Co-N}_{\text{axial}}$  bond distance for  $[\text{Co}(\text{salophen})(N\text{-Me-Pipz})(\text{OAc})]$  by  $\sim 0.019 \text{ \AA}$ . The average  $\text{Co-N}_{\text{chelate}}$  bond distance for  $[\text{Co}(\text{salophen})(\text{Pip})_2]^+$  is longer than the average  $\text{Co-N}_{\text{chelate}}$  bond distance by  $\sim 0.011 \text{ \AA}$ . For  $[\text{Co}(\text{salophen})(N\text{-MePipz})(\text{OAc})]$ , the highly non-planar chelate conformation permits closer approach of the bulky axial ligand, leading to a measurably shorter  $\text{Co-N}_{\text{axial}}$  distance. In the bis(piperidine) analogue, a less ruffled chelate conformation favours enhanced chelate····axial ligand nonbonded interactions and this, in turn, is likely to require longer  $\text{Co-N}_{\text{axial}}$  distances to alleviate some of the steric strain in the direction of the axial ligands.

## Chapter Six: Thermodynamics

### 6.1 Introduction

Stability constants are defined as equilibrium constants that express the tendency of a species to form from its component parts. Generally, the larger the stability constant the more stable the species. Stability constants or equilibrium constants for metal complex formation have been used as an efficient assessment for the affinity of a ligand for a metal ion in solution. It has also served as a quantitative indication of the success or failure of ligand design. The earliest quantitative measurements were pioneered by von Euler<sup>102</sup> and Bodlander<sup>103</sup> and were concerned only with the determination of empirical formulas and overall formation constants.<sup>104</sup>

For the system;



Where M is a metal and L is the ligand, the stability constant can be calculated as follows:

$$K = \frac{[ML]}{[M][L]} \quad (1)$$

The total concentration of the metal is given by:

$$[M]_{total} = [M] + [ML] \quad (2)$$

From equation (1):

$$[ML] = K[M][L] \quad (3)$$

Hence equation (3) becomes:

$$\begin{aligned} [M]_{total} &= [M] + K[M][L] \\ &= [M](1 + K[L]) \end{aligned} \quad (4)$$

Arranging equation (4) gives:

$$[M] = \frac{[M]_{total}}{(1 + K[L])} \quad (5)$$

Equation (5) illustrates that the concentration of M depends on the stability constant, K, and the free concentration of the ligand. There are various methods of determining stability constants, such as potentiometry, spectrophotometry, NMR spectroscopy, ion exchange, reaction kinetics and others.<sup>104</sup>

For our study on stability constants, we chose the method of spectroscopic titrations using UV-visible spectrophotometry. While results have been obtained and the stability constants calculated, it must be said that these results in some cases are not entirely reliable. The main reason is that the spectral changes accompanying ligand replacement were very small. This, coupled with overlapping stepwise binding constants  $K_1$  and  $K_2$ , made accurate fits of the experimental data and thus accurate estimation of thermodynamic variables difficult.

## **6.2 Experimental**

UV-visible spectra and titration data were collected with a Perkin Elmer Lambda 45 double beam scanning spectrophotometer using DMSO solutions in 1.0 cm path length quartz cuvettes. The method for the titrations was based on the addition of small aliquots of a solution of amine to a solution of [Co(salophen)(OAc)] and then recording a UV-visible spectrum after addition in order to monitor the progress of the reaction.

The amines used (butylamine, benzylamine,  $\alpha$ -methylbenzylamine, piperidine, dibutylamine and *N*-methylpiperazine) were freshly distilled and dried over CaH<sub>2</sub> and stored over activated molecular sieves (4 Å).

### **6.2.1 Preparation of [Co(salophen)(OAc)] Stock Solution**

200.9 mg [Co(salophen)(OAc)] was placed into a 50 ml volumetric flask and made up to the mark with DMSO. An initial spectrum of this solution was recorded and it was found that the recorded spectrum was off scale. The original stock solution was then diluted by taking 5 ml of the original stock solution and placing it into a 50 ml volumetric flask and making it up to the mark using DMSO. The concentration of the new stock solution was  $9.25 \times 10^{-4}$  M.

### **6.2.2 Preparation of Amine Stock Solutions**

Two stock solutions of approximate concentration  $5 \times 10^{-3}$  M (Solution A) and  $5 \times 10^{-1}$  M (Solution B) were prepared. The stock solutions were prepared by transferring the volume of the amine required, using a Hamilton microlitre syringe, into a 50 ml volumetric flask and making it up to the mark using DMSO.

### 6.2.3 The Titration

Before the actual titration was carried out, qualitative spectral scans were acquired. This was done by placing [Co(salophen)(OAc)] and DMSO in the cuvette and adding the respective amine dropwise. After each addition of the amine, the spectrum was recorded. This was done to establish at what wavelengths the greatest change was occurring.

The reference cell and the titration cell were filled with 2 ml of DMSO. To the titration cell, 100  $\mu$ l of [Co(salophen)(OAc)] stock solution was added using an Eppendorf pipette (Netherler – Hinz gmbH) and the spectrum was recorded. A magnetic flea was placed in the titration cell in order to stir the solution.

The UV/visible spectrophotometer was set to scan spectra between 1100 nm and 330 nm. The thermostat was initially set at 25 °C. Before running a baseline, the contents of the cells were stirred in the spectrometer for 1 minute. After a baseline was run the initial spectrum was recorded. Absorbance data were recorded at various wavelengths. 4  $\mu$ l of Solution A was added to the titration cell using a 10  $\mu$ l Hamilton syringe and stirred for 1 minute before recording the absorbance readings at different wavelengths. The corrected absorbance due to dilution effects was calculated at each wavelength.

For the titration of [Co(salophen)(OAc)] with benzylamine, the ligand was added to the reference cell and the titration cell. This procedure allowed for cancellation of the absorbance contribution from the free ligand at shorter wavelengths.

The next aliquot of ligand was added and the process was repeated until the end of the reaction. The titration was then repeated with the same ligand at variable temperatures, i.e., 30 °C, 35 °C, 40 °C and 45 °C.

The entire process was carried out with primary amines (butylamine, benzylamine and  $\alpha$ -methylbenzylamine) and secondary amines (piperidine, *N*-methylpiperazine and dibutylamine).

**Table 6.2.3.1:** Typical titrant volumes for titration.

<b>Addition Number</b>	<b>[Amine] / M</b>	<b>Volume (Aliquot) of titrant / <math>\mu\text{l}</math></b>
1	$5 \times 10^{-3}$	4
2		13
3		21
4		30
5		40
6		45
7		94
8		150
9		217
10	$5 \times 10^{-1}$	3
11		5.5
12		16
13		33
14		51
15		118
16		256
17		435

## 6.3 Results and Discussion

### 6.3.1 Titration Spectra for Primary Amines

The titration spectra for butylamine, benzylamine and  $\alpha$ -methylbenzylamine have the same spectral shape and as a result the mechanism for the reaction between  $[\text{Co}(\text{salophen})(\text{OAc})]$  and the above mentioned amines can be assumed to be the same. The titration results for each primary ligand used will be discussed in detail.

#### 6.3.1.1 Titration Spectra for $[\text{Co}(\text{salophen})(\text{BuNH}_2)_2](\text{OAc})$

Figure 6.3.1.1 shows the titration spectra for  $[\text{Co}(\text{salophen})(\text{BuNH}_2)_2](\text{OAc})$  at 25 °C and at the specified butylamine concentrations.

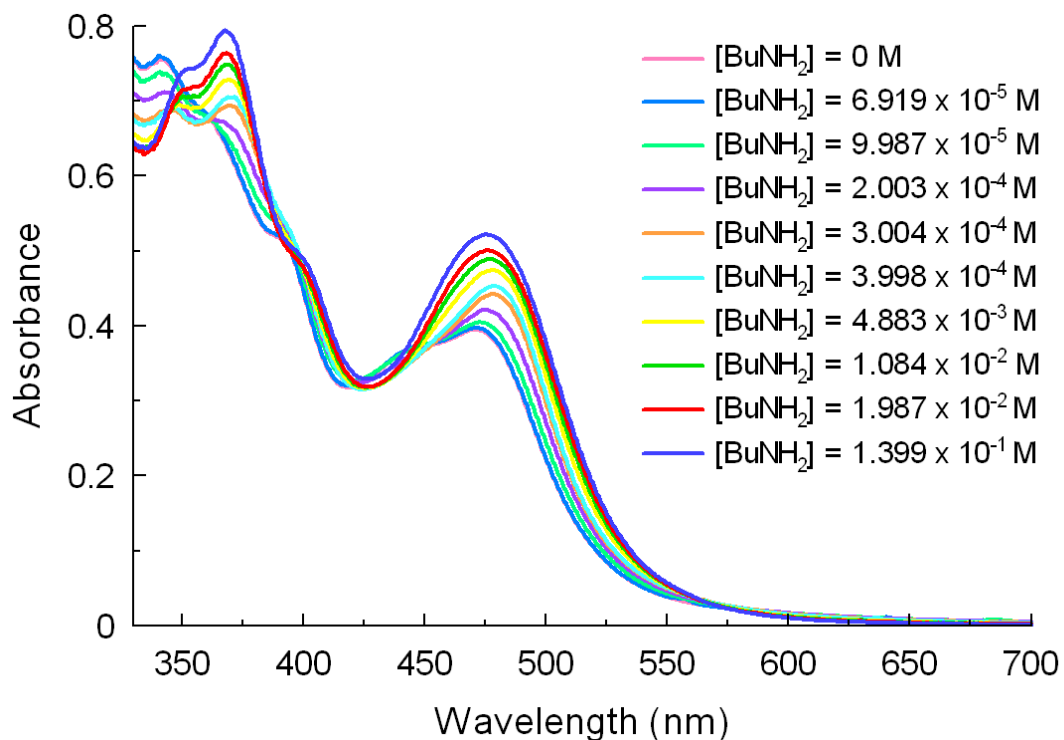


**Figure 6.3.1.1:** Superimposed titration spectra, showing the typical spectral progression for the reaction between  $[\text{Co}(\text{salophen})(\text{OAc})]$  and  $\text{BuNH}_2$ , at specified concentrations of the ligand at 25 °C. These spectra have been corrected for dilution.

The initial spectrum at 0 M concentration of butylamine, shows the spectrum of [Co(salophen)(OAc)], with a prominent peak at 472 nm and two shoulders at 362 nm, 391 nm. As the butylamine is added, even at a low concentration of  $9.987 \times 10^{-5}$  M, the shoulder at 362 nm begins to decrease in intensity. At concentrations of  $3.004 \times 10^{-4}$  M a peak at 364 nm and a peak at 470 nm begin to grow. At concentrations of  $1.987 \times 10^{-2}$  M and above, prominent peaks can be seen at 364 nm and 470 nm and two shoulders are observed at 354 nm and 390 nm.

**Figure 6.3.1.2** shows the titration spectra for [Co(salophen)(BuNH<sub>2</sub>)<sub>2</sub>](OAc) at 45 °C and at the specified butylamine concentrations. Absorption spectra for [Co(salophen)(BuNH<sub>2</sub>)<sub>2</sub>](OAc) at 0 °C, 35 °C and 40 °C are available in **Appendix D.4**.

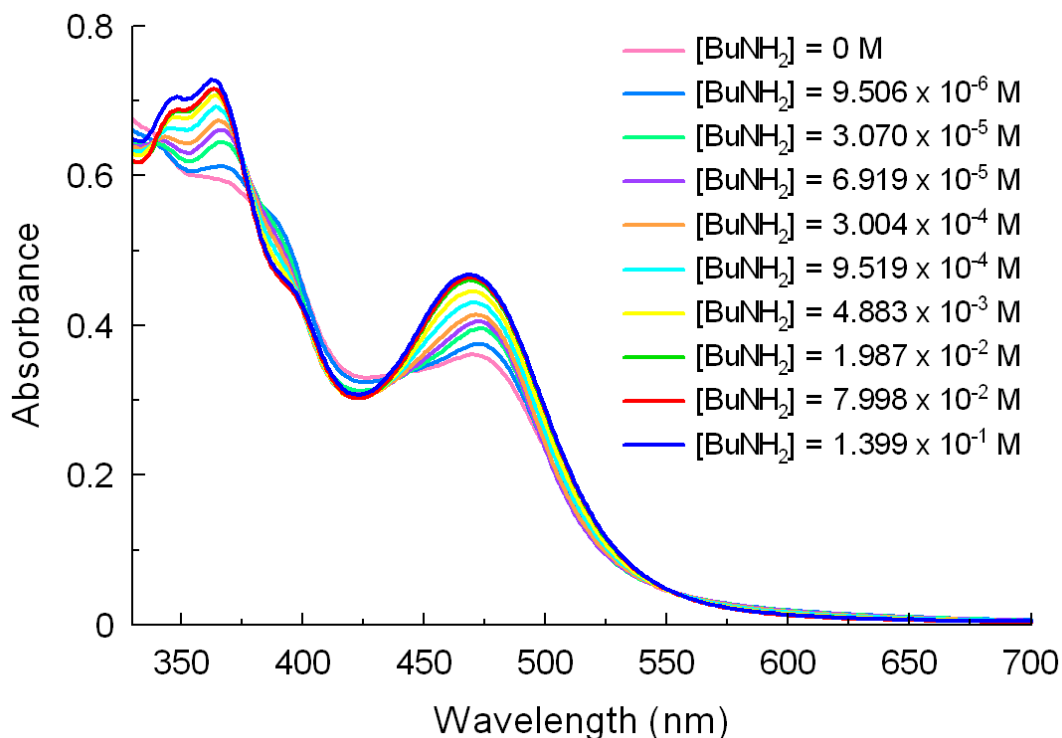


**Figure 6.3.1.2:** Superimposed titration spectra, showing the typical spectral progression for the reaction between [Co(salophen)(OAc)] and BuNH<sub>2</sub>, at specified concentrations of the ligand at 45 °C. These spectra have been corrected for dilution.

At 45 °C and at low concentrations of  $3.070 \times 10^{-5}$  M, the ill-defined maxima (below 400 nm) of the [Co(salophen)(OAc)] complex disappears immediately and the bands of the complex begin to appear. The shoulder at 390 nm appears to be more intense at higher temperatures.

### 6.3.1.2 Titration Spectra for [Co(salophen)(BzNH<sub>2</sub>)<sub>2</sub>](OAc)

Figure 6.3.1.3 shows the titration spectra for [Co(salophen)(BzNH<sub>2</sub>)<sub>2</sub>](OAc) at 25 °C and at the specified benzylamine concentrations. Spectra for this system are presented here owing to some subtle differences relative to the spectra for the butylamine analogue. These differences appear in the region below 375 nm and may reflect the aromatic nature of benzylamine.

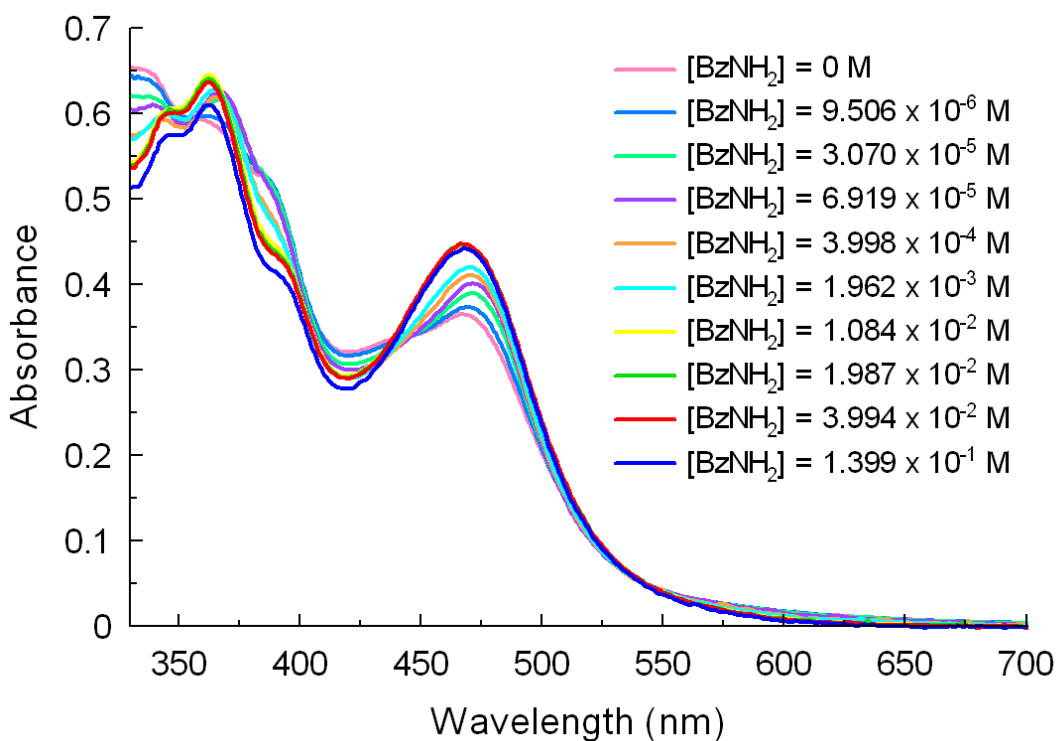
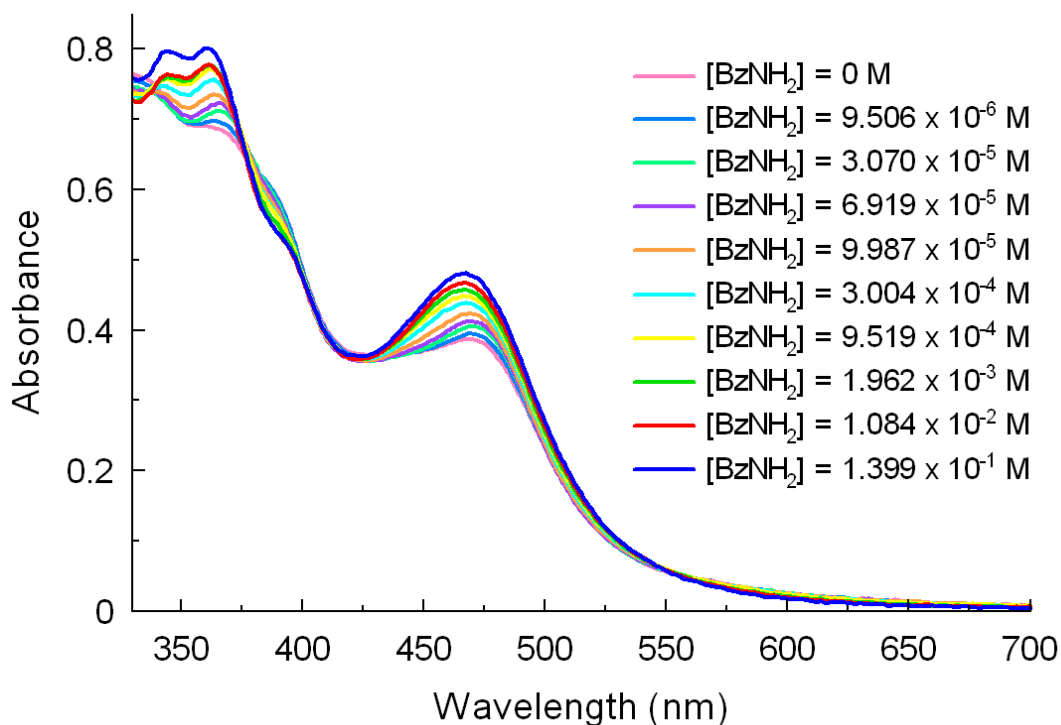


Figure 6.3.1.3: Superimposed titration spectra, showing the typical spectral progression for the reaction between [Co(salophen)(OAc)] and BzNH<sub>2</sub>, at specified concentrations of the ligand at 25 °C. These spectra have been corrected for dilution.

The initial spectrum at 0 M concentration of benzylamine, shows the spectrum of [Co(salophen)(OAc)] with a peak at 468 nm and two shoulders at 365 nm, 388 nm. At low concentrations of the ligand, the shoulder at 365 nm decreases in intensity and eventually disappears. A shoulder at 394 nm begins to appear, even at low concentrations of  $3.070 \times 10^{-5}$  M of the ligand. At concentrations of  $9.987 \times 10^{-5}$  M, a peak at 362 nm appears. A peak at 343 nm begins to appear at concentrations of  $1.987 \times 10^{-2}$  M. At concentrations of  $1.399 \times 10^{-1}$  M, prominent bands at 343 nm, 362 nm and 467 nm are observed and a shoulder at 394 nm is observed.

**Figure 6.3.1.4** shows the titration spectra for [Co(salophen)(BzNH<sub>2</sub>)<sub>2</sub>](OAc) at 45 °C and at the specified benzylamine concentrations. Absorption spectra for [Co(salophen)(BzNH<sub>2</sub>)<sub>2</sub>](OAc) at 30 °C, 35 °C and 40 °C are available in **Appendix D.5**.



**Figure 6.3.1.4:** Superimposed titration spectra, showing the typical spectral progression for the reaction between [Co(salophen)(OAc)] and BzNH<sub>2</sub>, at specified concentrations of the ligand at 45 °C. These spectra have been corrected for dilution.

At higher temperatures, the peak at 343 nm and 362 nm appears at low concentrations of the ligand. The shoulder at 394 nm is less intense at higher temperatures.

### 6.3.1.3 Titration Spectra for [Co(salophen)( $\alpha$ -MeBzNH<sub>2</sub>)<sub>2</sub>](OAc)

**Figure 6.3.1.5:** shows the titration spectra for [Co(salophen)( $\alpha$ -MeBzNH<sub>2</sub>)<sub>2</sub>] at 25 °C and at the specified  $\alpha$ -methylbenzylamine concentrations. These traces are very similar to the spectra of butylamine and benzylamine.

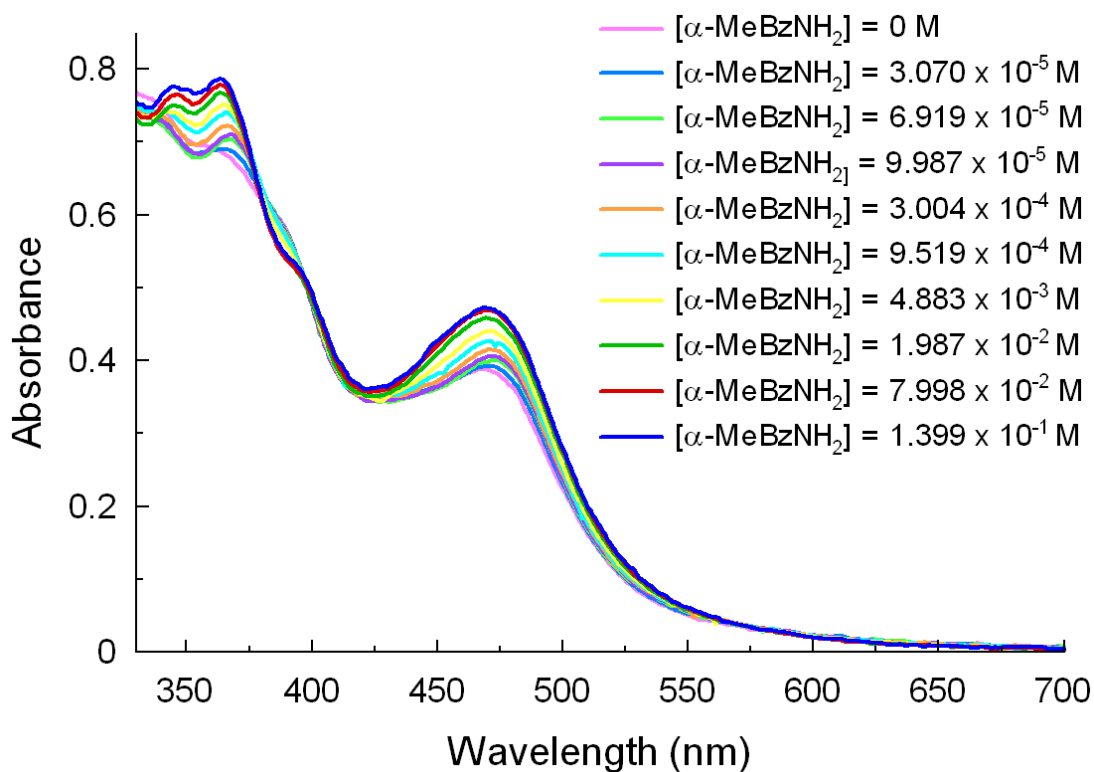


**Figure 6.3.1.5:** Superimposed titration spectra, showing the typical spectral progression for the reaction between [Co(salophen)(OAc)] and  $\alpha$ -MeBzNH<sub>2</sub>, at specified concentrations of the ligand at 25 °C. These spectra have been corrected for dilution.

The initial spectrum at 0 M concentration of  $\alpha$ -methylbenzylamine, shows the spectrum of [Co(salophen)(OAc)] with peak at 469 nm and two shoulders at 367 nm and 392 nm. At low concentrations of the ligand, the shoulder of the [Co(salophen)(OAc)] complex at 367 nm

decreases in intensity and eventually disappears and a peak at 370 nm begins to appear. At concentrations of  $9.519 \times 10^{-4}$  M, a peak at 342 nm appear. At high ligand concentrations of  $1.399 \times 10^{-1}$  M, prominent bands can be seen at 342 nm, 360 nm and 477 nm.

**Figure 6.3.1.6** shows the titration spectra for  $[\text{Co}(\text{salophen})(\alpha\text{-MeBzNH}_2)_2](\text{OAc})$  at 45 °C and at the specified  $\alpha$ -methylbenzylamine concentrations. Absorption spectra for  $[\text{Co}(\text{salophen})(\alpha\text{-MeBzNH}_2)_2](\text{OAc})$  at 30 °C, 35 °C and 45 °C are available in **Appendix D.6**.

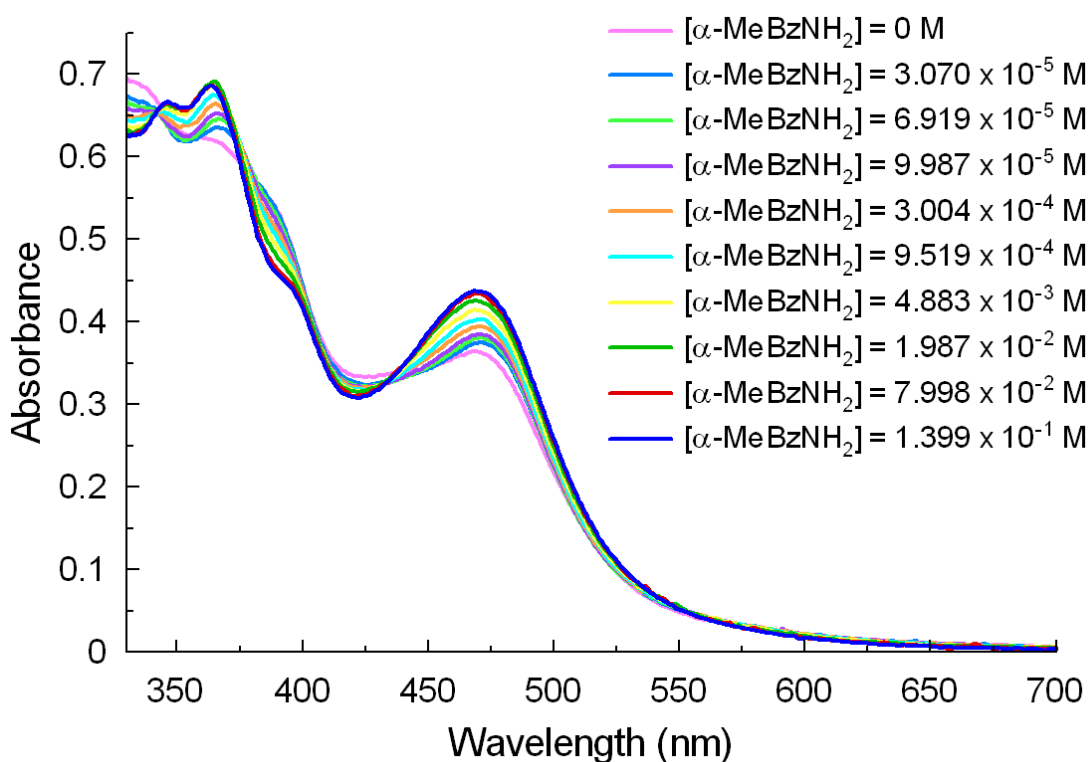


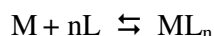
**Figure 6.3.1.6:** Superimposed titration spectra, showing the typical spectral progression for the reaction between  $[\text{Co}(\text{salophen})(\text{OAc})]$  and  $\alpha\text{-MeBzNH}_2$ , at specified concentrations of the ligand at 45 °C. These spectra have been corrected for dilution.

### 6.3.2 Analysis of Titration Results for Primary Amines

Each reaction was studied over a range of ligand concentrations ( $10^{-5}$  –  $10^{-1}$  M) and titrations were carried out at five different temperatures. The absorbance was recorded at wavelengths

where the greatest change in absorbance was observed at each concentration at the set temperature. At each of these wavelengths, a plot of absorbance versus  $\log$  [ligand] was obtained. The curve obtained was fitted by non-linear regression.

A model (**Model 1**) was derived in order to determine the stability constants for the reactions. This model was based on a mechanism where two ligands bind successively to the axial binding sites of the  $[\text{Co}(\text{salophen})]^+$  complex. The equilibrium constants  $K_1$  and  $K_2$  are easily distinguished. The derivation of this Model 1 is available in **Appendix D.1**.



### 6.3.2.1 Analysis of titration results for $[\text{Co}(\text{salophen})(\text{BuNH}_2)_2](\text{OAc})$

The absorbance, for the titration between  $[\text{Co}(\text{salophen})(\text{OAc})]$  and butylamine, was recorded at 364 nm and 475 nm. **Figure 6.3.2.1** shows the absorbance versus  $\log$   $[\text{BuNH}_2]$  at 25 °C and 364 nm and illustrates a typical fit of the model to the data.

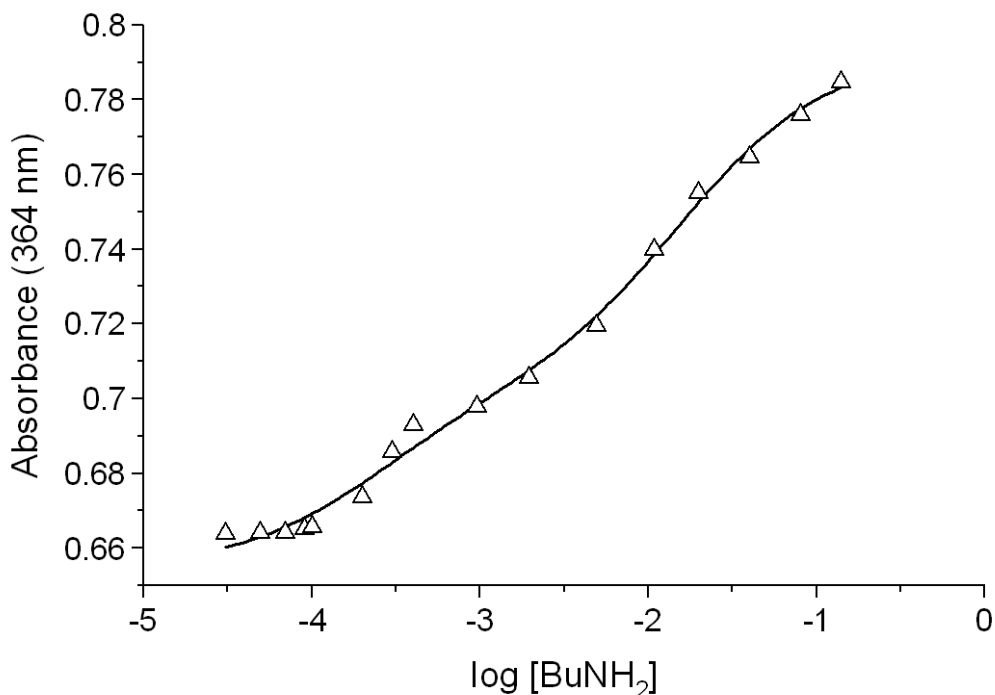


**Figure 6.3.2.1:** Reaction of  $[\text{Co}(\text{salophen})(\text{OAc})]$  with butylamine at 25 °C in DMSO, showing the typical shape of an equilibrium process consistent with the derived model.

Absorbance versus  $\log [\text{BuNH}_2]$  plots for the reaction of  $[\text{Co}(\text{salophen})(\text{OAc})]$  with butylamine at 30 °C, 35 °C, 40 °C and 45 °C and at 364 nm and 475 nm are available in **Appendix D.7**.

**Table 6.3.2.1:** Equilibrium constants obtained from the reaction between  $[\text{Co}(\text{salophen})(\text{OAc})]$  and butylamine at different temperatures.

Temperature (°C)	364 nm		475 nm	
	$K_1 / \text{M}^{-1}$	$K_2 / \text{M}^{-1}$	$K_1 / \text{M}^{-1}$	$K_2 / \text{M}^{-1}$
25	$4.1(0.4) \times 10^3$	$6.3(0.4) \times 10^1$	$5.7(0.5) \times 10^3$	$4.6(0.7) \times 10^1$
30	$1.1(0.07) \times 10^4$	$2.8(0.3) \times 10^2$	$2.7(0.3) \times 10^3$	$5.2(0.4) \times 10^2$
35	$1.8(0.1) \times 10^4$	$7.9(0.9) \times 10^2$	$8.6(0.4) \times 10^3$	$8.7(11) \times 10^1$
40	$4.1(0.3) \times 10^3$	$8.4(1.5) \times 10^0$	$3.4(0.1) \times 10^3$	$4.3(0.9) \times 10^2$
45	$1.0(0.04) \times 10^4$	$4.2(1.6) \times 10^2$	$5.7(0.2) \times 10^3$	$2.1(0.4) \times 10^2$

As the temperature increases,  $K_1$  and  $K_2$  are expected to decrease. From the data in **Table 6.3.2.1**, this is not observed. There is substantial scatter in the data and no reasonable trend exists for  $K_1$  or  $K_2$  at either of the analysis wavelengths. From **Figure 6.3.2.1**, it is evident that strong overlap of  $K_1$  and  $K_2$  occurs such that the separate binding steps are not clearly delineated. The estimation of  $K_1$  and  $K_2$  therefore becomes difficult when using non-linear regression methods. This problem clearly underpins the scattered values of  $K_1$  and  $K_2$  in **Table 6.3.2.1**. Attempts were made to linearise the data by plotting a graph of  $\log \{(A_0 - A_\infty)\}$  versus  $\log [\text{amine}]_{\text{free}}$ .  $\beta_2$  and  $n$  can be obtained from the slope and y-intercept respectively. However, linearising the data did not decrease the scattering of the values.

### 6.3.2.2 Analysis of titration results for $[\text{Co}(\text{salophen})(\text{BzNH}_2)_2](\text{OAc})$

Absorbances for the titration between  $[\text{Co}(\text{salophen})(\text{OAc})]$  and benzylamine were recorded at 472 nm. **Figure 6.3.2.2** shows the absorbance versus  $\log [\text{BzNH}_2]$  at 30 °C and 472 nm and illustrates a fit of the model to the data.

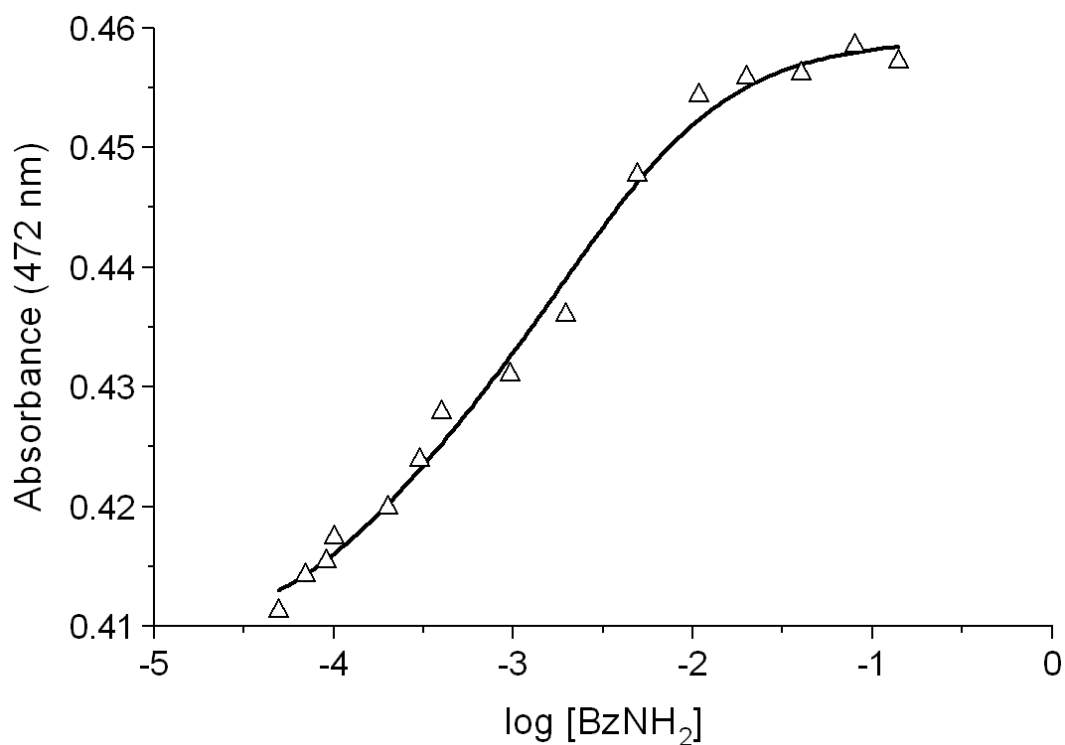


**Figure 6.3.2.2:** Reaction of [Co(salophen)(OAc)] with benzylamine at 30 °C in DMSO, showing the typical shape of an equilibrium process consistent with the derived model.

As can be seen in **Figure 6.3.2.2**, the spectral changes accompanying ligand replacement are not large (viz.: 0.05 A units), which is typical of low spin Co(III). It is also evident from the shape of the curve that the system has strongly overlapped  $K_1$  and  $K_2$  values.

Equilibrium processes for the reaction between [Co(salophen)(OAc)] and benzylamine at 25 °C, 35 °C, 40 °C and 45 °C are available in **Appendix D.8**.

**Table 6.3.2.2:** Table of equilibrium constants obtained from the reaction between [Co(salophen)(OAc)] and benzylamine at different temperatures.

Temperature (°C)	472 nm	
	$K_1 / M^{-1}$	$K_2 / M^{-1}$
25	$3.6(0.3) \times 10^2$	$5.9(1.3) \times 10^0$
30	$4.9(0.6) \times 10^3$	$3.3(0.3) \times 10^2$
35	$1.5(0.1) \times 10^4$	$4.0(0.3) \times 10^2$
40	$3.9(0.2) \times 10^3$	$3.4(1.2) \times 10^0$
45	$7.9(0.3) \times 10^3$	$3.2(0.4) \times 10^1$

Again there is no trend in the  $K_1$  and  $K_2$  values and the data shows a great amount of scatter.

### 6.3.2.3 Analysis of titration results for [Co(salophen)( $\alpha$ -MeBzNH<sub>2</sub>)<sub>2</sub>](OAc)

The absorbance for the titration between [Co(salophen)(OAc)] and  $\alpha$ -methylbenzylamine was recorded at 366 nm and 473 nm. **Figure 6.3.1.8** shows the absorbance versus log [ $\alpha$ -MeBzNH<sub>2</sub>] at 25 °C and 366 nm and illustrates a typical fit of the model to the data. In this case two independent processes appear to be better delineated from the shape of the curve.

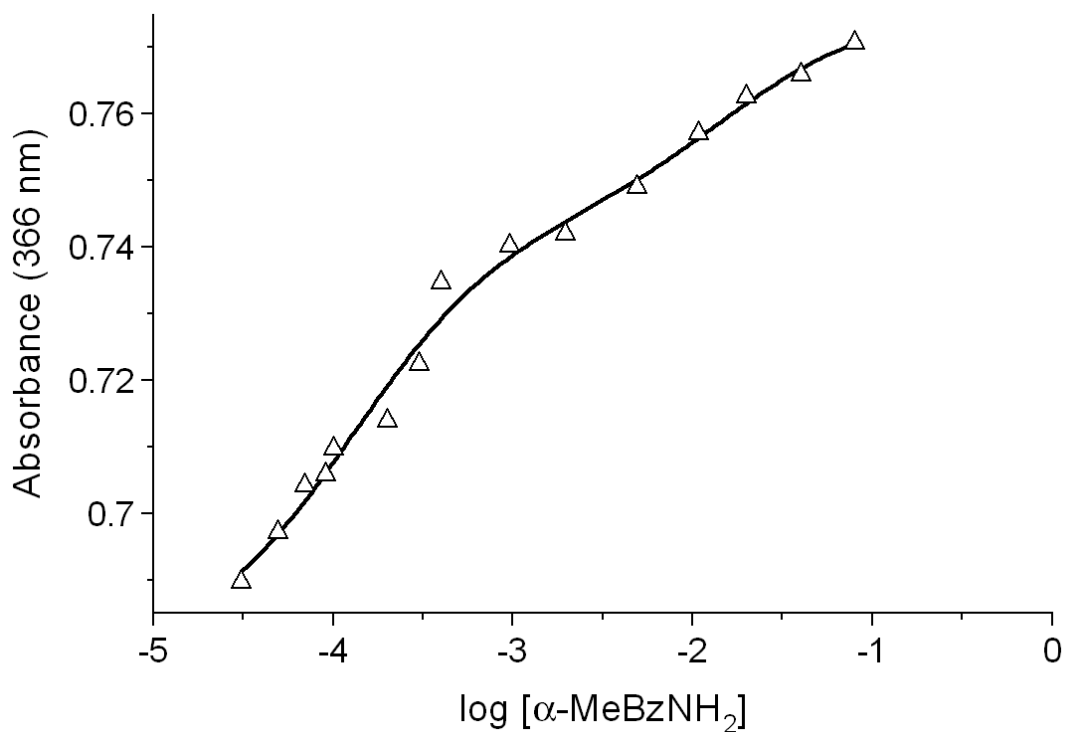


**Figure 6.3.2.3:** Reaction of [Co(salophen)(OAc)] with  $\alpha$ -methylbenzylamine at 25 °C in DMSO, showing the typical shape of an equilibrium process consistent with the derived model.

Equilibrium processes for the reaction between [Co(salophen)(OAc)] and  $\alpha$ -methylbenzylamine at 30 °C, 35 °C, 40 °C and 45 °C are available in **Appendix D.9**.

**Table 6.3.2.3:** Table of equilibrium constants obtained from the reaction between [Co(salophen)(OAc)] and  $\alpha$ -methylbenzylamine at different temperatures.

Temperature (°C)	366 nm		473 nm	
	$K_1 / M^{-1}$	$K_2 / M^{-1}$	$K_1 / M^{-1}$	$K_2 / M^{-1}$
25	$8.0(0.5) \times 10^3$	$6.4(1.0) \times 10^1$	$1.0(0.05) \times 10^4$	$9.1(0.5) \times 10^1$
30	$9.2(0.4) \times 10^3$	$2.4(0.3) \times 10^2$	$8.0(0.4) \times 10^3$	$2.2(0.1) \times 10^2$
35	$7.2(0.9) \times 10^3$	$4.6(1.8) \times 10^2$	$6.7(0.5) \times 10^3$	$8.1(1.1) \times 10^1$
40	$7.1(0.3) \times 10^3$	$2.1(1.7) \times 10^1$	$7.0(0.4) \times 10^3$	$4.6(0.4) \times 10^1$
45	$1.4(0.05) \times 10^4$	$5.2(0.7) \times 10^2$	$7.8(0.3) \times 10^3$	$5.8(0.3) \times 10^1$

From **Table 6.3.2.3**, there is no trend in the values of  $K_1$  and  $K_2$  at either of the wavelengths. The  $K$  values do not decrease with an increase in temperature as would be expected. As with butylamine and benzylamine, there is substantial scatter in the data. This is attributed to the strong overlap between  $K_1$  and  $K_2$  and the difficulty of obtaining these values accurately for a system with intrinsically small absorption changes.

### 6.3.3 Titration Spectra for Secondary Amines

The absorption spectra for the secondary amines differ from those of the primary amines. *N*-methylpiperazine, dibutylamine and piperidine have the same spectral shape and hence the reaction of  $[\text{Co}(\text{salophen})(\text{OAc})]$  with these amines can be assumed to follow the same mechanistic pathway. The titration results for the secondary amines used will be discussed in detail.

#### 6.3.3.1 Titration Spectra for $[\text{Co}(\text{salophen})(\text{N-MePipz})_2](\text{OAc})$

**Figure 6.3.3.1** shows the titration spectra for the reaction between  $[\text{Co}(\text{salophen})(\text{OAc})]$  and *N*-methylpiperazine at 25 °C and at the specified *N*-methylpiperazine concentrations.

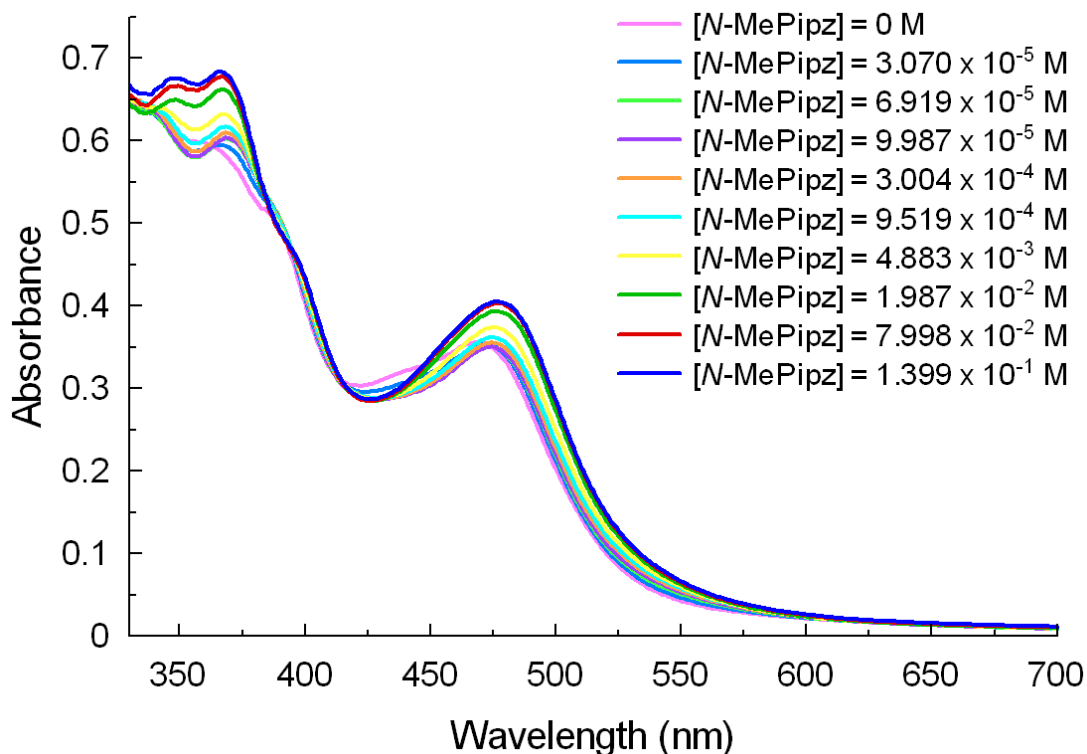


**Figure 6.3.3.1:** Superimposed titration spectra, showing the typical spectral progression for the reaction between  $[\text{Co}(\text{salophen})(\text{OAc})]$  and *N*-MePipz, at specified concentrations of the ligand at 25 °C. These spectra have been corrected for dilution.

As with the reaction with the primary amines, the initial spectrum at 0 M concentration of *N*-methylpiperzine shows the spectrum of  $[\text{Co}(\text{salophen})(\text{OAc})]$ , with a prominent peak at 469 nm and two shoulders at 365 nm, 388 nm. At concentrations of  $9.987 \times 10^{-5}$  M, a peak at 372 nm appears while at low concentrations the shoulders of  $[\text{Co}(\text{salophen})(\text{OAc})]$  decrease in intensity and eventually disappear as more ligand is added. At high concentrations of the ligand, prominent bands are observed at 343 nm, 372 nm and 477 nm. A shoulder is also observed at 390 nm.

**Figure 6.3.3.2** shows the titration spectra for  $[\text{Co}(\text{salophen})(\text{N-MePipz})_2](\text{OAc})$  at 45 °C and at the specified *N*-methylpiperzine concentrations. Absorption spectra for  $[\text{Co}(\text{salophen})(\text{N-MePipz})_2](\text{OAc})$  at 30 °C, 35 °C and 40 °C are available in **Appendix D.10**.

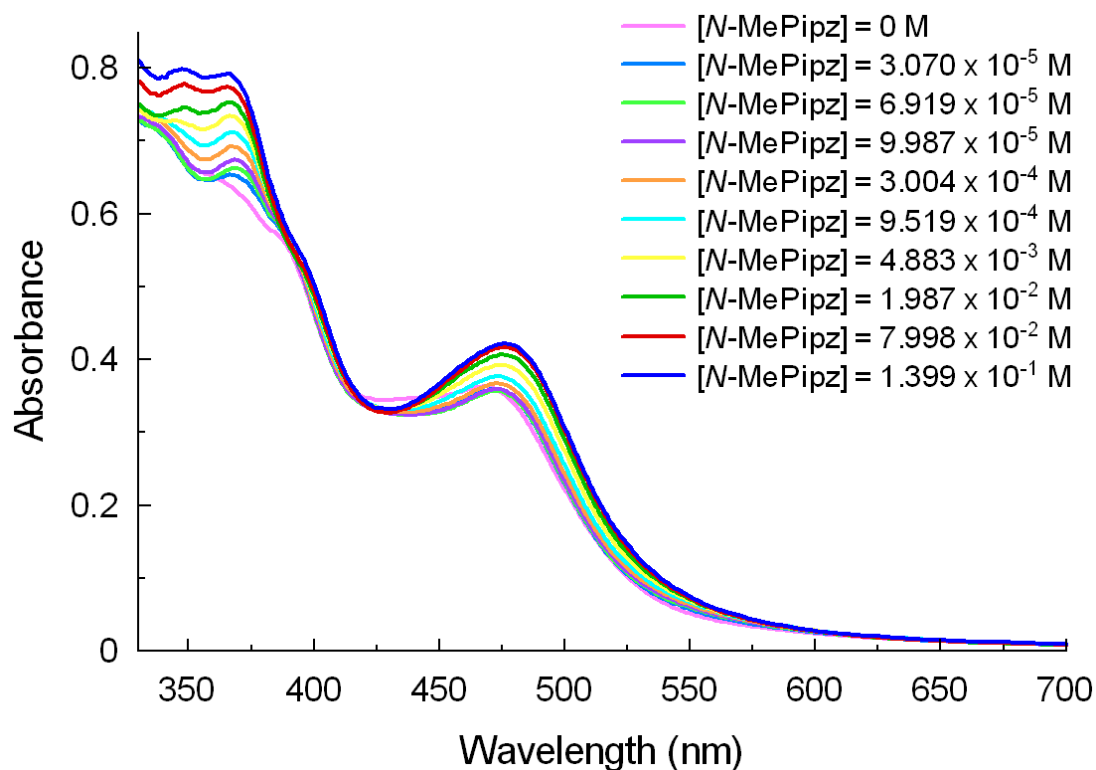


**Figure 6.3.3.2:** Superimposed titration spectra, showing the typical spectral progression for the reaction between  $[\text{Co}(\text{salophen})(\text{OAc})]$  and  $N\text{-MePipz}$ , at specified concentrations of the ligand at  $45 \text{ }^\circ\text{C}$ . These spectra have been corrected for dilution.

When comparing the spectra at  $25 \text{ }^\circ\text{C}$  and  $45 \text{ }^\circ\text{C}$  (**Figure 6.3.3.1** and **Figure 6.3.3.2**), there are small variations between the spectra mainly below  $400 \text{ nm}$ . The peak at  $343 \text{ nm}$  is sharp at  $25 \text{ }^\circ\text{C}$ , but at  $45 \text{ }^\circ\text{C}$ , this peak appears broad and almost flattened. At  $45 \text{ }^\circ\text{C}$ , the peak at  $472 \text{ nm}$  is sharp as compared to the peak at  $25 \text{ }^\circ\text{C}$ .

### 6.3.3.2 Titration Spectra for $[\text{Co}(\text{salophen})(\text{Bu}_2\text{NH})_2](\text{OAc})$

**Figure 6.3.3.3** shows the titration spectra for the reaction between  $[\text{Co}(\text{salophen})(\text{OAc})]$  and dibutylamine at  $25 \text{ }^\circ\text{C}$  and at the specified dibutylamine concentrations.

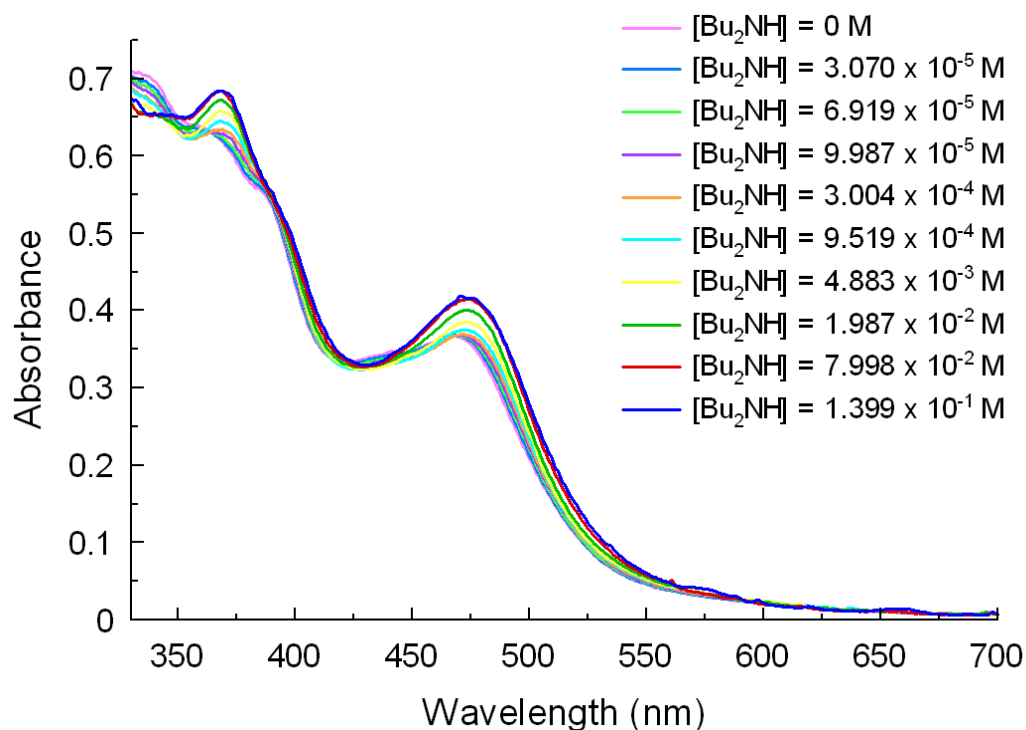


**Figure 6.3.3.3:** Superimposed titration spectra, showing the typical spectral progression for the reaction between [Co(salophen)(OAc)] and Bu<sub>2</sub>NH, at specified concentrations of the ligand at 25 °C. These spectra have been corrected for dilution.

The initial spectrum at 0 M concentration of dibutylamine shows the spectrum of [Co(salophen)(OAc)], with a peak at 468 nm and two shoulders at 363 nm, 389 nm. At low concentrations of the ligand, the peak at 468 nm and the shoulder at 363 nm decrease in intensity and eventually disappear. At concentrations of  $3.004 \times 10^{-4}$  M, a peak at 370 nm appears. At high concentrations of the ligand, prominent bands are observed at 370 nm and 477 nm. A shoulder is also observed at 390 nm.

**Figure 6.3.3.4** shows the titration spectra for [Co(salophen)(Bu<sub>2</sub>NH)<sub>2</sub>](OAc) at 45 °C and at the specified dibutylamine concentrations. Absorption spectra for [Co(salophen)(Bu<sub>2</sub>NH)<sub>2</sub>](OAc) at 30 °C, 35 °C and 40 °C are available in **Appendix D.11**.

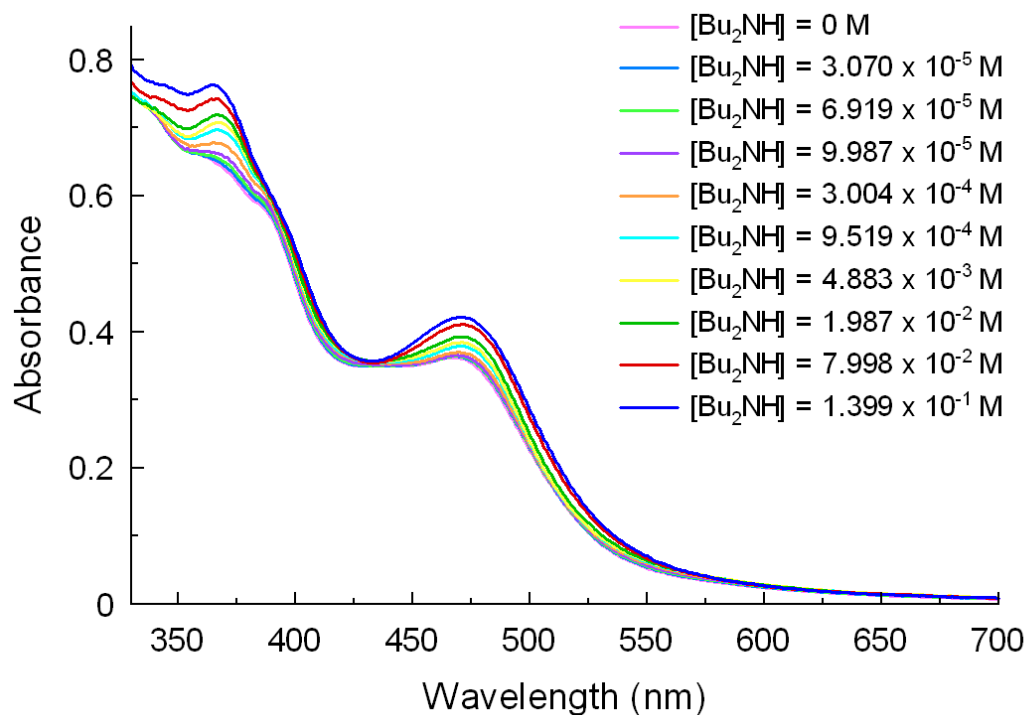


**Figure 6.3.3.4:** Superimposed titration spectra, showing the typical spectral progression for the reaction between  $[\text{Co}(\text{salophen})(\text{OAc})]$  and  $\text{Bu}_2\text{NH}$ , at specified concentrations of the ligand at  $45\text{ }^\circ\text{C}$ . These spectra have been corrected for dilution.

As the temperature increases the band at  $477\text{ nm}$  does not change significantly and the greatest change is observed in the region below  $400\text{ nm}$ . The peak at  $370\text{ nm}$  becomes broad as can be seen in **Figure 6.3.3.4**.

When comparing the spectra at  $25\text{ }^\circ\text{C}$  for *N*-MePipz and  $\text{BuNH}_2$  (**Figures 6.3.3.1** and **6.3.3.3**, respectively), the greatest difference lies in the peak at about  $372\text{ nm}$ . For the *N*-MePipz spectra, this band is broad and not as sharp as the band in the  $\text{BuNH}_2$  spectra at the same wavelength.

### 6.3.3.3 Titration Spectra for $[\text{Co}(\text{salophen})(\text{Pip})_2](\text{OAc})$

**Figure 6.3.3.5** shows the titration spectra for the reaction between  $[\text{Co}(\text{salophen})(\text{OAc})]$  and piperidine at  $25\text{ }^\circ\text{C}$  and at the specified piperidine concentrations.

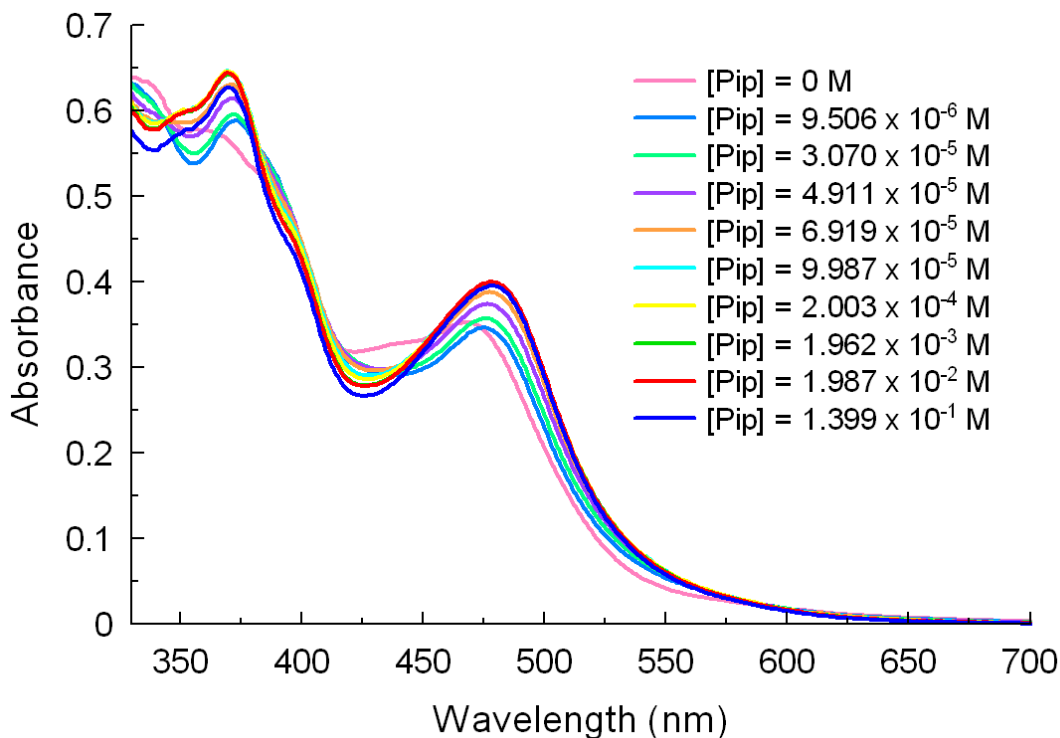


**Figure 6.3.3.5:** Superimposed titration spectra, showing the typical spectral progression for the reaction between  $[\text{Co}(\text{salophen})(\text{OAc})]$  and Pip, at specified concentrations of the ligand at 25 °C. These spectra have been corrected for dilution.

The initial spectrum at 0 M concentration of piperidine shows the spectrum of  $[\text{Co}(\text{salophen})(\text{OAc})]$ , with a prominent peak at 468 nm and two shoulders at 368 nm and 388 nm. At low concentrations of the ligand, the peak at 468 nm and the shoulder at 368 nm decrease in intensity and eventually disappear. A peak at 360 nm begins to appear at low concentrations of the ligand. At high concentrations of the ligand, prominent bands are observed at 375 nm and 478 nm.

**Figure 6.3.3.6** shows the titration spectra for  $[\text{Co}(\text{salophen})(\text{Pip})_2](\text{OAc})$  at 45 °C and at the specified piperidine concentrations. Absorption spectra for  $[\text{Co}(\text{salophen})(\text{Pip})_2](\text{OAc})$  at 30 °C, 35 °C and 40 °C are available in **Appendix D.12**.

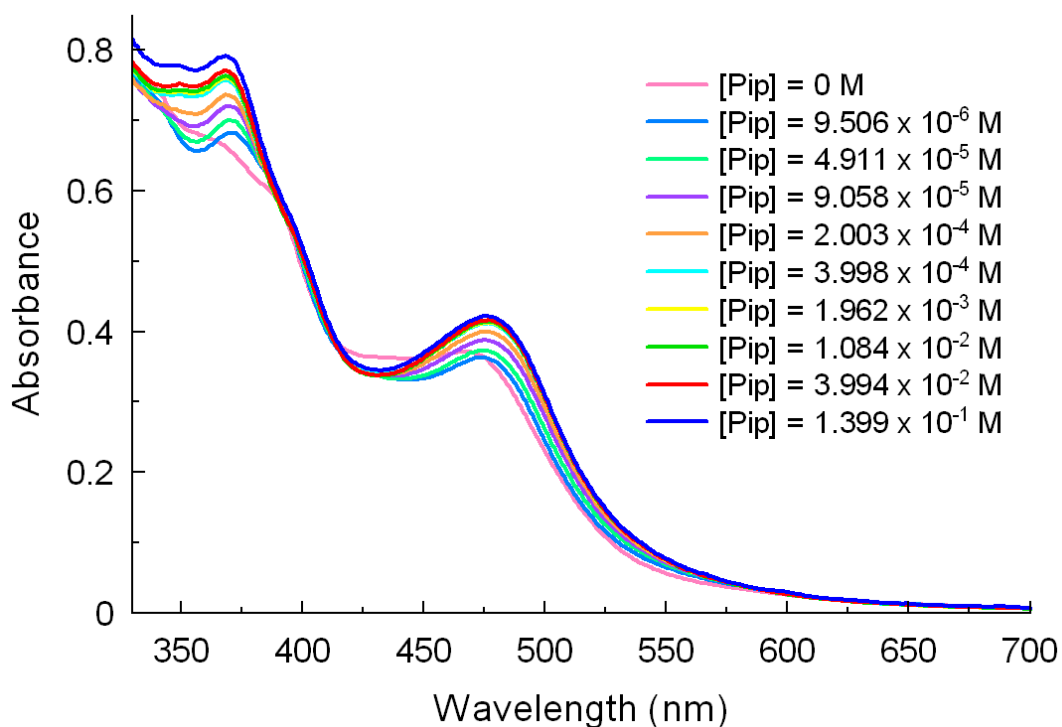


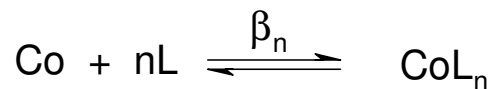
**Figure 6.3.3.6:** Superimposed titration spectra, showing the typical spectral progression for the reaction between  $[\text{Co}(\text{salophen})(\text{OAc})]$  and Pip, at specified concentrations of the ligand at  $45\text{ }^\circ\text{C}$ . These spectra have been corrected for dilution.

### 6.3.4 Analysis of Titration Results for Secondary Amines

As with the primary amines, each reaction was studied over a range of ligand concentrations ( $10^{-5} - 10^{-1}\text{ M}$ ) and titrations were carried out at five different temperatures. Absorbances were recorded at wavelengths where the greatest change was observed. At each of these wavelengths, a plot of absorbance versus  $\log[\text{ligand}]$  was obtained. The curve obtained was fitted by non-linear regression methods to an appropriate binding isotherm.

For *N*-methylpiperazine and dibutylamine, the model used to fit the data for the primary amines was used. For piperidine, the titration curve showed only one process taking place. Hence a new model (**Model 2**) had to be derived. This new model is based on a concerted mechanism, with the coordination of *n* axial ligands simultaneously. This model is used when  $K_1$  and  $K_2$  overlap significantly and cannot be adequately resolved. One stability

constant is obtained which represents both processes, denoted,  $\beta_2$  (where  $\beta_2 = K_1 \times K_2$ ). The derivation of Model 2 is available in **Appendix D.2**. It represents the equilibrium



where  $n \cong 2$ .

### 6.3.4.1 Analysis of titration results for [Co(salophen)(*N*-MePipz)<sub>2</sub>](OAc)

The absorbance for the titration between [Co(salophen)(OAc)] and *N*-methylpiperazine was recorded at 369 nm and 477 nm. **Figure 6.3.4.1** shows the absorbance versus log [*N*-MePipz] at 25 °C and illustrates a fit of the model (Model 1) to the data.

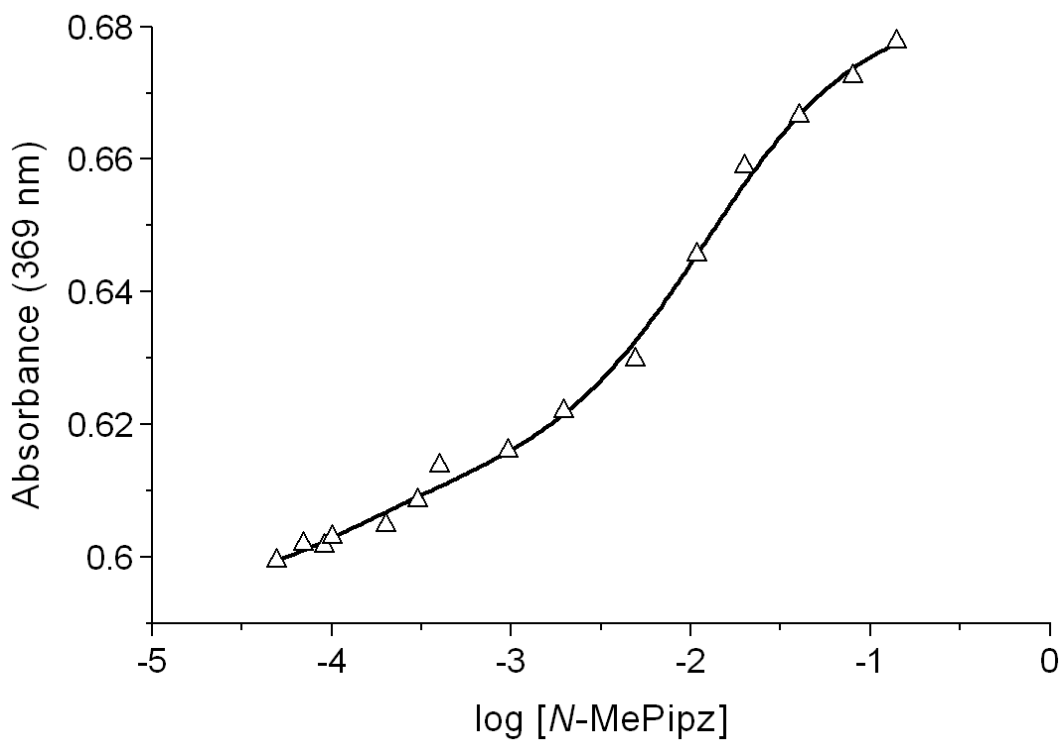


**Figure 6.3.4.1:** Reaction of [Co(salophen)(OAc)] with *N*-methylpiperazine at 25 °C in DMSO, showing the typical shape of an equilibrium process consistent with the derived model (step-wise coordination of two ligands).

Equilibrium processes for the reaction between [Co(salophen)(OAc)] and *N*-methylpiperazine at 30 °C, 35 °C, 40 °C and 45 °C are available in **Appendix D.13**.

**Table 6.3.4.1:** Table of equilibrium constants obtained from the reaction between [Co(salophen)(OAc)] and *N*-methylpiperazine at different temperatures.

Temp (°C)	369 nm			477 nm		
	$K_1 / M^{-1}$	$K_2 / M^{-1}$	${}^a\beta_2 / M^{-2}$	$K_1 / M^{-1}$	$K_2 / M^{-1}$	${}^a\beta_2 / M^{-2}$
25	$8.2(0.5) \times 10^3$	$8.1(1.0) \times 10^1$	$6.6 \times 10^5$	$3.3(0.5) \times 10^3$	$9.2(0.5) \times 10^1$	$3.1 \times 10^5$
30	$4.7(0.4) \times 10^3$	$1.2(0.3) \times 10^2$	$5.5 \times 10^5$	$2.8(0.4) \times 10^3$	$1.4(0.1) \times 10^2$	$3.9 \times 10^5$
35	$7.7(0.9) \times 10^3$	$1.1(18) \times 10^1$	$8.5 \times 10^5$	$3.5(0.5) \times 10^3$	$1.0(0.1) \times 10^2$	$3.5 \times 10^5$
40	$1.0(0.03) \times 10^4$	$1.8(0.2) \times 10^2$	$1.8 \times 10^6$	$4.1(0.4) \times 10^3$	$1.9(0.04) \times 10^2$	$7.9 \times 10^5$
45	$6.0(0.5) \times 10^3$	$4.8(7.3) \times 10^1$	$2.9 \times 10^5$	$2.2(0.3) \times 10^3$	$6.0(0.3) \times 10^1$	$1.3 \times 10^5$

$${}^a\beta_2 = K_1 \times K_2$$

From the data in **Table 6.3.4.1**, there is no definite trend in the  $K$  values or the  $\beta_2$  values. As the temperature increases,  $\beta_2$  is expected to decrease for an exergonic reaction. However this is not observed. This can be attributed to the very small spectral change that occurs. There is also no agreement between the  $\beta_2$  values at 369 nm and 477 nm.

#### 6.3.4.2 Analysis of titration results for [Co(salophen)(Bu<sub>2</sub>NH)<sub>2</sub>](OAc)

The absorbance for the titration between [Co(salophen)(OAc)] and dibutylamine was recorded at 370 nm and 477 nm. **Figure 6.3.4.2** shows the absorbance versus log [Bu<sub>2</sub>NH<sub>2</sub>] at 25 °C and illustrates a fit of the model to the data.

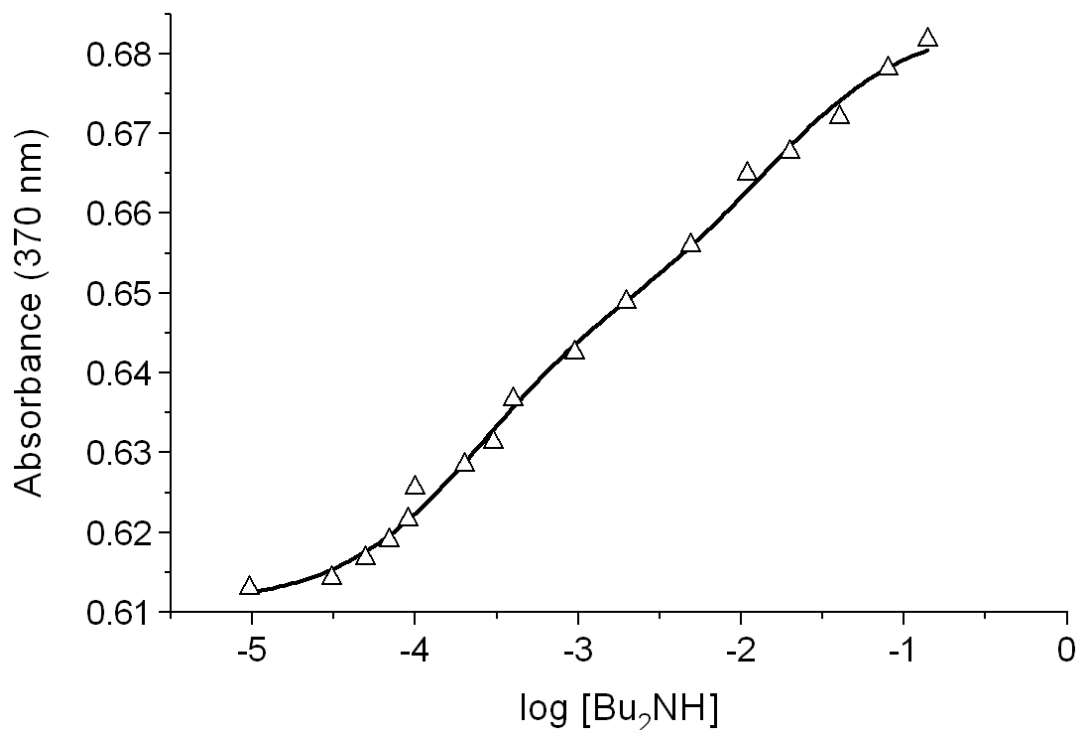


**Figure 6.3.4.2:** Reaction of [Co(salophen)(OAc)] with dibutylamine at 25 °C in DMSO, showing the typical shape of an equilibrium process consistent with the derived model.

Equilibrium processes for the reaction between [Co(salophen)(OAc)] and dibutylamine at 30 °C, 35 °C, 40 °C and 45 °C are available in **Appendix D.14**.

**Table 6.3.4.2:** Table of equilibrium constants obtained from the reaction between [Co(salophen)(OAc)] and dibutylamine at different temperatures.

Temp (°C)	370 nm			477 nm		
	$K_1 / M^{-1}$	$K_2 / M^{-1}$	${}^a\beta_2 / M^{-2}$	$K_1 / M^{-1}$	$K_2 / M^{-1}$	${}^a\beta_2 / M^{-2}$
25	$4.2(0.5) \times 10^3$	$6.4(1.0) \times 10^1$	$2.7 \times 10^5$	$5.5(0.5) \times 10^3$	$5.4(0.5) \times 10^1$	$2.9 \times 10^5$
30	$4.7(0.4) \times 10^3$	$7.2(2.7) \times 10^1$	$3.4 \times 10^5$	$6.7(0.4) \times 10^3$	$6.1(1.2) \times 10^1$	$4.1 \times 10^5$
35	$6.3(0.9) \times 10^3$	$2.1(18) \times 10^1$	$1.3 \times 10^5$	$4.8(0.5) \times 10^3$	$1.7(1.1) \times 10^1$	$8.1 \times 10^4$
40	$3.8(0.3) \times 10^3$	$8.4(1.7) \times 10^1$	$3.2 \times 10^5$	$2.2(0.4) \times 10^3$	$3.0(0.4) \times 10^1$	$6.7 \times 10^4$
45	$4.8(0.5) \times 10^3$	$7.6(73) \times 10^0$	$3.7 \times 10^4$	$3.0(0.3) \times 10^3$	$8.9(3.4) \times 10^0$	$2.7 \times 10^4$

$${}^a\beta_2 = K_1 \times K_2$$

As with *N*-methylpiperzine, there is no distinct trend in the  $K$  values and the  $\beta_2$  values. The  $\beta_2$  values at both wavelengths do not agree with each other.

### 6.3.4.3 Analysis of titration results for $[\text{Co}(\text{salophen})(\text{Pip})_2](\text{OAc})$

The absorbance for the titration between  $[\text{Co}(\text{salophen})(\text{OAc})]$  and piperidine was recorded at 478 nm. Figure 6.3.4.3 shows the absorbance versus  $\log [\text{Pip}]$  at 25 °C and illustrates a fit of the model to the data. The shape of the curve is distinct from each of the other titrations as the second phase is absent.

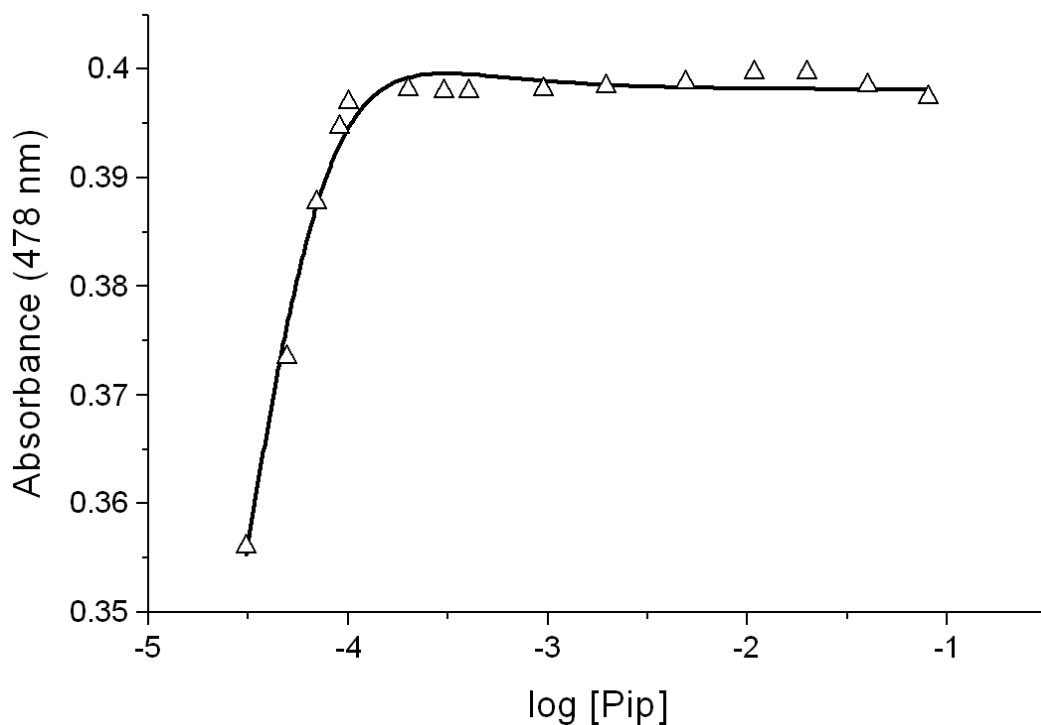


**Figure 6.3.4.3:** Reaction of  $[\text{Co}(\text{salophen})(\text{OAc})]$  with piperidine at 25 °C in DMSO, showing the typical shape of an equilibrium process consistent with the derived model.

Equilibrium processes for the reaction between  $[\text{Co}(\text{salophen})(\text{OAc})]$  and piperidine at 30 °C, 35 °C, 40 °C and 45 °C are available in **Appendix D.15**.

**Table 6.3.4.3:** Table of  $K_1$  values obtained from the reaction between [Co(salophen)(OAc)] and piperidine at 478 nm and at different temperatures.

Temperature (°C)	n	$^aK_1 / M^{-1}$
25	1	$2.0(12) \times 10^4$
30	1	$1.3(60) \times 10^4$
35	1	$1.4(24) \times 10^4$
40	1	$1.3(0.05) \times 10^4$
45	1	$4.8(0.2) \times 10^5$

### 6.3.5 Obtaining Thermodynamic Data from the van't Hoff Plot

From the derived binding isotherms, the stability constants can be determined from the spectroscopic data. Using the stability constants, the thermodynamic parameters,  $\Delta H$  and  $\Delta S$ ; can be determined for each reaction. A van't Hoff plot is obtained by plotting the natural log of the equilibrium constant versus the inverse of absolute temperature.

The van't Hoff plot is based on the equation:

$$-RT \ln K = \Delta H - T\Delta S$$

Derived from the Gibb's Equation:

$$\Delta G = \Delta H - T\Delta S \quad \text{and}$$

$$\Delta G = -RT \ln K$$

Rearranging affords the van't Hoff equation:

$$\ln K = \frac{-\Delta H}{R} \left( \frac{1}{T} \right) + \frac{\Delta S}{R}$$

The derivation of the van't Hoff equation can be found in **Appendix D.3**.

From the plot of  $\ln K$  versus  $1/T$ ,  $\Delta H$  is calculated from the slope of the graph and  $\Delta S$  is obtained from the y-intercept. If the reaction has a large negative  $\Delta H$  value, then the reaction is potentially favourable and exothermic. However, if  $\Delta H$  is positive, then the reaction is endothermic and requires heat in order to take place. The reaction will then only be favourable if  $\Delta S$  is large and positive.

### 6.3.5.1 Thermodynamic Data

**Table 6.3.5.1** to **Table 6.3.5.5** list thermodynamic data for the reaction of  $[\text{Co}(\text{salophen})(\text{OAc})]$  with primary amines butylamine, benzylamine and  $\alpha$ -methylbenzylamine. A typical plot of  $\ln K_2$  vs.  $1/T$  is shown in **Figure 6.3.5.1** for the reaction of  $[\text{Co}(\text{salophen})(\text{OAc})]$  and dibutylamine. While measurements were carried out at five temperatures, straight lines for the van't Hoff plots were only drawn through three data points. This was observed for all the van't Hoff plots.

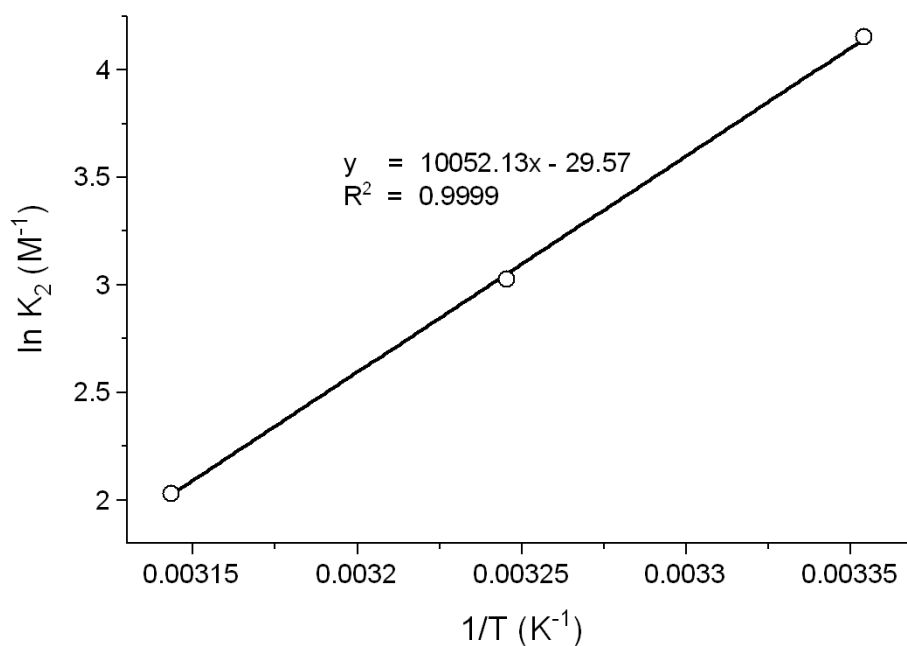


**Figure 6.3.5.1:**  $K_2$  van't Hoff plot for the reaction of  $[\text{Co}(\text{salophen})(\text{OAc})]$  and dibutylamine at 370 nm in DMSO.

**Table 6.3.5.1:** Thermodynamic data for the reaction of [Co(salophen)(OAc)] with butylamine at 364 nm in DMSO.

<b>Butylamine</b>							
	25 °C	30 °C	35 °C	40 °C	45 °C	$\Delta H$ (kJ mol <sup>-1</sup> )	$\Delta S$ (J mol <sup>-1</sup> K <sup>-1</sup> )
$K_1$ (x 10 <sup>3</sup> M <sup>-1</sup> )	4.1(0.4)	10.9(0.7)	17.9(1.1)	4.1(0.2)	10.5(0.3)	113(21)	449(68)
$K_2$ (x 10 <sup>2</sup> M <sup>-1</sup> )	0.6(0.04)	2.8(0.3)	7.9(0.9)	0.08(0.01)	4.2(1.6)	193(17)	682(56)
<sup>a</sup> $\beta_2$ (x 10 <sup>5</sup> M <sup>-2</sup> )	2.5(0.3)	30.1(3.9)	141.6(18.3)	0.3(0.06)	44.0(16.5)	307(38)	1136(124)

<sup>a</sup>Calculated  $\beta_2 = K_1 \times K_2$ .

**Table 6.3.5.2:** Thermodynamic data for the reaction of [Co(salophen)(OAc)] with butylamine at 475 nm in DMSO.

<b>Butylamine</b>							
	25 °C	30 °C	35 °C	40 °C	45 °C	$\Delta H$ (kJ mol <sup>-1</sup> )	$\Delta S$ (J mol <sup>-1</sup> K <sup>-1</sup> )
$K_1$ (x 10 <sup>3</sup> M <sup>-1</sup> )	5.7(0.5)	2.7(0.3)	8.6(0.4)	3.4(0.1)	5.7(0.2)	37(16)	186(53)
$K_2$ (x 10 <sup>2</sup> M <sup>-1</sup> )	0.5(0.07)	5.2(0.4)	0.9(1.1)	4.3(0.9)	2.1(0.4)	59(6)	229(21)
<sup>a</sup> $\beta_2$ (x 10 <sup>5</sup> M <sup>-2</sup> )	2.6(0.5)	14.2(1.7)	7.5(9.6)	14.7(3.0)	11.9(2.5)	88(7)	400(22)

<sup>a</sup>Calculated  $\beta_2 = K_1 \times K_2$ .

The van't Hoff plots for butylamine are available in **Appendix D.7**.

**Table 6.3.5.3:** Thermodynamic data for the reaction of [Co(salophen)(OAc)] with benzylamine at 472 nm in DMSO.

<b>Benzylamine</b>							
	25 °C	30 °C	35 °C	40 °C	45 °C	$\Delta H$ (kJ mol <sup>-1</sup> )	$\Delta S$ (kJ mol <sup>-1</sup> K <sup>-1</sup> )
$K_1$ (x 10 <sup>3</sup> M <sup>-1</sup> )	0.4(0.03)	4.9(0.6)	15.2(1.0)	3.9(0.2)	7.9(0.3)	285(63)	1(0.2)
$K_2$ (x 10 <sup>2</sup> M <sup>-1</sup> )	0.06(0.01)	3.3(0.3)	4.1(0.3)	0.03(0.01)	0.3(0.04)	324(166)	1(0.5)
<sup>a</sup> $\beta_2$ (x 10 <sup>5</sup> M <sup>-2</sup> )	0.02(0.0005)	16.3(2.6)	61.7(6.6)	0.1(0.05)	2.6(0.3)	611(228)	2(0.7)

<sup>a</sup>Calculated  $\beta_2 = K_1 \times K_2$ .

The van't Hoff plots for benzylamine are available in **Appendix D.8**.

**Table 6.3.5.4:** Thermodynamic data for the reaction of [Co(salophen)(OAc)] with  $\alpha$ -methylbenzylamine at 366 nm in DMSO.

<b><math>\alpha</math>-methylbenzylamine</b>							
	25 °C	30 °C	35 °C	40 °C	45 °C	$\Delta H$ (kJ mol <sup>-1</sup> )	$\Delta S$ (J mol <sup>-1</sup> K <sup>-1</sup> )
$K_1$ (x 10 <sup>3</sup> M <sup>-1</sup> )	8.0(0.5)	9.2(0.4)	7.2(0.8)	7.1(0.3)	14.0(0.5)	21(1)	146(3)
$K_2$ (x 10 <sup>2</sup> M <sup>-1</sup> )	0.6(0.1)	2.4(0.3)	4.6(1.8)	0.2(0.2)	5.2(0.7)	151(26)	541(87)
<sup>a</sup> $\beta_2$ (x 10 <sup>5</sup> M <sup>-2</sup> )	5.1(0.9)	21.6(2.7)	33.6(13.8)	1.5(1.2)	72.5(10.6)	64(2)	333(5)

<sup>a</sup>Calculated  $\beta_2 = K_1 \times K_2$ .

**Table 6.3.5.5:** Thermodynamic data for the reaction of [Co(salophen)(OAc)] with  $\alpha$ -methylbenzylamine at 473 nm in DMSO.

<b><math>\alpha</math>-methylbenzylamine</b>							
	25 °C	30 °C	35 °C	40 °C	45 °C	$\Delta H$ (kJ mol <sup>-1</sup> )	$\Delta S$ (J mol <sup>-1</sup> K <sup>-1</sup> )
$K_1$ (x 10 <sup>3</sup> M <sup>-1</sup> )	10.4(0.5)	8.0(0.4)	6.7(0.5)	7.0(0.4)	7.8(0.3)	-33(4)	-34(12)
$K_2$ (x 10 <sup>2</sup> M <sup>-1</sup> )	0.9(0.05)	2.2(0.1)	0.8(0.1)	0.5(0.04)	0.6(0.03)	-124(20)	-365(64)
<sup>a</sup> $\beta_2$ (x 10 <sup>5</sup> M <sup>-2</sup> )	9.5(0.7)	17.9(1.3)	5.5(0.8)	3.2(0.3)	4.6(0.3)	-53(10)	-64(32)

<sup>a</sup>Calculated  $\beta_2 = K_1 \times K_2$ .

The van't Hoff plots for  $\alpha$ -methylbenzylamine are available in **Appendix D.9**.

For the butylamine and benzylamine systems,  $\Delta H$  was found to be positive. Positive  $\Delta H$ 's were also found for  $\alpha$ -methylbenzylamine at 366 nm.

**Table 6.3.5.6** to **Table 6.3.5.9** lists the thermodynamic data for the secondary amines *N*-methylpiperazine, dibutylamine and piperidine.

**Table 6.3.5.6:** Thermodynamic data for the reaction of [Co(salophen)(OAc)] with *N*-methylpiperazine at 369 nm in DMSO.

<b><i>N</i>-methylpiperazine</b>							
	25 °C	30 °C	35 °C	40 °C	45 °C	$\Delta H$ (kJ mol <sup>-1</sup> )	$\Delta S$ (J mol <sup>-1</sup> K <sup>-1</sup> )
$K_1$ (x 10 <sup>3</sup> M <sup>-1</sup> )	8.2(0.5)	4.7(0.4)	7.7(0.9)	10.5(0.3)	6.0(0.5)	-12(5)	34(15)
$K_2$ (x 10 <sup>2</sup> M <sup>-1</sup> )	0.8(0.1)	1.2(0.3)	1.1(1.8)	1.8(0.2)	0.5(0.7)	-50(15)	-126(47)
<sup>a</sup> $\beta_2$ (x 10 <sup>5</sup> M <sup>-2</sup> )	6.6(0.9)	5.5(1.7)	8.5(1.4)	18.4(1.9)	2.9(4.4)	-32(2)	4(6)

<sup>a</sup>Calculated  $\beta_2 = K_1 \times K_2$ .

**Table 6.3.5.7:** Thermodynamic data for the reaction of [Co(salophen)(OAc)] with *N*-methylpiperazine at 477 nm in DMSO.

<b><i>N</i>-methylpiperazine</b>							
	25 °C	30 °C	35 °C	40 °C	45 °C	$\Delta H$ (kJ mol <sup>-1</sup> )	$\Delta S$ (J mol <sup>-1</sup> K <sup>-1</sup> )
$K_1$ (x 10 <sup>3</sup> M <sup>-1</sup> )	3.3(0.5)	2.8(0.4)	3.5(0.5)	4.1(0.4)	2.2(0.3)	-11(5)	37(16)
$K_2$ (x 10 <sup>2</sup> M <sup>-1</sup> )	0.9(0.05)	1.4(0.1)	1.0(0.1)	1.9(0.04)	0.6(0.03)	-48(15)	-117(48)
<sup>a</sup> $\beta_2$ (x 10 <sup>5</sup> M <sup>-2</sup> )	3.1(0.5)	3.9(0.5)	3.5(0.5)	7.9(?)	1.3(0.2)	-60(15)	-90(50)

<sup>a</sup>Calculated  $\beta_2 = K_1 \times K_2$ .

The van't Hoff plots for *N*-methylpiperazine are available in **Appendix D.13**.

**Table 6.3.5.8:** Thermodynamic data for the reaction of [Co(salophen)(OAc)] with dibutylamine at 370 nm in DMSO.

<b>Dibutylamine</b>							
	25 °C	30 °C	35 °C	40 °C	45 °C	$\Delta H$ (kJ mol <sup>-1</sup> )	$\Delta S$ (J mol <sup>-1</sup> K <sup>-1</sup> )
$K_1$ (x 10 <sup>3</sup> M <sup>-1</sup> )	4.2(0.5)	4.7(0.4)	6.3(0.8)	3.8(0.3)	4.8(0.5)	31(8)	173(27)
$K_2$ (x 10 <sup>1</sup> M <sup>-1</sup> )	6.4(1.0)	7.2(2.7)	2.1(18.2)	8.4(1.7)	0.8(7.3)	-84(1)	-246(5)
<sup>a</sup> $\beta_2$ (x 10 <sup>5</sup> M <sup>-2</sup> )	2.7(0.5)	3.4(1.3)	1.3(11.4)	3.2(0.7)	0.4(3.5)	-116(12)	-277(37)

<sup>a</sup>Calculated  $\beta_2 = K_1 \times K_2$ .

**Table 6.3.5.9:** Thermodynamic data for the reaction of [Co(salophen)(OAc)] with dibutylamine at 477 nm in DMSO.

<b>Dibutylamine</b>							
	25 °C	30 °C	35 °C	40 °C	45 °C	$\Delta H$ (kJ mol <sup>-1</sup> )	$\Delta S$ (J mol <sup>-1</sup> K <sup>-1</sup> )
$K_1$ (x 10 <sup>3</sup> M <sup>-1</sup> )	5.5(0.5)	6.7(0.4)	4.8(0.5)	2.2(0.4)	3.0(0.3)	-42(4)	-66(12)
$K_2$ (x 10 <sup>1</sup> M <sup>-1</sup> )	5.4(0.5)	6.1(1.2)	1.7(1.1)	3.0(0.4)	0.9(0.3)	-71(10)	-205(33)
<sup>a</sup> $\beta_2$ (x 10 <sup>4</sup> M <sup>-2</sup> )	29.3(3.9)	41.1(8.6)	8.1(5.2)	6.7(1.4)	2.7(1.1)	-145(2)	-372(7)

<sup>a</sup>Calculated  $\beta_2 = K_1 \times K_2$ .

The van't Hoff plots for dibutylamine are available in **Appendix D.14**.

**Table 6.3.5.10:** Thermodynamic data for the reaction of [Co(salophen)(OAc)] with piperidine at 478 nm in DMSO.

<b>Piperidine</b>							
	25 °C	30 °C	35 °C	40 °C	45 °C	$\Delta H$ (kJ mol <sup>-1</sup> )	$\Delta S$ (J mol <sup>-1</sup> K <sup>-1</sup> )
$K_1$ (x 10 <sup>4</sup> M <sup>-1</sup> )	2(12)	1.3(60)	1.4(24)	1.3(0.05)	48(1.7)	-25(4)	-0.59(13)

The van't Hoff plots for piperidine are available in **Appendix D.15**.

Negative  $\Delta H$ 's were found for all secondary amines which suggest that the reaction was spontaneous.

All three primary amines and secondary amines had similar titration spectra. The model derived was based on two consecutive equilibria whereby one amine binds to the first axial site and then in a second step, the other amine binds to the other available site to yield the bis(ligated) product. From the shape of the titration curve with absorbance plotted against the log of ligand concentration, one can distinctly see two processes taking place with a change in slope along the curve. The titration curves were different for the primary amines and the secondary amines. Thus the primary and secondary amines will be discussed separately.

## Primary Amines

From the titration curves for the primary amines, two processes can be seen distinctly. However, at some wavelengths the two processes overlapped and as a result the  $K_1$  and  $K_2$  values overlapped significantly. We calculated  $\beta_2$  values ( $K_1 \times K_2$ ) in an effort to obtain a more accurate overall binding constant for the uptake of two equivalents of the added ligand.

$K_1$  represents the affinity for the binding of the first ligand to the Co(III) complex. The larger the stability constant, the greater is the affinity of the ligand for the complex. On average,  $\alpha$ -methylbenzylamine has a larger  $K_1$  value, over the studied temperature range, than butylamine and benzylamine. This suggests that  $\alpha$ -methylbenzylamine has a larger affinity to coordinate to the available axial site of Co(III) to give  $[\text{Co}(\text{salophen})(\text{L})(\text{OAc})]$  in the first step than the other two primary amines.

Over the studied temperature range, an averaged  $K_2$  for all primary amines was found to be 10 to 100 fold smaller than  $K_1$ . This is due to the fact that dissociation of the acetate ion has to occur first, which requires energy before the binding of the second ligand takes place.  $K_2$  for  $\alpha$ -methylbenzylamine was found to be larger than that of the other primary amines.

This result, i.e. the fact that  $\alpha$ -methylbenzylamine is the strongest binding ligand, is consistent with the high  $\sigma$ -donor power of the ligand first noted by Munro, Shabalala and Brown<sup>68</sup> based on extensive <sup>59</sup>Co NMR and DFT data for  $[\text{Co}(\text{TPP})\text{L}_2]\text{SbF}_6$  complexes.

Benzylamine showed a much greater change in enthalpy than butylamine and the change in enthalpy for both reactions were found to be positive, an unexpected result. At 473 nm,  $\alpha$ -methylbenzylamine showed large negative changes in enthalpy. This suggests that the reaction was exothermic. In using linear regression to fit the data, the greatest error will occur in obtaining the y-intercept. This means that the value of  $\Delta S$  will have the greatest uncertainty and a relatively large standard deviation. The change in absorbance over the given temperature range was very small. This lead to a significant overlap of K values and a definite trend could not be established due to the data being scattered. Due to this factor values of  $\Delta H$  and  $\Delta S$  are subject to considerable experimental errors. The graphs obtained from the van't Hoff plots did not produce reliable fits and as a result the thermodynamic data

obtained is not a true measure of the system being studied. A more feasible method of determining stability constants is clearly required, e.g. titration calorimetry and / or potentiometry.

### Secondary Amines

With the titration of *N*-methylpiperazine and dibutylamine with [Co(salophen)(OAc)],  $K_1$  and  $K_2$  were easily distinguishable from the titration curves. The process was the same as that of the primary amines. A  $\beta_2$  value was also calculated for *N*-methylpiperazine and dibutylamine. On average, *N*-methylpiperazine, was found to have higher values of  $K_1$  than dibutylamine over the studied temperature range. The  $K_2$  values were found to be 10 to 100 fold smaller than the  $K_1$  values at all temperatures and  $K_2$  values for dibutylamine were found to be much smaller than those for *N*-methylpiperazine.

The changes in enthalpy for all secondary amines were found to be negative. As with the primary amines, the graphs obtained for the van't Hoff plots were not reliable and neither was the data that was obtained. The fundamental problem in all titrations was that the overall change in absorbance was small ( $< 0.1$ ) and proper delineation of  $K_1$  and  $K_2$  was thus not feasible by non-linear regression analysis of the titration data.

For the titration between piperidine and [Co(salophen)(OAc)], neither  $K_1$  nor  $K_2$  could be distinguished from the titration curves because of significant overlap of the two processes. As a result, the process was treated as a single concerted process and one equilibrium constant,  $\beta_2$ , was obtained which was a product of  $K_1$  and  $K_2$ . Since  $\beta_2$  is the product of  $K_1$  and  $K_2$ , one would expect  $\beta_2$  to be much larger than either equilibrium constant of *N*-methylpiperazine and dibutylamine; this is true for the above system. However, even though  $\Delta H$  was found to be negative, the van't Hoff plot obtained was not reliable (refer to **Appendix D.15, Figure D.15.5**).

When comparing the primary amines and secondary amines, it was found that the primary amines had much larger  $K_1$  and  $K_2$  values than the secondary amines. This is fully consistent with the fact that sterically bulky amines endure greater repulsion from the salophen chelate and thus bind more weakly than unrestricted primary amines.

## Comparisons with the Literature

Asadi *et al.*<sup>105</sup> have carried out extensive work on the thermodynamic properties of cobalt Schiff base complexes. Their work focussed on the Schiff bases BAE (bis(acetylaceton)ethylenediimine) and BBE (bis(benzolaceton)ethylenediimine) and phosphine axial ligands. Asadi *et al.*<sup>106</sup> also worked on the thermodynamic properties of cobalt Schiff base complexes involving the Schiff base acacen (bis(acetylaceton)(ethylene diimine)) and tertiaryphosphines as acceptors and *n*-propyl, *n*-butyl and *sec*-butyl as donors. In both cases, Asadi *et al.*<sup>105,106</sup> carried out their titrations spectrophotometrically and the equilibrium constants were calculated using Ketelaar's equation.

## Chapter Seven: Conclusions and Future Work

The main aim of this work was to synthesise and characterise (structurally and spectroscopically) a range of cobalt(III) Schiff base complexes and to determine the binding constants of these complexes.

Four novel crystal structures of  $[\text{Co}(\text{salophen})\text{L}_2]\text{X}$  derivatives, where  $\text{L} = \text{BuNH}_2$ ,  $\text{BzNH}_2$ ,  $N\text{-MePipz}$  and  $\text{Pip}$  and  $\text{X} = \text{solvent-derived Cl}^-$ , have been presented in this thesis. All the complexes with the exception of  $[\text{Co}(\text{salophen})(N\text{-MePipz})(\text{OAc})]$  crystallised as the bis-ligated complex. All complexes with the exception of  $[\text{Co}(\text{salophen})(\text{BzNH}_2)_2]\text{Cl}\cdot\text{CH}_2\text{Cl}_2$  crystallised in the triclinic space group and all of the complexes had solvent or a counter ion present in the lattice. In every complex, the ligand was non-planar. For  $[\text{Co}(\text{salophen})(\text{BuNH}_2)_2]\text{CH}_2\text{Cl}_2\cdot\text{Cl}^-$  and  $[\text{Co}(\text{salophen})(\text{BzNH}_2)_2]\text{Cl}\cdot\text{CH}_2\text{Cl}_2$ , interesting hydrogen bonding existed between the oxygen atoms of the chelate and the hydrogen atoms on the nitrogens of the axial ligands. There were also short contacts between the  $\text{CH}_2\text{Cl}_2$  molecules of the solvent and the hydrogen atoms of the chelate. For  $[\text{Co}(\text{salophen})(N\text{-MePipz})(\text{OAc})]\cdot n\text{H}_2\text{O}$ , hydrogen bonding between the oxygen atoms of the water molecules (present as solvent) and the hydrogens of the chelate was observed. In  $[\text{Co}(\text{salophen})(\text{Pip})_2](\text{OAc})$  hydrogen bonding between the oxygen atoms of the acetate ion and the hydrogen atoms bound to the axial nitrogen atom was observed.

Importantly, by variation of the synthetic method, we could prepare both  $[\text{Co}(\text{salophen})(N\text{-MePipz})(\text{OAc})]$ , a mixed ligand complex, and  $[\text{Co}(\text{salophen})(\text{Pip})_2](\text{OAc})$ .

Extensive studies were carried out in order to determine the binding constants of the  $[\text{Co}(\text{salophen})\text{L}_2](\text{OAc})$  complexes, where  $\text{L} = \text{butylamine}$ ,  $\text{benzylamine}$ ,  $\alpha\text{-methylbenzylamine}$ ,  $N\text{-methylpiperazine}$ ,  $\text{dibutylamine}$  and  $\text{piperidine}$ . It was found that the spectral changes accompanying ligand replacement were generally very small. This, coupled with strong overlapping of the stepwise binding constants  $K_1$  and  $K_2$ , made accurate fitting of the experimental data and thus accurate estimation of thermodynamic variables  $\Delta\text{H}$ ,  $\Delta\text{S}$  and  $\Delta\text{G}$  difficult. While results have been obtained for the thermodynamic data, in some

cases these results were not entirely reliable due to the problems associated with deconvolution of the association constants from the spectroscopic data.

For the primary amines, it was found that on average  $\alpha$ -methylbenzylamine had a larger  $K_1$  value than butylamine and benzylamine over the studied temperature range. This means that  $\alpha$ -methylbenzylamine has a larger affinity to coordinate to the available axial site of Co(III) to give  $[\text{Co}(\text{salophen})(\alpha\text{-MeBzNH}_2)(\text{OAc})]$  in the first step compared to the other two primary amines.

It was found that over the studied temperature range,  $K_2$  for all primary amines was 10 to 100 fold smaller than  $K_1$ . This is due to the fact that dissociation of the acetate ion has to occur first which requires energy before the binding of the second ligand takes place.  $K_2$  for  $\alpha$ -methylbenzylamine was found to be larger than  $K_2$  for the other two primary amines.

For the secondary amines, *N*-methylpiperazine was found to have higher values of  $K_1$  than dibutylamine over the studied temperature range. As with the primary amines, the  $K_2$  values were found to be 10 to 100 fold smaller than the  $K_1$  values at all temperatures. The  $K_2$  value for dibutylamine was found to be much smaller than those of *N*-methylpiperazine.

It was found that the primary amines had much larger  $K_1$  and  $K_2$  values than the secondary amines. This was consistent with the fact that sterically bulky amines endure greater repulsion from the salophen chelate and thus bind weakly than the unrestricted primary amines.

Future work on these complexes includes investigations by density functional theory (DFT) calculations, to obtain a relationship between the theoretical data and the experimental data. We also plan on investigating the redox potential of these systems by cyclic voltammetry.

## References

- 
- <sup>1</sup> Holm, R. H.; Everett Jr., G. W.; Chakravorty, A. *Prog. Inorg. Chem.* **1966**, *7*, 83-214.
- <sup>2</sup> Jones, C. J. In *Inorganic Experiments*, Woollins, J. D., Eds; VCH Publishers: New York, **1994**; pp 127-130.
- <sup>3</sup> Atwood, D. A.; Harvey, M. J. *Chem Rev.* **2001**, *101*, 37-52.
- <sup>4</sup> Cort, A. D.; Gasparri, F.; Lunazzi, L.; Mandolini, L.; Mazzanti, A.; Pasquini, C.; Pierini, M.; Rompietti, R.; Schiaffino, L. *J. Org. Chem.* **2005**, *70*, 8877-8883.
- <sup>5</sup> Cozzi, P. G. *Chem. Soc. Rev.* **2004**, *33*, 410-421.
- <sup>6</sup> El-Medani, S.; Ali, O. M. A.; Ramadan, R. M. *J. Mol. Struct.* **2005**, *738*, 171-177.
- <sup>7</sup> Venkataramanan, N. S.; Kuppuraj, G.; Rajagopal, S. *Coordination Chemistry Reviews* **2005**, *249*, 1249-1268.
- <sup>8</sup> Monash University, *Synthetic and Catalytic Chemistry* [Online] Available: <http://www.chem.monash.edu.au/synthetic-chem/schiffbase/html>.
- <sup>9</sup> Ribeiro da Silva, M. D. M. C.; Gonçalves, J. M.; Silva, A. L. R.; Oliveira, P. C. F. C.; Schröder, B.; Ribeiro da Silva, M. A. V. *J. Mol. Cata. A: Chemical* **2004**, *224*, 207-212.
- <sup>10</sup> Gaur, S. *Asian J. Chem.* **2003**, *15*, 250-254.
- <sup>11</sup> Amirnasr, M.; Mahmoudkhani, A. H.; Gorji, A.; Dehghanpour, S.; Bijanzadeh, H. R. *Polyhedron* **2002**, *21*, 2733-2742.
- <sup>12</sup> Yamada, S. *Coord. Chem. Rev.* **1999**, *190-192*, 537-555.
- <sup>13</sup> Tuna, F.; Patron, L.; Rivière, E.; Boillot, M-L. *Polyhedron* **2000**, *19*, 1643-1648.

- 
- <sup>14</sup> Franceschi, F.; Solari, E.; Floriani, C.; Rosi, M.; Chiesi-Villa, A.; Rizzoli, C. *Chem. Eur. J.* **1999**, *5*, 708-721.
- <sup>15</sup> Djebbar-Sid, S.; Benali-Baitich, O.; Deloume, J. P. *J. Mol. Struct.* **2001**, *569*, 121-128.
- <sup>16</sup> Zhang, Y-L.; Ruan, W-J.; Zhao, X-J.; Wang, H-G.; Zhu, Z-A. *Polyhedron* **2003**, *22*, 1535-1545.
- <sup>17</sup> Dreos, R.; Nardin, G.; Randaccio, L.; Siega, P.; Tauzher, G.; Vrdoljak, V. *Inorg. Chim. Acta* **2003**, *349*, 239-248.
- <sup>18</sup> Migita, K. T.; Migita, C. T.; Iwaizumi, M. *J. Chem. Soc. Dalton Trans.* **1984**, 1195-1201.
- <sup>19</sup> Pui, A. *Croatia Chemica Acta* **2002**, *75*, 165-173.
- <sup>20</sup> Park, S.; Mathur, V. K.; Planalp, R. P. *Polyhedron* **1998**, *17*, 325-330.
- <sup>21</sup> University of the West Indies, Mona Campus *Dioxygen Uptake by Co(salen)* [Online] Available: [http://wwwchem.uwimona.edu.jm/lab\\_manuals/c31lex2.html](http://wwwchem.uwimona.edu.jm/lab_manuals/c31lex2.html).
- <sup>22</sup> Ortiz, B.; Park, Su-M. *Bull. Korean Chem. Soc.* **2000**, *21*, 405-411.
- <sup>23</sup> Combes, A. *C. R. Acad. Fr.* **1889**, *108*, 1252.
- <sup>24</sup> Canali, L.; Sherrington, D. C. *Chem. Soc. Rev.* **1999**, *28*, 85-93.
- <sup>25</sup> Nishinaga, A.; Yamato, H.; Abe, T.; Maruyama, K.; Matsuura, T. *Tetrahedron Letters* **1988**, *29*, 6309.
- <sup>26</sup> Fukuda, T.; Katsuki, T. *Synlett*, **1995**, 825.
- <sup>27</sup> Jacobsen, E. N.; Kakiuch, F.; Konsler, R. G.; Larrow, J. F.; Tokunaga, M. *Tetrahedron Letters* **1997**, *38*, 773.

- 
- <sup>28</sup> Brandes, B. D.; Jacobsen, E. N. *Tetrahedron: Asymmetry* **1997**, *8*, 3927.
- <sup>29</sup> Isse, A. A.; Gennaro, A.; Vianello, E. *Electrochim. Acta* **1997**, *13-14*, 2065-2071.
- <sup>30</sup> Arena, F.; Floriani, C.; Chiesi-Villa, A.; Guastini, C. *Inorg. Chem.* **1986**, *25*, 4589-4596.
- <sup>31</sup> Koh, S.; Jeon, B.; Kim, H.; Park, K.; Kim, H. *Bull. Korean Chem. Soc.* **2004**, *25*, 471-474.
- <sup>32</sup> Zare H. R.; Memarzadeh, F.; Gorji, A.; Ardakani, M. M. *J. Braz. Chem. Soc.* **2005**, *16*, 571-577.
- <sup>33</sup> Yuan, R.; Chai, Y-Q.; Liu, D.; Gao, D.; Li, J-Z.; Yu, R-Q. *Anal. Chem.* **1993**, *65*, 2572-2575.
- <sup>34</sup> Vol'pin, M. E.; Novodarova, G. N. *J. Mol. Catal.* **1992**, *74*, 153-162.
- <sup>35</sup> Cameron, J. H.; Turner, S. C. *J. Chem. Soc. Dalton Trans.* **1992**, 3285-3289.
- <sup>36</sup> Pui, A.; Berdan, I.; Morgenstern-Badarau, R.; Gref, A.; Perrée-Fauvet, M. *Inorg. Chim. Acta* **2001**, *320*, 167-171.
- <sup>37</sup> Migita, K.; Chikira, M.; Iwaizumi, M. *J. Chem. Soc. Dalton Trans.* **1983**, 2281-2286.
- <sup>38</sup> Tsumaki, T. *Bull. Chem. Soc. Japan* **1938**, *13*, 252.
- <sup>39</sup> Busetto, C.; Cariati, F.; Fusi, A.; Gulloti, M.; Morazzoni, F.; Pasini, A.; Ugo, R.; Valenti, V. *J. Chem. Soc., Dalton Trans.* **1973**, 754-765.
- <sup>40</sup> Hobday, M. D.; Smith, T. D. *Coord. Chem. Rev.* **1972**, *9*, 311-337.
- <sup>41</sup> Calvin, M.; Bailes, R. H.; Wilmarth, W. K. *J. Am. Chem. Soc.*, **1946**, *68*, 2254-2256.

- 
- <sup>42</sup> Gall, R. S.; Rogers, J. F.; Schaefer, W. P.; Christoph, G. G. *J. Am. Chem. Soc.* **1976**, *98*, 5135-5144.
- <sup>43</sup> Vogt, L. H.; Faigenbaum, H. M.; Wiberley, S. E. *Chem Rev.* **1963**, *63*, 269-277.
- <sup>44</sup> Ohashi, Y.; Nakamura, M. *Bull. Chem. Soc. Jpn.* **1994**, *67*, 2921-2926.
- <sup>45</sup> Jones, R. D.; Summerville, D. A.; Basolo, F. *Chem. Rev.* **1979**, *79*, 139-179.
- <sup>46</sup> Basolo, F.; Hoffman, B. M.; Ibers, J. A. *Acc. Chem. Res.* **1975**, *8*, 384-392.
- <sup>47</sup> Kurzak, K.; Kuźniarska-Biernacka, I.; Żurowska, B. *J. Soln. Chem.* **1999**, *28*, 133-151.
- <sup>48</sup> Chen, D.; Martell, A. E. *Inorg. Chem.* **1987**, *26*, 1026-1030.
- <sup>49</sup> Sheikshoaie, I.; Fabian, W. M. F. *Dyes and Pigments* **2006**, *70*, 91-98.
- <sup>50</sup> Di Bella, S.; Fragalà, I.; Ledoux, I.; Marks, T. J. *J. Am. Chem. Soc.* **1995**, *117*, 9481-9485.
- <sup>51</sup> Marzilli L. G.; Summers, M. F.; Bresciani-Pahor, N.; Zangrando, E.; Charland, J-P.; Randaccio, L. *J. Am. Chem. Soc.* **1985**, *107*, 6880-6888.
- <sup>52</sup> Chemaly, S.; Pratt, J. M. *J. Chem. Soc., Dalton Trans.* **1980**, 2259-2266.
- <sup>53</sup> Calligaris, M.; Minichelli, D.; Nardin, G.; Randaccio, L. *J. Chem. Soc. (A)* **1971**, 2720.
- <sup>54</sup> Asbell, P. A.; Epstein, S. P.; Wallace, J. A.; Epstein A. B.; Stewart, C. C.; Burger, R. M. *Cornea* **1998**, *17*, 550.
- <sup>55</sup> Blum, O.; Haiek, A.; Cwikel, D.; Dori, Z.; Meade, T. J.; Gray, H. B. *Proc. Natl. Acad. Sci. USA* **1998**, *95*, 6659-6662.
- <sup>56</sup> Louie, A. Y.; Meade, T. J. *Proc. Natl. Acad. Sci. USA* **1998**, *95*, 6663-6668.

- 
- <sup>57</sup> Takeuchi, T.; Böttcher, A.; Quezada, C. M.; Meade, T. J.; Gray, H. B. *Bioorganic and Medicinal Chemistry* **1999**, *7*, 815-819.
- <sup>58</sup> Osinsky, S.; Levitin, I.; Bubnovskaya, L.; Sigan, A.; Ganusevich, I.; Kovelskaya, A.; Valkovskaya, N.; Campanella, L.; Wardman, P. *Experimental Oncology* **2004**, *26*, 140-144.
- <sup>59</sup> Amirnasr, M.; Schenk, K. J.; Gorji, A.; Vafazadeh, R. *Polyhedron* **2001**, *20*, 695-702.
- <sup>60</sup> *ORTEP-3 for Windows*, v1.08 (Farrugia, L. J. *J. Appl. Cryst.* **1997**, *30*, 565). This program is based on *ORTEP-III* v1.03 (Burnett, M. N.; Johnson, C. K. Oak Ridge National Laboratory report ORNL-6895, 1996).
- <sup>61</sup> International Union of Crystallography, *CheckCIF*, [Online] Available: <http://www.iucr.org/>.
- <sup>62</sup> Gall, R. S.; Schaefer, W. P. *Inorg. Chem.* **1976**, *15*, 2758-2763.
- <sup>63</sup> Matsumoto, N.; Imaizumi, M.; Ohyoshi, A. *Polyhedron* **1983**, *2*, 137-139.
- <sup>64</sup> Nakamoto, N. In *Infrared and Raman Spectroscopy of Inorganic and Coordination Compounds Part A: Theory and Applications in Inorganic Chemistry*, 5<sup>th</sup> ed., John Wiley & Sons: New York, **1997**, 1-6.
- <sup>65</sup> Pavia, D. L.; Lampman, G. M.; Kriz, G. S. *Introduction to Spectroscopy* 3<sup>rd</sup> ed., Brooks/Cole Thomson Learning: Australia, **2001**, 75.
- <sup>66</sup> Kumar, D. N.; Garg, B. S. *Spectrochim. Acta Part A* **2006**, *64*, 141-147.
- <sup>67</sup> Ware, D. C.; Mackie, D. S.; Brothers, P. J.; Denny, W. A. *Polyhedron* **1995**, *14*, 1641-1646.
- <sup>68</sup> Munro, O. Q.; Shabalala, S. C.; Brown, N. J. *Inorg. Chem.* **2001**, *40*, 3303-3317.

- 
- <sup>69</sup> *CrysAlis CCD* and *CrysAlis RED*, Version 170, Oxford Diffraction Ltd., Abingdon, UK, **2002**.
- <sup>70</sup> Subrahmanyam, C.; Seshasayee, M.; Aravamudan, G. *Cryst. Struct. Comm.* **1982**, *11*, 1719-1723.
- <sup>71</sup> Pahor, N. B.; Calligaris, M.; Delise, P.; Dodic, G.; Nardin, G.; Randaccio, L. *J. Chem. Soc. Dalton Trans* **1976**, 2478-2483.
- <sup>72</sup> Kabak, M.; Elmali, A.; Elerman, Y.; Durlu, T. N. *J. Mol. Struct.* **2000**, *553*, 187-192.
- <sup>73</sup> Kannappan, R.; Tanase, S.; Tooke, D. M.; Spek, A. L.; Mutikainen, I.; Turpeinen, U.; Reedijk, J. *Polyhedron* **2004**, *23*, 2285-2291.
- <sup>74</sup> Çakir, Ö.; Elerman, Y.; Elamli, A. *Analytical Sciences* **2002**, *18*, 377-378.
- <sup>75</sup> Wang, Y.; Parkin, S.; Atwood, D. *Inorg. Chem.* **2002**, *41*, 558-565.
- <sup>76</sup> Zhang, K-L.; Xu, Y.; Song, Y.; Zhang, Y.; Wang, Z.; You, X-Z. *J. Mol. Struct.* **2001**, *570*, 137-143.
- <sup>77</sup> Kitaura, R.; Onoyama, G.; Sakamoto, H.; Matsuda, R.; Noro, S.; Kitagawa, S. *Angew. Chem. Int. Ed.* **2004**, *43*, 2684-2687.
- <sup>78</sup> Naskar, S.; Biswas, S.; Mishra, D.; Adhikary, B.; Falvello, L. R.; Soler, T.; Schwalbe, C. H.; Chattopadhyay, S. K. *Inorg. Chim. Acta* **2004**, *357*, 4257-4264.
- <sup>79</sup> Marinovich, A. F.; O' Mahony, S.; Waters, J. M.; Waters, T. N. M. *Croatica Chemica Acta* **1999**, *72*, 685-703.
- <sup>80</sup> Nishida, Y.; Kino, K.; Kida, S. *J. Chem. Soc. Dalton Trans.* **1987**, 1157-1161.

- 
- <sup>81</sup> Hori, A.; Ozawa, T.; Yoshida, H.; Imori, Y.; Kuribayashi, Y.; Nakano, E.; Azuma, N. *Inorg. Chim. Acta* **1998**, *281*, 207-213.
- <sup>82</sup> Works, C. F.; Jocjer, C. J.; Bart, G. D.; Bu, X.; Ford, P. C. *Inorg. Chem.* **2002**, *41*, 3728-3739.
- <sup>83</sup> Biswas, S.; Mitra, K.; Schwalbe, C. H.; Lucas, C. R.; Chattopadhyay, S. K.; Adhikary, B. *Inorg. Chim. Acta* **2005**, *358*, 2473-2481.
- <sup>84</sup> Gallo, E.; Solari, E.; Re, N.; Floriani, C.; Chiesi-Villa, A.; Rizzoli, C. *J. Am. Chem. Soc.* **1997**, *119*, 5144-5154.
- <sup>85</sup> Chen, C.; Huang, D.; Zhang, X.; Chen, F.; Zhu, H.; Liu, Q.; Zhang, C.; Liao, D.; Li, L.; Sun, L. *Inorg. Chem.* **2003**, *42*, 3540-3548.
- <sup>86</sup> Yao, H. H.; Huang, W. T.; Lo, J. M.; Liao, F. L.; Wang, S. L. *Eur. J. Solid State Inorg. Chem.* **1997**, *34*, 355-366.
- <sup>87</sup> Hernández-Molina, R.; Mederos, A.; Gili, P.; Domínguez, S.; Núñez, P.; Germain, G.; Debaerdemaeker, T. *Inorg. Chim. Acta* **1997**, *256*, 319-325.
- <sup>88</sup> Shen, Y-Z.; Pan, Y.; Wang, L-Y.; Dong, G.; Jin, X-P.; Huang, X-Y.; Hu, H. *J. Org. Chem.* **1999**, *590*, 242-247.
- <sup>89</sup> Gambarotta, S.; Fiallo, M. L.; Floriani, C.; Chiesi-Villa, A.; Guastini, C. *J. Chem. Soc., Chem. Commun.* **1982**, 503-505.
- <sup>90</sup> Floriani, C.; Fiallo, M.; Chiesi-Villa, A.; Guastini, C. *J. Chem. Soc. Dalton Trans.* **1987**, 1367-1376.
- <sup>91</sup> Cummins, D.; Mckenzie, E. D.; Milburn, H. *J. Chem. Soc. Dalton Trans.* **1976**, 130-135.

- 
- <sup>92</sup> Kennedy, B. J.; Fallon, G. D.; Gatehouse, B. M. K.C.; Murray, K. S. *Inorg. Chem.* **1984**, *23*, 580-588.
- <sup>93</sup> Summers, M. F.; Marzilli, L. G.; Bresciani-Pahor, N.; Randaccio, L. *J. Am. Chem. Soc.* **1984**, *106*, 4478-4485.
- <sup>94</sup> Sheldrick, G. M. *SHELXS-97, Program for solution of crystal and structures*, University of Göttingen, Germany, **1997**.
- <sup>95</sup> Farrugia, L. J. *J. Appl. Crystallogr.* **1999**, *32*, 837-838.
- <sup>96</sup> Sheldrick, G.M. *SHELXL-97, Program for refinement of crystal structures*, University of Göttingen, Germany, **1997**.
- <sup>97</sup> Blessing, R. H. *Acta Cryst.* **1995**, *A51*, 33-38.
- <sup>98</sup> V.d. Sluis, P. and Spek, A. L. *Acta Crystallogr., Sect. A.* **1990**, *46*, 194-201.
- <sup>99</sup> Setsune, J.; Ishimaru, Y.; Moriyama, T.; Kitao, T. *Chem. Commun.* **1991**, 556-557.
- <sup>100</sup> Steiner, T. *Angew. Chem. Int. Ed.* **2002**, *41*, 48-76.
- <sup>101</sup> Nishio, M. *CrystEngComm.* **2004**, *6*, 130-158.
- <sup>102</sup> von Euler, H. *Ber.*, **1903**, 1854.
- <sup>103</sup> Bodlander, G.; Storbeck, O.Z. *Anorg. Chem.*, **1902**, *31*, 1.
- <sup>104</sup> Martell, A. E.; Motekaitis, R. J. *Determination and Use of Stability Constants* VCH Publishers, Inc. New York, **1992**.
- <sup>105</sup> Asadi, M.; Sarvestani, A. H.; Asadi, Z.; Setoodehkhah, M.; *Synthesis and Reactivity in Inorganic, Metal-Organic and Nano-Metal Chemistry* **2005**, *35*, 639-644.

---

<sup>106</sup> Asadi, M.; Ahmadi, M. B.; Mohammadi, K.; Asadi, Z.; Sarvestani, A. H. *J. Chem. Thermodynamics* **2004**, *36*, 141-146.